Spectroscopic Analysis of Yellow Diamonds

by

Mei Yan Lai

A thesis submitted in partial fulfillment of the requirements for the degree of

Master of Science

Department of Earth and Atmospheric Sciences

University of Alberta

Abstract

This research was motivated by the common recovery of yellow diamonds from kimberlites at Chidliak, Ekati and Qilalugaq in recent years, giving Canada the potential to become the new major source of fancy yellow diamonds. This thesis focuses on the analysis of yellow diamonds recovered from the Chidliak CH-7 and the Ekati Misery kimberlites in northern Canada. Physical properties including morphology, surface features and colours are recorded and displayed statistically. Further analyses include the extensive use of equipment – long wave ultraviolet (LWUV) (365 nm) light to detect fluorescence properties, Fourier transform infrared (FTIR) spectroscopy to detect the mid-IR absorption, UV-VIS-NIR spectroscopy to detect the visible light absorption, scanning electron microscope (SEM) cathodoluminescence (CL) imaging to reveal the internal growth structures, and secondary ion mass spectrometry (SIMS) to detect the carbon isotope composition and localized nitrogen concentration. The studied yellow diamonds are dominated by Type Ib/IaA, suggesting that the presence of C-centres is the major factor responsible for the yellow colouration of diamonds from both localities. The orange, yellow and green UV-excited fluorescence detected in some yellow diamonds indicates that the existence of additional optical centres modifies the colours. The discovery of diamonds from both kimberlites composed of B′-centre containing colourless cores and C-centre containing yellow outer layers, alongside with nitrogen thermometry results and evidence of distinct growth zones through different CL responses and distinct carbon isotope compositions, suggest that two or more episodes of diamond formation may be a common feature for yellow diamonds from Canada’s Arctic. Analysis of carbon isotope compositions provides preliminary results on the source parageneses of the yellow diamonds, where CH-7 yellow diamonds show a wide range of $\delta^{13}C$, indicative of an eclogitic (or websteritic) origin, whereas Misery yellow diamonds display a confined range of $\delta^{13}C$, in agreement with the range of mantle carbon and hence are thought to be mainly peridotitic.

Acknowledgements

First of all, I would like to express my deepest gratitude to my supervisor, Dr. Thomas Stachel, for providing me with this invaluable chance to work alongside him on diamond research. I am grateful for him to be always supportive throughout my research. His knowledge and guidance have been very inspiring to me, and my interest in the field of diamond research grew day by day from his inspiration. He is not only a supervisor, but also a mentor in my life.

I am thankful to Dr. Herman Grütter (Peregrine Diamonds Ltd.) for donating the Chidliak diamonds for this project. I would also like to thank Jon Carlson and Kimberly Ferguson (Dominion Diamond Mines) for donating the Ekati diamonds for this project and teaching me tremendous amounts of knowledge about diamond exploration. I am very grateful to have had the chance to visit the Ekati mine during my candidature and learn the whole exploration procedure, from drilling to kimberlite processing and diamond recovery. This was an unforgettable experience, which has been very helpful to my research and will definitely assist my future career.

I also would like to express my thanks to Dr. Jeff Harris for giving us an informative and delightful lecture about the characteristics of diamonds. Furthermore, special thanks to Dr. Mike Breeding (Gemological Institute of America) for teaching me the analytical techniques and the spectral features of yellow diamonds. In particular, I would like to thank him for discussing with me regarding my data and providing me with advice.

I am grateful to Dr. Richard Stern and Robert Dokken (Canadian Centre for Isotopic Microanalysis) as they have assisted me with SIMS analysis, CL imaging and sample preparation.

I would also like to show appreciation to all my teammates for their valuable inputs – especially Theetso Motsamai for being a very supportive teammate and always answering my questions about diamond geology. Many thanks to Dr. Graham Pearson and Anetta Banas, for organizing the Diamond Exploration and Research Training School (DERTS). The program has provided us numerous opportunities to explore the diamond field, and I feel privileged to be one of the members.

Finally, I would like to extend my thanks to Dr. Kiaran Lawson for always teaching me computational skills and assisting me in solving software issues. He has always been very helpful and supportive – words cannot express how grateful I am.

Table of contents

List of tables

List of figures

List of symbols

at. ppm — atomic part per million

cm^{-1} — wavenumber

cps — counts per second

ct. — carat

eV — electron volt

kV — kilovolt

nA — nanoampere

km — kilometre

mm — millimetre

nm — nanometre

µm — micrometre

s — second

ms — millisecond

ns — nanosecond

Ma — mega annum, million years

Ga — giga annum, billion years

% — percent

%A — the proportion of nitrogen in the form of A-center in diamond

%B — the proportion of nitrogen in the form of B-center in diamond

‰ — per mil

^{12}C — carbon-12

^{13}C — carbon-13

$\delta^{13}C$ — carbon isotope composition expressed as the normalized difference of the $^{13}C/^{12}C$ ratio of an unknown relative to the $^{13}C/^{12}C$ ratio of international VPDB standard

σ — standard deviation

× — times

° — degree

°C — degree Celsius

Ω — ohm

List of abbreviations

CCD — charge-coupled device

CL — cathodoluminescence

EM — electron multiplier

FTIR — Fourier transform infrared

IR — infrared

LWUV — long wave ultraviolet

NIR — near infrared

PL — photoluminescence

SEM — scanning electron microscope

SIMS — secondary ion mass spectrometry

SWUV — short wave ultraviolet

UV — ultraviolet

VIS — visible

1. Introduction

Diamond has exceptional physical and chemical properties, enabling it to be one of the most valuable gemstones in the jewelry market. When a diamond is cut and polished to ideal proportions, its high refractive index (an average value of 2.42 over the visible spectrum (Driscoll and Vaughan, 1978)) gives it the so-called "fire", which is the dispersion of white light into a spectrum. Combining this enchanting optical phenomenon with its chemical inertness and extreme hardness, gem-quality diamond is constantly popular among jewelry collectors.

From a geological point of view, diamond is more than just a piece of fascinating gemstone. Diamond gives important information of the mantle deep down in the Earth, where there is no access for direct sampling. The deepest borehole in the world, Kola SG-3, was drilled for geophysical studies (Popov et al., 1999), but the project could not proceed to the planned depth due to technical problems. The borehole reached a final depth of about 12.2 km – only approximately one third of the average thickness of the continental crust. Given that there is no physical way to reach further into the mantle with the current technology, diamonds formed in the mantle provide a window for scientists to probe the interior of the Earth.

During the crystallization of diamond, minerals in the proximity are trapped and become inclusions inside. The inclusions being encapsulated in diamond reflect the pressure and temperature conditions and the chemical composition of the Earth's mantle at the site of diamond formation. Moreover, the impurities incorporated in the diamond lattice, such as nitrogen, provide information on the thermal history of the diamond during its residence in the mantle.

1.1. Formation of diamonds

Formation of diamond mainly happens in the mantle, or very rarely occurs under exceptionally high-pressure conditions, such as in meteorite impact sites or during continental plate collision. Diamonds formed as a result of the latter conditions are usually very small and do not have commercial value.

Diamond forms in the mantle where the pressure is sufficient to stabilize its crystal lattice. Approximately 99 % of diamonds worldwide are derived from lithospheric mantle, whereas diamonds having sublithospheric origin are rare (Stachel and Harris, 2008). The region favourable for diamond crystallization, known as the diamond window, is constrained by the local geotherm, the graphite/diamond transition and the mantle adiabat (Fig. 1.1).

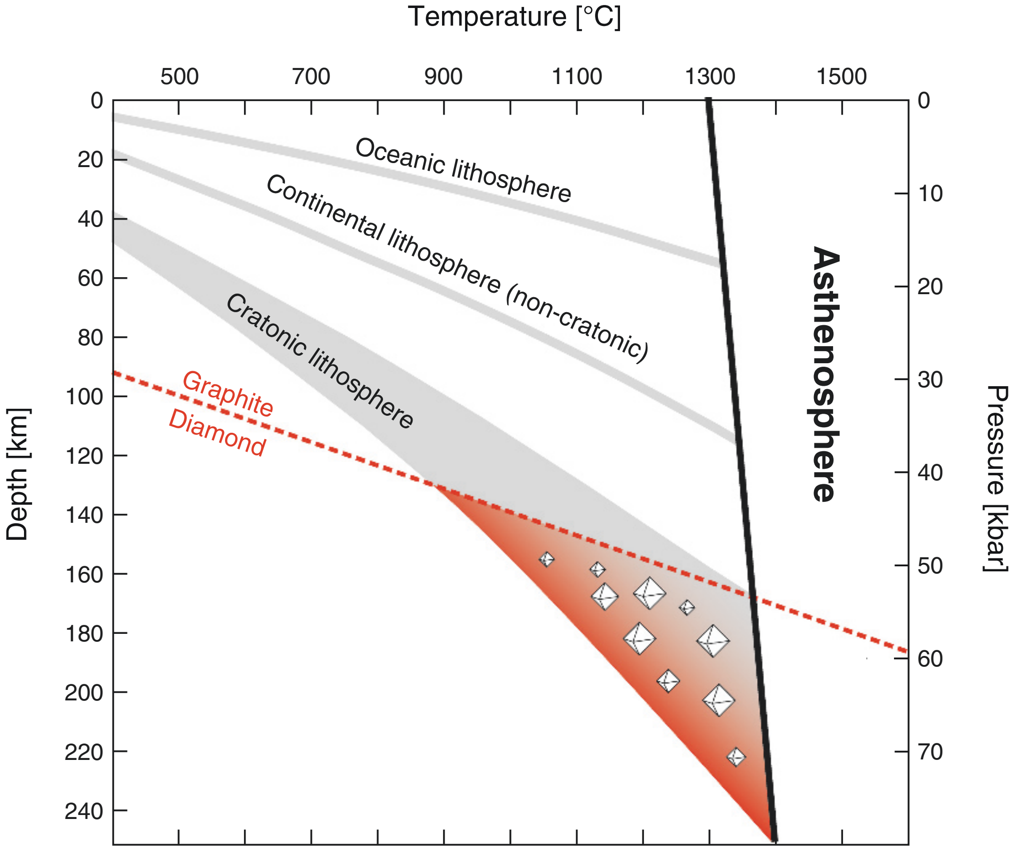

Figure 1.1: Plot of depth, pressure and temperature demonstrating the diamond window in the lithosphere (shaded in red), constrained by the local conductive geothermal gradient (shaded in grey), the graphite/diamond transition (red dashed line) and the mantle adiabat (black line) (taken from Fig. 1-03 of Tappert and Tappert (2011)).

It has been observed that primary (volcanic) diamond deposits are linked to ancient cratons (Clifford, 1966), and regions with high diamond potential are more likely to be found on cratons with relatively low geothermal gradients. Cratons are the oldest portions of the continental lithosphere that have remained stable for billions of years. In other words, cratons are tectonically inactive and therefore have a decrease in mantle heat flow, and lower heat generation as the radiogenic heat generating elements, K, Th and U, are increasingly depleted along with increasing crustal age (Pollack and Chapman, 1977). Additionally, heat transfer in the lithosphere occurs slowly through conduction, instead of efficient convection which happens in the asthenosphere, leading to a lower geothermal gradient within thick cratonic regions. There is a downward deflection of lithospheric mantle where it is colder than the asthenospheric mantle at a comparable depth, which creates a lithospheric mantle keel beneath cratons. Alongside with this thickening of subcratonic lithospheric mantle, the diamond stability field deflects upwards, as the lower temperature of the mantle keel at sufficiently high pressure favours the crystallization and preservation of diamond (Fig. 1.2). Thus, the low geothermal gradients of subcratonic lithospheric mantle result in a large diamond window.

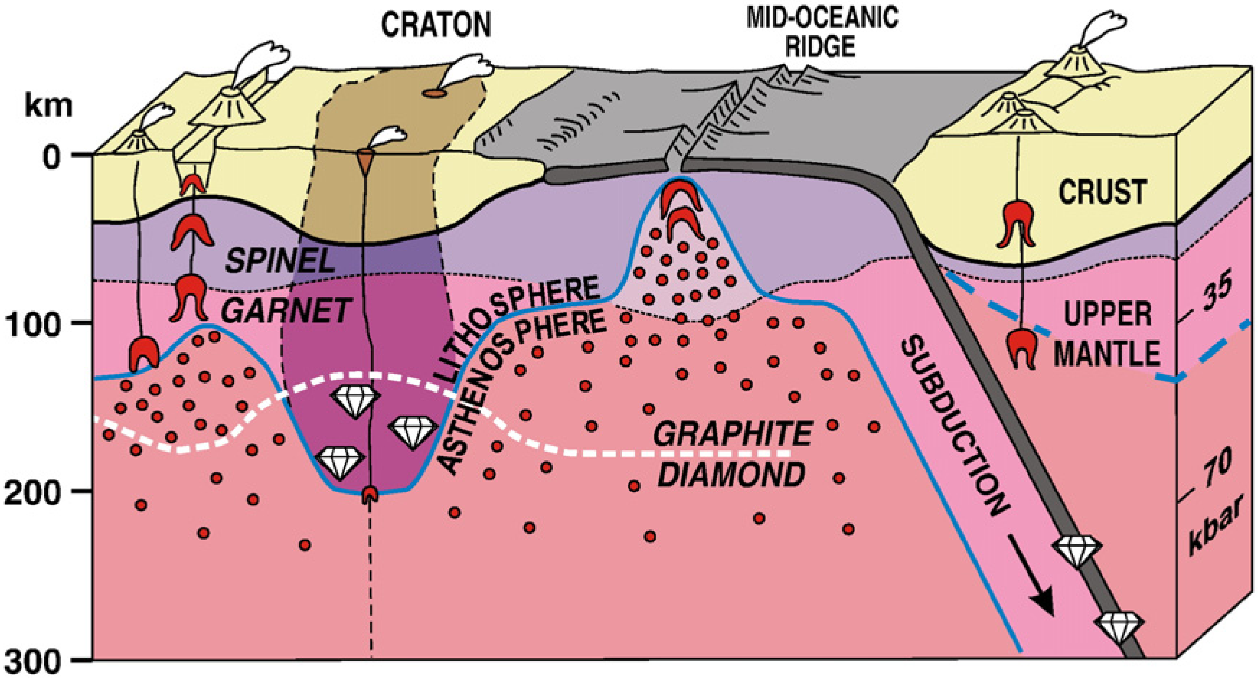

Figure 1.2: A schematic diagram of the Earth's crust and the upper mantle down to the depth of 300 km, showing the mantle keel of subcratonic lithosphere where it overlaps with the diamond stability field. The region enclosed between the graphite-diamond transition and the base of the lithosphere is known as the diamond window (taken from Fig. 1 of Stachel and Harris (2008)).

There are three possible diamond forming mechanisms in the mantle: (1) direct phase transition from graphite to diamond; (2) crystallization of diamond in a subsolidus CHO fluid saturated with carbon, and (3) redox reactions which include reduction of carbonates (CO_3^{2-}) or oxidation of methane (CH_4) to release free carbon for precipitation of diamonds (Stachel and Luth, 2015). The first mechanism, however, is only limited to the formation of polycrystalline diamonds, as the transition to diamond involves the breakage of graphite bonds which requires an extremely high activation energy. Under these kinetic conditions, the phase transition from graphite to diamond will take place so rapidly that it results not in gem quality but in polycrystalline diamond (Stachel et al., 2006). Moreover, CL images of diamonds revealed that there is growth zoning in gem-quality, monocrystalline diamonds, where the carbon isotopic compositions and nitrogen concentrations vary across different zones, implying that they grow layer by layer in a slow and episodic process, which cannot be achieved by a direct phase transition. Thus, precipitation of diamonds from carbon-saturated subsolidus CHO fluid and redox reactions seem to be the most acceptable mechanisms for the formation of monocrystalline diamonds (Stachel and Harris, 2009).

1.1.1. Source parageneses of diamonds

Diamonds can be broadly assigned to two main source groups according to their inclusions – subcratonic lithospheric diamonds and sublithospheric diamonds (which can possibly form as deep as 410 – 800 km within the transition zone and the lower mantle (Harte, 2010)). Lithospheric diamonds contain inclusions encompassing the peridotitic, eclogitic and websteritic suites, whereas sublithospheric diamonds contain inclusions formed at extremely high pressure such as majoritic garnet and ferropericlase (Stachel et al., 2005).

Of inclusion-bearing diamonds formed in subcratonic lithospheric mantle, diamonds with peridotitic inclusions dominate the worldwide database and make up 65 %, followed by eclogitic diamonds and relatively rare websteritic diamonds, with proportions of 33 % and 2 %, respectively (Stachel and Harris, 2008).

Employing another robust technique, carbon isotopic analysis, the source parageneses of diamonds can be better understood. Carbon is the major element in diamond; by analysing the ratio of its two stable isotopes, ^{12}C and ^{13}C, the origin of carbon forming the diamonds and its geologic history is revealed. The carbon isotopic signature of diamond is represented by $\delta^{13}C$, which is the normalized difference of its $^{13}C/^{12}C$ ratio relative to the $^{13}C/^{12}C$ ratio of the international VPDB standard. Typically, $\delta^{13}C$ values of inclusion-bearing diamonds are plotted as histograms to show the relationship between the distribution of values and possible sources of carbon. $\delta^{13}C$ values of diamonds worldwide mainly fall in the range of –38.5 to +5 ‰, where peridotitic, eclogitic and websteritic diamonds have a common mode in distribution at approximately –5 ‰, correlating with mantle derived carbon (Cartigny, 2005; Stachel, 2014).

1.1.1.1. Peridotitic diamond source

Peridotitic diamonds are commonly referred to as P-type diamonds. P-type diamonds are further divided into harzburgitic, lherzolitic and wehrlitic parageneses based on the composition of garnet inclusion, in which harzburgitic diamonds are dominant and constitute approximately 86 % among the studied peridotitic diamonds (Stachel and Harris, 2008).

The inclusion suite of peridotitic diamonds typically has characteristics of high Mg in olivine, orthopyroxene and clinopyroxene, and high Cr in garnet (Stachel, 2014), while having low Ca and Al in them compared to the same minerals found in peridotite nodules in kimberlite (Harte et al., 1980).

The range of $\delta^{13}C$ in peridotitic diamonds is from –26.4 to +0.2 ‰ (Cartigny, 2005), where more than 95 % of peridotitic diamonds lie in a confined interval within the range of mantle values, which is –8 to –2 ‰ (Shirey and Shigley, 2013), implying that mantle carbon likely is the main source of peridotitic diamond formation.

1.1.1.2. Eclogitic diamond source

Eclogitic diamonds, also known as E-type diamonds, have an inclusion suite with compositions distinctly different from that of peridotitic diamonds: mineral inclusions in E-type diamonds have low concentrations of Mg and Cr, while exhibiting high concentrations of Na, Ca and Al (Stachel, 2014).

Compared to peridotitic diamonds, eclogitic diamonds have a much wider spread of $\delta^{13}C$ values, ranging from –41 ‰ (De Stefano et al., 2009) to +2.9 ‰ (Davies et al., 2003). The strongly negative values are considered to be related to former organic matter, whereas the positive values correlate with marine carbonates, suggesting that eclogitic diamonds have a subduction origin (Kirkley et al., 1991).

However, this proposition is controversial and was questioned by Cartigny (2005), because re-equilibration of carbon isotopic ratios of subducted organic substances and carbonates occurs as temperature increases, leading to a homogenization of the carbon isotopic composition of subducted carbonaceous materials. Thus, the presence of a wide range of $\delta^{13}C$ in diamonds cannot readily be related to subduction processes. Instead, Cartigny (2005) proposed that eclogitic diamonds are derived from mantle carbon involving carbon isotopic fractionation in an open system. However, this model cannot explain the distribution of $\delta^{13}C$ extending to very low values.

1.1.1.3. Websteritic diamond source

Websteritic diamonds have inclusions showing transitional compositions between those in peridotitic and ecologitic diamonds (Aulbach et al., 2002).

The range of $\delta^{13}C$ values in websteritic diamonds is not well established as inclusion-bearing websteritic diamonds are rare. From the reported data of different localities worldwide, the distribution of $\delta^{13}C$ in websteritic diamonds does not seem to have any pattern, and is strongly correlated with localities (Stachel et al., 2009). Similar to eclogitic diamonds, it can have very low $\delta^{13}C$ values down to –41 ‰ (De Stefano et al., 2009).

1.2. Diamond mining

Diamonds can be transported to the surface of the Earth by three types of magmas – kimberlite, lamproite and ultramafic lamprophyre, in which only the first magma is common for the occurrence of diamond. Lamproite magma is not usually diamondiferous, but there are a few exceptions including the Argyle diamond mine (Chapman et al., 1996) and the Ellendale diamond mine (Jenke and Cowan, 1994), which are the major deposits of pink and yellow diamonds, respectively. Ultramafic lamprophyre only scarcely hosts diamonds and it is not economically significant. All of them are suggested to erupt quickly but their volcanic emplacement has never been observed (Shirey and Shigley, 2013).

If the diamond-bearing primary deposits are exposed in the air instead of being buried under the surface of the Earth, they can be weathered and eroded. Subsequently, diamonds in these deposits will be washed away and concentrated in new environments such as riverbeds, to form secondary deposits, which are commonly referred to as placer diamonds.

1.3. Morphologies of diamonds

1.3.1. Octahedron and cuboid

Gem-quality, monocrystalline diamonds have two basic growth forms, known as octahedron and cuboid. Yet, most of the diamonds are not perfectly symmetrical - some of them have distorted shapes, where a dominant growth is observed in one or more particular directions. Common examples of distorted diamonds are elongated octahedra and re-entrant cubes. It is believed that the morphology of diamonds is related to the growth rate and the degree of carbon supersaturation in the diamond growing fluids, in which octahedral diamond originates from a slow spiral growth mechanism in fluids of low carbon supersaturation (Sunagawa, 1984).

1.3.2. Dodecahedron/tetrahexahedron

Diamonds with blunt edges are frequently observed and are considered the result of resorption happening during kimberlite/lamproite emplacement. It is observed from cathodoluminescence (CL) images, which show the internal growth structure of diamonds, that resorption can also happen during mantle residence. Resorption is a process of dissolution on the surface of diamonds, caused by surrounding oxidizing agents at high temperature. This occurs in diamonds of any shape. Sharp edges and corners are most susceptible to resorption (Moore and Lang, 1974), so they are rounded in the beginning of the process. As the dissolution continues, the faces of octahedral diamonds, for example, wear off progressively until they disappear completely. These diamonds then transform to a new shape called dodecahedron (McCallum et al., 1994). A similar process occurs in cubic diamonds, where their transformed shape is sometimes called tetrahexahedron.

1.3.3. Twin, parallel intergrowth and aggregate

A common morphology derived from the basic octahedron is a triangular shaped diamond named macle. It is a form of contact twinning where two components of the twin are connected along a compositional plane parallel to $\{111\}$. Another frequently observed form of twinning are interpenetrant twins where two components of the twins are connected along internal crystal planes (Tappert and Tappert, 2011).

Parallel intergrowths can be mistakenly identified as twins as they look quite similar in appearances. The main difference between them is the orientation of the components participating in the crystals, in which two or more components in parallel intergrowths are oriented in a parallel direction, while one component in twins rotates with respect to the other component about an axis in the crystal (Tappert and Tappert, 2011).

Aggregates form from a few diamonds clustering together. Unlike twins and parallel intergrowths, aggregates do not show a pattern of crystal orientation. Additionally, the clustered diamonds can be of different colours and types.

1.3.4. Irregular diamond/fragment

Irregular diamonds do not have a well-defined shape. Harris et al. (1975) defined that diamonds are categorized as irregular if they show less than 50 % of any of the recognizable shapes mentioned above.

Diamond fragments exhibit obvious fracture planes which are usually smooth. For diamonds recovered from primary deposits, fragmentation can happen during mantle residence, kimberlite/lamproite emplacement or mining. For diamonds recovered from secondary deposits, fragments usually result from collision with rocks during transportation in rivers.

1.3.5. Fibrous overgrowth

Fibrous overgrowth is a layer of rough coating encompassing a typically monocrystalline diamond core. It can occur in any shape of diamond and usually is poorly transparent to opaque. The monocrystalline core and fibrous coat grow in two different stages – smooth spiral growth and rough columnar growth, respectively (Sunagawa, 1990), where the former stage occurs slowly in diamond forming fluids of low carbon supersaturation, whereas the latter stage occurs rapidly in fluids of high carbon supersaturation (Sunagawa, 1984).

1.3.6. Polycrystalline diamond

Similar to fibrous diamonds, polycrystalline diamonds also grow rapidly under high carbon supersaturation (Sunagawa, 1984). Polycrystalline diamond is a cluster of randomly oriented submillimetre crystallites (Sunagawa, 1990). Hence, it does not have a well-defined shape, usually appears dull, and has a rough texture.

1.4. Surface features of diamonds

1.4.1. Growth-related features

Flat triangular plates are observed on octahedral faces of diamonds and they are known as the only growth-related feature (Stachel, 2014). They can appear as pyramidically overlapping growth layers or imbricating triangular plates of any thickness (Tappert and Tappert, 2011).

1.4.2. Resorption-related features

1.4.2.1. Shield-shaped lamina

When resorption occurs on the triangular growth plates of diamonds, the edges become rounded, resulting in thinner shield-shape laminae (Orlov, 1977).

1.4.2.2. Trigon and tetragon

Triangular pits, also known as trigons, are another feature limited to octahedral faces of diamonds.

They appear commonly as negative trigons (orientation opposite to that of the octahedral face) or rarely as positive trigons (same orientation as that of the octahedral face), depending on the conditions of the etching fluid, e.g. temperature (Omar et al., 1954). Occasionally, trigons with opposite orientations can combine to form hexagons (Evans and Sauter, 1961; Stachel, 2014).

Tetragons result from etching similar to trigons and are observed as squared pits limited to cubic faces of diamonds. Analogous to trigons, tetragons can also be classified as negative tetragons (rotated by 45° with respect to the orientation of the cubic face) and positive tetragons (sides parallel to the cubic face), in which the former ones are more frequently observed. Similar to trigons, the temperature of the etching fluid is one of the crucial factors which determine the orientation of tetragons (Evans and Sauter, 1961).

1.4.2.3. Terrace and hillock

On the progression of resorption, dodecahedral diamond can be further etched to develop edges surrounding the conjunction of three rhombic dodecahedral faces and parallel to sides of these rhombic faces. This pattern is called terraces, and its stepped texture is related to the growth structure of octahedral faces (Moore and Lang, 1974).

Hillock is another resorption-related feature restricted to dodecahedral faces of diamonds. They are aligned along the major diagonals of the rhombic faces of dodecahedral diamonds, or if the dodecahedron is not well-developed, they are oriented parallel to the sides of remnant octahedral faces. The formation of hillock is also related to the octahedral growth structure of diamond (Tappert and Tappert, 2011).

1.4.3. Deformation-related feature

Plastic deformation lines are sets of parallel lines, sometimes crossing each other when the sets of lines orient in different directions, formed under high shear stress in the stability field of diamond, which causes dislocation of atoms in the diamond lattice. It is suggested that plastic deformation occurs during kimberlite/lamproite emplacement where the diamonds are squeezed by neighbouring rocks (Fisher, 2009). A temporal connection to kimberlite magmatism is reinforced by experimental results that some deformation-related defects are unlikely to survive for extended time periods in the mantle at high temperature (Collins et al., 2000).

1.4.4. Other features

Occasionally, some rounded pits with variable depths can be observed on dodecahedral faces of diamonds, which are known as corrosion sculpture and shallow depression. At first glance, they look similar to another circular feature, named the micro-disk, which is also found on dodecahedral faces. However, this latter circular feature is slightly protruded from the surface of diamond instead of forming a pit. It is believed that the micro-disk pattern is a result of the adhesion of bubbles which protect the underlying surface from etching (Pandeya and Tolansky, 1961).

Other surface features, including the percussion mark and the scratch mark, are frequently observed on diamonds recovered from secondary deposits. Similar to fragmentation of diamonds during transportation in a river, these surface features are linked to the collision of diamonds with bedrock (Tappert and Tappert, 2011).

1.5. Diamond Type classification

Diamond is one of the allotropes of carbon, forming a stable structure of a covalently bonded face-centred cubic crystal lattice. Natural diamonds usually contain trace impurities such as hydrogen, boron and nitrogen. The incorporation of these trace impurities during the crystallization of diamond distorts its microstructure, and alters its physical properties such as colour and electrical conductivity.

The most common substitutional impurity in the diamond lattice is nitrogen, due to its similar ionic radius and charge to carbon (Goldschmidt, 1937). A Fourier transform infrared (FTIR) spectrometer is the essential instrument to quantitatively analyse the concentration and configuration of nitrogen atoms in diamond, hence identifying the Type of diamonds. Based on their nitrogen content, diamonds can be classified into two main types, namely Type I and Type II (Fig. 1.3).

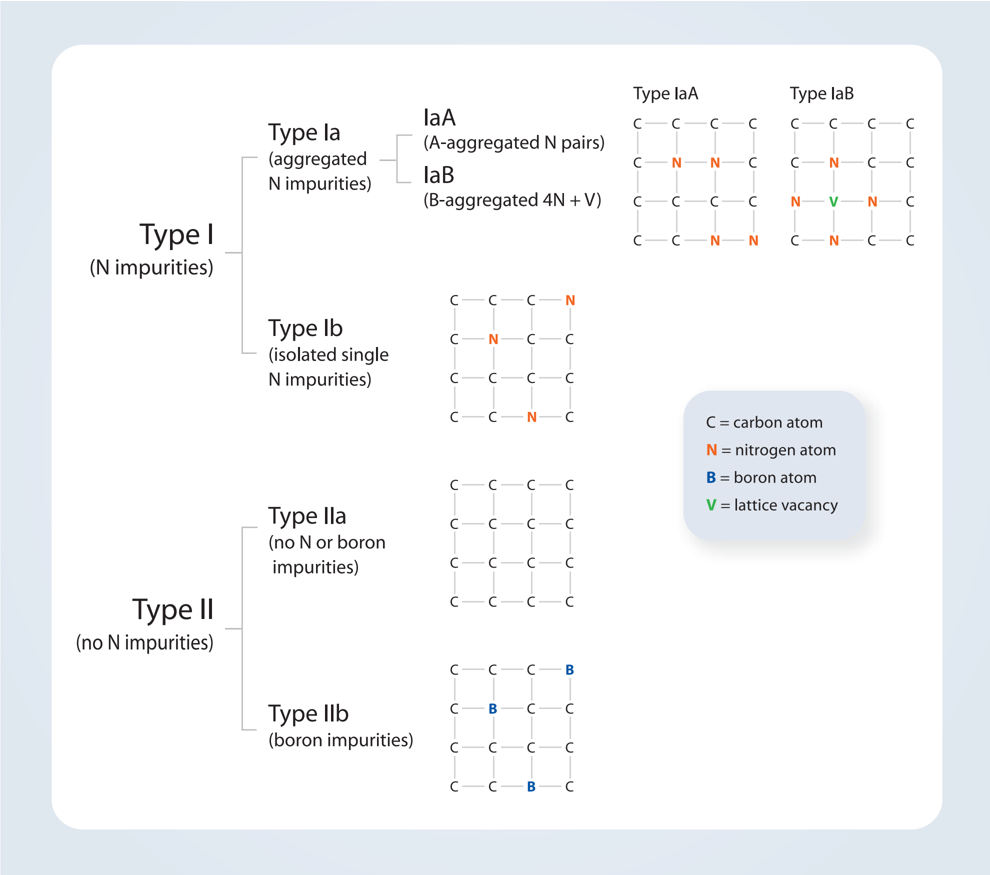

Figure 1.3: The diamond Type classification system based on the occurrence and configuration of impurities in the diamond lattice (taken from Fig. 2 of Breeding and Shigley (2009)).

1.5.1. Type I diamonds

Type I diamonds contain detectable (FTIR) amounts of nitrogen. With respect to the arrangement of nitrogen atoms in the diamond lattice, Type I diamonds are subdivided into Type Ia (aggregated nitrogen atoms) and Type Ib (single substituted nitrogen atoms, known as C-centres). Nitrogen aggregates appear in two configurations: they are nitrogen pairs (known as A-centres; (Davies, 1976)), and rings of four nitrogen atoms symmetrically surround a vacancy (known as B-centres; (Jones et al., 1992)). This further separates Type Ia diamonds into Type IaA and Type IaB respectively.

The degree of nitrogen aggregation is dependent on the concentration, the time averaged residence temperature and the residence period of diamonds in Earth's mantle (Taylor et al., 1990). C-centres are considered to be the original form of incorporated nitrogen impurities in the diamond lattice when diamonds crystallize. After the diamonds reside in the mantle for sufficient time, C-centres migrate and combine to form A-centres. This process occurs readily due to its relatively low activation energy, so pure Type Ib diamonds are very rare in nature (Taylor et al., 1996). That means even geologically young diamonds contain measurable concentration of A-centres instead of solely possessing C-centres (Collins, 2001), and are known as mixed Type Ib/IaA diamonds. As the aggregation proceeds, A-centres further migrate and combine to form B-centres. However, this process requires a high activation energy (Taylor et al., 1990), so the complete transition from A-centres to B-centres is rarely achieved before the diamonds are brought to the surface of the Earth. Thus, pure Type IaB diamonds are uncommon (Dobrinets et al., 2013) and diamonds usually contain significant concentrations of both A-centres and B-centres instead, which are grouped as mixed Type IaAB.

1.5.2. Type II diamonds

Type II diamonds, on the contrary, do not contain FTIR measurable nitrogen impurities (detection limit of FTIR is typically around 5 – 10 at. ppm). Type II diamonds are subdivided into Type IIa (absence of boron impurities) and Type IIb (single substituted boron atoms).

1.5.3. Relative abundances of diamond types

A vast majority of natural diamonds belong to Type Ia, constituting approximately 98 % in proportion. This is followed by Type IIa diamonds which are far less abundant, comprising a population of less than 2 %. Type Ib and Type IIb diamonds are scarce in nature, where each totals less than 0.1 % of all natural diamonds (Dobrinets et al., 2013).

1.6. Colours of diamonds

The colour of diamond perceived by human eye is a result of selective light absorption or emission by its optical defects in the visible spectrum. Optical defects are created by incorporated trace impurities, vacancies and dislocations in the lattice, enabling the diamonds to absorb or emit light of particular wavelengths. The absorption features corresponding to optical defects of diamonds are commonly detected using UV-VIS-NIR spectrometer, where they appear as broad absorption bands or sharp absorption peaks in the absorption spectrum. Pure diamonds without any defects in the lattice have a wide band gap of 5.5 eV, corresponding to a wavelength of 225 nm which lies in the ultraviolet region. This implies that pure diamonds do not absorb visible light and thus appear colourless.

In the case of coloured diamonds, the colour often results from a combination of multiple optical defects with different absorption features or even light emissions, leading to a wide variety of body colours of diamonds. Broad absorption bands usually have a stronger impact on a diamond's colour than the sharp absorption features (Shigley and Breeding, 2015).

1.6.1. Brown

Brown is the most abundant colour among all coloured diamonds and results from defect caused by plastic deformation (Wilks and Wilks, 1994), which is believed to be vacancy clusters (Fisher, 2009). Brown colour can be found in diamonds of any Type, but is especially common in Type IIa diamonds, as the presence of A- and B-centres somewhat restricts the diamond lattice from being distorted by plastic deformation (Nailer et al., 2007). The absorption characteristic of brown diamonds is a continuum steadily rising from the near infrared region towards the shorter wavelengths of the visible spectrum.

1.6.2. Yellow

Yellow is the second most abundant diamond colour, in which the colour saturated yellow diamonds are popular among jewelry collectors – reflected by the statistic that they are the most frequently submitted coloured diamonds to the Gemological Institute of America for analysis (King et al., 2005). Nitrogen-related defects are believed to be the primary cause for the yellow colour, supported by the fact that none of the yellow diamonds recovered so far belong to Type II. The most common optical defects causing the yellow colouration in diamonds are C-centres, N3 and N2 centres (N stands for naturally occurring), and the 480 nm band.

C-centres result in a steady rise in absorption from about 500 nm towards the blue end of the visible spectrum, which appears to be quite similar to the absorption feature of brown diamonds, but with much lower absorption in the yellow and red spectral regions (Dobrinets et al., 2013). Indeed, extremely high concentrations of C-centres can cause a very deep yellow colour, with a brownish tint, of diamonds (Collins, 2001). Furthermore, C-centres absorb light effectively, even just a very small portion in the lattice is enough to cause a vibrant yellow colour (Kitawaki, 2007).

N3 and N2 centres are the so-called "cape peaks", which absorb light at 415 and 478 nm, respectively. N3 centres have the physical structure of three nitrogen atoms surrounding a vacancy (N_3V) in the diamond lattice (Bursill and Glaisher, 1985), which is an intermediate form of nitrogen aggregation from A- to B-centres. The N2 centre is a vibronic transition (changes in vibrational and electronic energy levels simultaneously) of the N3 centre, and it always accompanies N3 centre in the visible absorption spectra. They are responsible for most of the pale yellow coloured diamonds, which are named “cape yellow” diamonds. It is known that the N3 centre is active in both absorption and luminescence, while the N2 centre is only active in absorption (Dobrinets et al., 2013), suggesting that the N2 centre is more likely to be the decisive factor accountable for the intensity of yellow colour of these diamonds. Indeed, King et al. (2005) observed that the saturation of yellow colours in diamonds which exhibit the same peak intensity of the N3 centre, can be very different. Moreover, they noticed that the N2 centre absorbs more strongly in yellow diamonds with higher saturation than in the less saturated yellow diamonds.

The 480 nm band is a broad absorption feature in the visible spectrum yet it does not have a well-defined structure (Shigley and Breeding, 2013). It has a proposed structure attributed to electronic transitions of positively charged substitutional oxygen atoms in the diamond lattice (Gali et al., 2001; Hainschwang et al., 2008). Diamonds with the 480 nm band exhibit strong yellow fluorescence under long wave UV excitation (Collins and Mohammed, 1982).

1.6.3. Grey/black

Grey and black colours are also prevalent in diamonds recovered worldwide, but they detrimentally affect the value of diamonds as they are considered to be unfavourable colours. It is a high content of dark coloured inclusions such as graphite and sulfides that causes the grey appearance, or even an opaque black colour of diamonds when the abundance of these inclusions is extremely high (Titkov et al., 2003). A coat of graphitized material on diamonds may also be a cause of black colouration (Field, 1979).

1.6.4. Other colours

Diamonds very rarely appear in other colours such as green, blue, pink, red and purple. Green colouration is associated with natural irradiation by radioactive elements existing in close proximity to the diamonds, which can occur to any type of diamond. Blue colour is limited to Type IIb diamonds, attributing to the single substitutional boron in the diamond lattice. Pink, red and purple colours are the results of plastic deformation. They occur in any type of diamond and, similar to brown diamonds, they exhibit an absorption continuum in the visible spectrum, but with the presence of a more pronounced broad absorption band located at 550 nm (Dobrinets et al., 2013; Shigley and Breeding, 2013).

1.7. Diamond fluorescence

Diamond fluorescence is a type of luminescence where the diamonds absorb light at a certain wavelength, then emit light of longer wavelengths following the absorption. The most frequently used light sources for diamond studies are short wave ultraviolet (SWUV) and long wave ultraviolet (LWUV), which excite diamond fluorescence of different intensities and colours. A variety of defects in diamonds result in different fluorescence colours, with more than 500 nitrogen-related defects in diamonds that can emit fluorescence (Dobrinets et al., 2013). The occurrence of inconsistent fluorescent strength or colour in different areas of a diamond means that the defects in the diamond lattice are unevenly distributed. In some cases, it can serve as an indicator that a diamond grew in several stages (King and Wang, 2017).

1.8. Purpose of research

The market for fancy yellow diamonds has long been dominated by the Ellendale diamond mine located in Western Australia, which contributed approximately 50 % of the production of fancy yellow diamonds worldwide (Gem Diamonds, 2012). Along with the cessation of mining activities at Ellendale in 2015 (Government of Western Australia, 2015), the supply of fancy yellow diamonds to the market has dropped significantly.

However, it has been observed that the Ekati diamond mine constantly produces fancy yellow diamonds in recent years. A well-known example is the 65.93 ct. “Arctic Sun” diamond recovered from the Misery main pipe in 2016, which is by far the largest fancy yellow diamond recovered in North America (Dominion Diamond Mines, 2017).

The Chidliak advanced exploration property was also found to have potential for the existence of fancy yellow diamonds, as a previous evaluation assessed in 2014 on a diamond parcel from the CH-6 kimberlite revealed the presence of a number of small yellow diamonds (Nowicki et al., 2016).

This research is motivated by the frequent recovery of yellow diamonds from the above two mines located in Canada in recent years. As Canada may have the potential to be the new major source of fancy yellow diamonds, it is economically important to study the properties of the yellow diamonds from these two mines systematically in order to understand the causes of their colouration and the conditions of their formation.

1.9. Thesis outline

This thesis focuses on the observation and analysis of yellow diamonds from two localities in Canada. Observation includes the morphology, surface features, colours and fluorescence of diamonds, whereas analysis requires the extensive use of various instruments to investigate their spectroscopic characteristics and growth history.

Chapter 1, presented here, serves as an introduction regarding the origin and the basic properties of diamonds.

Chapter 2 reports the methodology for this research: (i) The use of FTIR to identify the different Types of diamonds and detect IR-active defects. This includes a discussion of the effects of spectral resolution and the deconvolution of FTIR spectra to calculate the nitrogen concentration in diamonds. (ii) The fluorescence properties of diamonds excited by UV light were also recorded. Visible absorption spectra were obtained from selected diamonds utilizing a UV-VIS-NIR spectrometer to investigate the relationship between the diamond colours and the lattice defects. CL imaging was performed with a scanning electron microscope (SEM) for investigating the internal growth structure of diamonds. (iii) This was followed by the analysis of carbon isotope compositions and nitrogen abundances using the secondary ion mass spectrometry (SIMS) technique to understand the growth events of diamonds and to draw inferences on the source paragenesis.

Diamonds from the Chidliak property and the Ekati diamond mine will be discussed individually in Chapters 3 and 4 respectively. These chapters will be dedicated to sample description, summarizing the observed physical properties of diamonds, showing statistics about the relative abundances of diamond colours in the parcels, and documenting the distribution of morphology in the yellow diamond subset. This is followed by the analysis and discussion of experimental results, where the mantle residence time of diamonds is calculated from the concentration and degree of aggregation of nitrogen. Furthermore, spectral features and CL images are examined. The distribution of carbon isotope compositions is compared with the global database, and the source paragenesis of the diamonds is deduced.

Finally, Chapter 5 will highlight the key features of diamonds in this research, discuss the similarities and differences observed between diamonds from the two localities, and summarize the experimental results.

2. Methodology

2.1. FTIR spectroscopy

The IR absorption spectra of diamonds were acquired using a Thermo Nicolet Nexus 470 FTIR spectrometer, equipped with a continuum IR microscope and a motorized stage, located in the De Beers Laboratory for Diamond Research at the University of Alberta. A mid-IR light source was used to collect diamond absorption spectra with a spectral range of $650-4000\ \mathrm{cm}^{-1}$. Diamonds were placed on the motorized stage and measured under a 15× magnification IR objective in transmittance mode. The spectra were acquired by averaging 200 scans at a spectral resolution of $1\ \mathrm{cm}^{-1}$ with an aperture size of 100 μm × 100 μm.

Diamonds were immersed in petrolether and placed in an ultrasonic bath for about 5 minutes, to remove any possible surface contamination prior to all measurements. The detector of the IR microscope was cooled to near liquid nitrogen temperature and was left to stand at least 30 minutes to stabilize before operation. A background spectrum was collected before sample measurement to compensate for the effect of atmospheric absorption. Throughout the measurements, the background spectrum was re-measured whenever the sample spectrum showed an undesirable signal contributed by the atmosphere.

The total nitrogen content and the nitrogen concentration in C-, A- and B-centres were calculated using the spectral deconvolution spreadsheet developed by David Fisher of De Beers Technologies. Initially, the original spectrum was corrected with manual baseline subtraction. Prior to spectral deconvolution, all spectra were normalized to a Type IIa reference spectrum in absorption coefficient (1 cm thickness).

Spectral deconvolution was conducted on normalized spectra in the spectral range between $1000-1400\ \mathrm{cm}^{-1}$, which corresponds to the nitrogen absorption region of diamonds. The relative abundances of nitrogen in C-, A- and B-centres, with a unit of at. ppm, were obtained via least squares fitting based on appropriate constraints set in the solver add-in of Excel. The constraints corresponding to A (A-centre), B (B-centre), C (C-centre) and D (platelet-related absorption, (Woods, 1986)) components were set based on the spectral features in three cases: (i) platelets peak present: A, B and $D \geq 0$, $C = 0$; (ii) C-centres present: A and $C \geq 0$, $B = 0$; (iii) B-centres present:

A and B ≥ 0, C = 0. The A-component was involved in the all three cases above, as all yellow diamonds analysed contain A-centres – this will be further discussed in detail in Chapters 3 and 4.

The results of spectral deconvolution are used to classify the types of diamonds. The calculation of relative proportions of A-, B- and C-centres is as follows, taking A-centre as an example:

$$\%A = \frac{concentration\ of\ nitrogen\ in\ A\text{-}centres}{Total\ concentration\ of\ nitrogen} \times 100$$

If C-centres are present with A-centres, the diamond will be categorized as Type Ib/IaA, regardless of the concentration of C-centres; if A-centres are present with B-centres, and the proportion of A-centres is > 90 %, then it is a Type IaA diamond; if B-centres are > 90 %, then it is classified as Type IaB; else it is a Type IaAB diamond. The relative proportions of A-, B- and C-centres, alongside with the total nitrogen content, are parameters in constraining the mantle residence time of diamonds, applying an appropriate time-averaged mantle residence temperature (Taylor et al., 1990; Taylor et al., 1996; Leahy and Taylor, 1997).

The choice of spectral resolution is of great importance in this research, as the high concentration of A-centres in some diamonds masks the C-centre peaks in the spectrum, especially when the concentration of C-centres is very low (Hainschwang et al., 2012b). Thus, tests on a diamond with a high concentration of A-centres were conducted using various spectral resolutions, to determine the optimum experimental condition for resolving the C-centre peaks (Fig. 2.1).

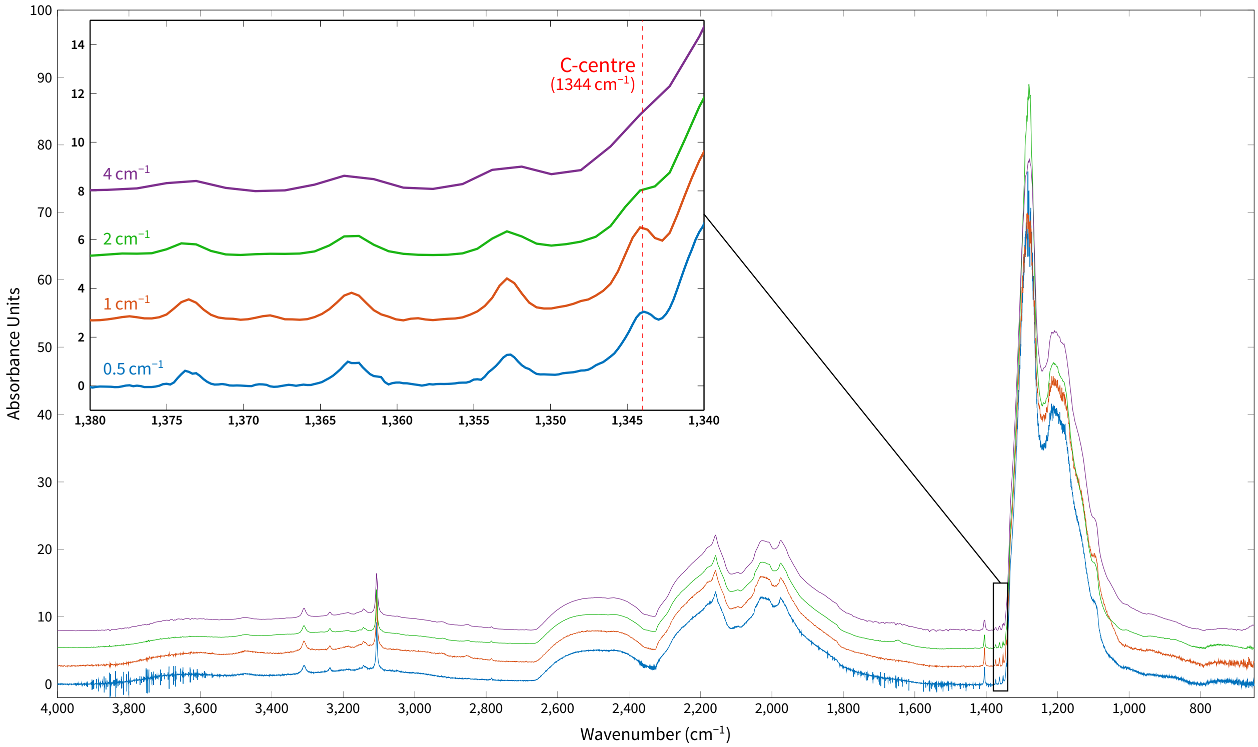

Figure 2.1: The IR absorption spectra of a diamond with high concentration of A-centre acquired with 4 cm^{-1} (purple), 2 cm^{-1} (green), 1 cm^{-1} (orange) and 0.5 cm^{-1} (blue).

It is observed that the C-centre peak at 1344 cm^{-1} in the spectrum of the above diamond is unrecognizable when a spectral resolution of 4 cm^{-1} is used. The peak becomes detectable at a spectral resolution of 2 cm^{-1}, but it was not well resolved. Spectral resolutions of 1 cm^{-1} and 0.5 cm^{-1} can reveal the peak equally well, however, the higher resolution of 0.5 cm^{-1} is achieved at the cost of a lower signal-to-noise ratio (given a fixed number of scans) (Blitz and Klarup, 2002), making some subtle spectral features unidentifiable. Thus, a spectral resolution of 1 cm^{-1} was adopted for the IR absorption measurements throughout this research, such that the 1344 cm^{-1} peak (and other minor peaks) was still resolvable while maintaining a sufficient signal-to-noise ratio.

While the relative abundance of nitrogen in A- and B-centres was obtained via spectral fitting, the C-centre concentration was calculated manually based on the absorption coefficient at the peak position of 1344 cm^{-1}. This approach is especially more accurate for diamonds having a high concentration of A-centre, as the 1344 cm^{-1} peak does not overlap with other components. The choice of spectral resolution has been shown to affect the calculation of C-centre concentrations significantly. Based on the factors corresponding to different spectral resolutions deduced by

Liggins (2010), the concentration of nitrogen in C-centres was calculated by multiplying the absorption coefficient at 1344 cm^{-1} by a factor of 37.

It has been observed that the 1344 cm^{-1} peak has a first overtone at 2688 cm^{-1}, and the absorption coefficient ratio of these two peaks was proven to be consistent for all C-centre bearing diamonds (Hainschwang et al., 2012b). This ratio is useful for the calculation of C-centre concentrations when the content of A-centres is extremely high so that it partially masks the 1344 cm^{-1} peak (Hainschwang et al., 2012b). The method for obtaining the absorption coefficients with respect to local baselines is shown in Fig. 2.2, using a synthetic Type Ib diamond as an example.

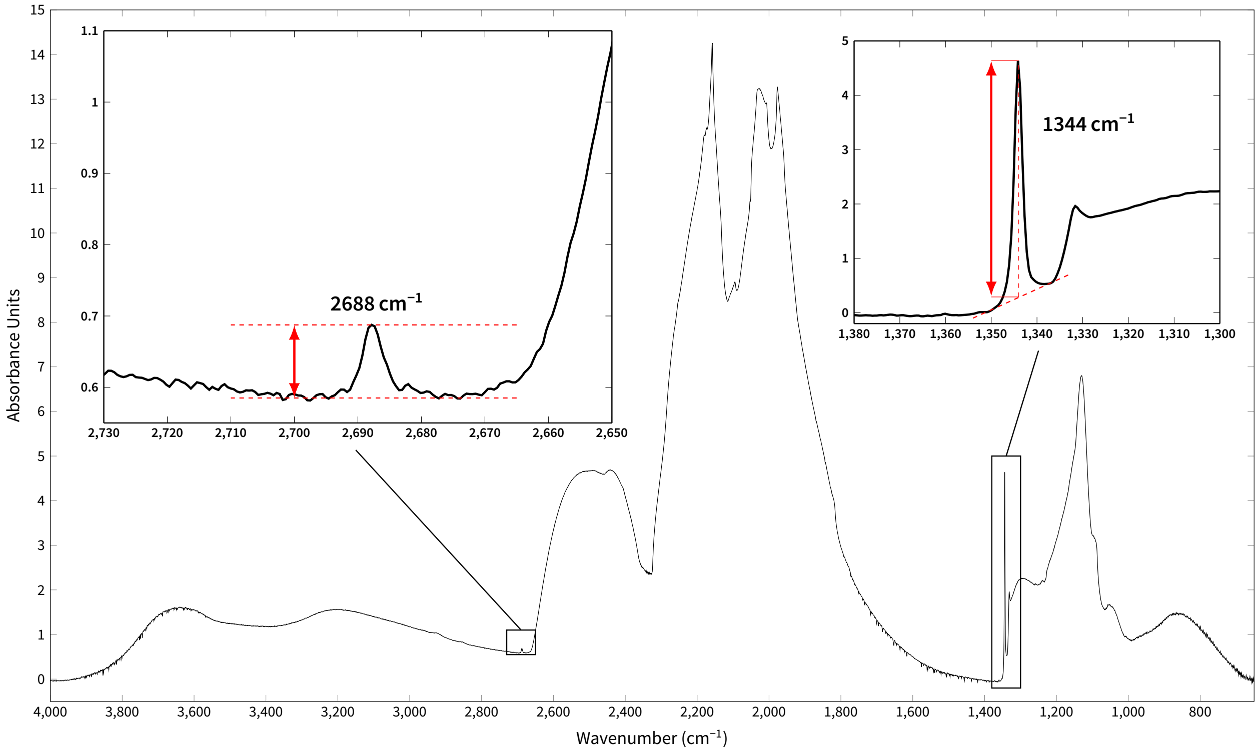

Figure 2.2: The IR absorption spectrum of a synthetic Type Ib diamond, to demonstrate the method for obtaining the absorption coefficients of the peaks at 1344 and 2688 cm^{-1}.

A graph was plotted to deduce the absorption coefficient ratio between these two peaks using 30 diamonds which consist of C-centres, including three synthetic Type Ib diamonds and 27 yellow diamonds from the Ekati mine and the Chidliak advanced exploration property. The deduced ratio was approximately 49, with a linear regression coefficient (R^2) of 0.998 (Fig. 2.3).

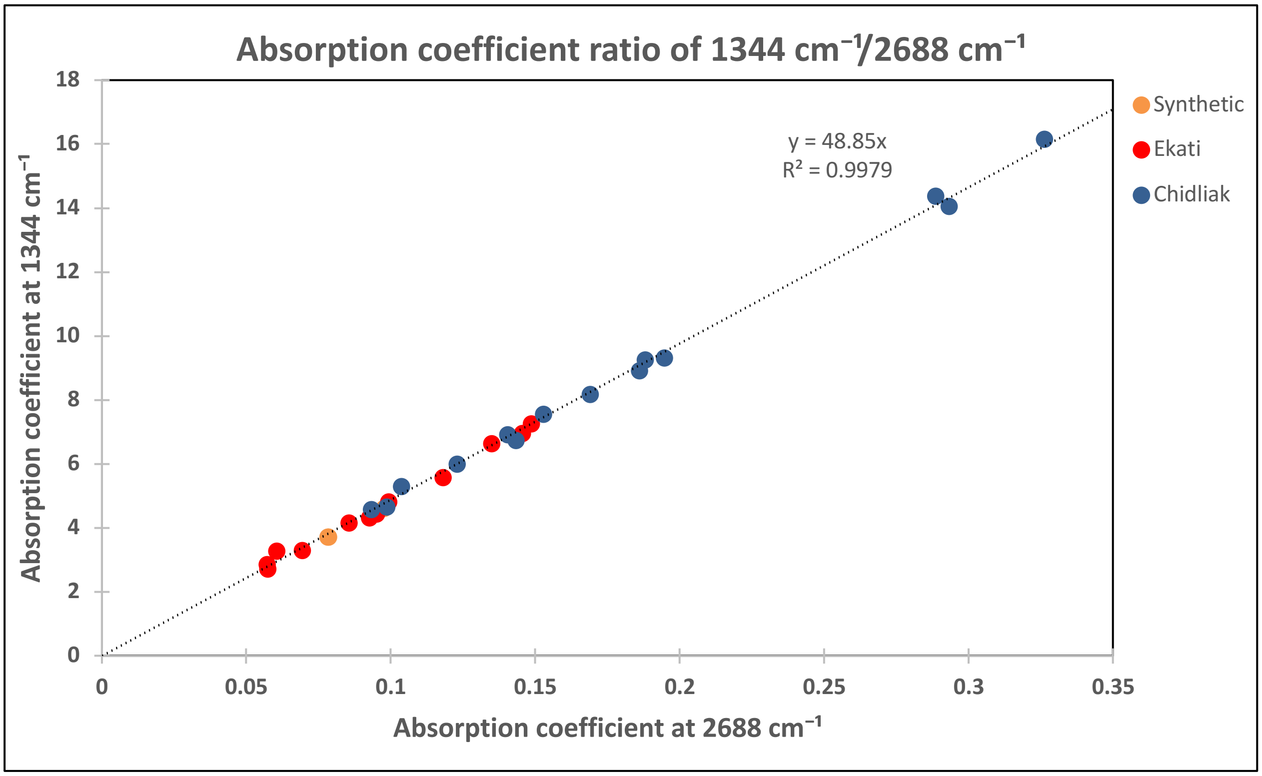

Figure 2.3: Plot of absorption coefficients at 1344 cm^{-1} and 2688 cm^{-1} to deduce the ratio between these two peaks.

In some circumstances, where the total concentration of nitrogen in diamonds was too high, the IR detector readings saturated, making the spectra impossible to be deconvoluted accurately. This phenomenon is common in diamonds with intense nitrogen absorptions (Taylor et al., 1990). Thus, in such cases diamonds were crushed and their fragments, with reduced optical path lengths, were re-measured.

2.2. Diamond fluorescence by UV light excitation

Fluorescence of diamond was observed using long wave ultraviolet (LWUV) light with a wavelength of 365 nm. Contaminant-free diamonds were placed under the binocular microscope, then the LWUV light was directed on the diamonds at an angle of about 45°. Fluorescent diamonds were viewed through a microscope in order to detect any non-uniform fluorescence distribution in the magnified images.

2.3. UV-VIS-NIR spectroscopy

Visible absorption spectra of diamonds were collected at the Gemological Institute of America (GIA) in Carlsbad, using an Ocean Optics HR 4000 CCD spectrometer with a spectral resolution of 1.4 nm. Diamonds were placed in an Avantes AvaSphere-30 integrating sphere, and were cooled to near liquid nitrogen temperature before and throughout the measurements. The integrating sphere was connected with the spectrometer and light source through Ocean Optics optical fibres with a diameter of 2 mm at the measurement port and illumination port, respectively. An Avantes AvaLight-HAL compact light source was utilized to provide a halogen light illumination (effective wavelength range: 400 – 2500 nm). The spectrum was collected in the spectral range of 400 – 700 nm, with an integration time of 990 ms for each scan, averaging the measurements over 50 scans.

2.4. CL imaging

Cathodoluminescence (CL) images of diamonds were obtained using a Zeiss EVO MA15 SEM equipped with a parabolic mirror coupling to a highly sensitive broadband photomultiplier tube (Robinson detector) and a Gatan ChromaCL system for grayscale images and colour images, respectively, in the Canadian Centre for Isotopic Microanalysis (CCIM) at the University of Alberta.

Prior to CL imaging, a selected subset of diamond fragments was embedded in three epoxy mounts, with smooth surfaces or fracture planes oriented parallel to the surfaces of the mounts, followed by grinding and polishing using metal-bonded diamond pads. The epoxy mounts were subsequently trimmed into smaller blocks and put in a new epoxy mount together with CCIM reference materials (vitreous carbon S0233A and diamond S0270 pressed into indium).

The mount was cleaned with alkaline lab soap and de-ionized water, then coated with 10 nm of Au to prevent the diamonds from charging during scanning electron microscope (SEM) operation. The SEM was operated at a voltage of 15 kV and a beam current of 3 – 5 nA to obtain both secondary electron and CL images (Stern et al., 2014).

2.5. SIMS analysis

After CL imaging was completed, an additional coating of 40 nm Au was applied on the epoxy mount. Then the mount was degassed under high vacuum for approximately 12 hours in the ion probe mount storage chamber, preceding SIMS analysis. The carbon isotope composition and nitrogen abundance of diamonds were then analysed sequentially using a Cameca IMS-1280 multicollector ion microprobe in the Canadian Centre for Isotopic Microanalysis (CCIM) at the University of Alberta (Stern et al., 2014).

The primary beam of $^{133}Cs^{+}$ ions was operated at an accelerating voltage of 10 kV and a beam current of 0.8 – 1.8 nA, in combination with the sample being held at a potential of 10 kV this induces an impact energy of 20 keV of $^{133}Cs^{+}$ ions bombarding the mount surface at an incidence angle of about 21° from the normal of mount surface. The primary beam diameter was approximately 12 µm. Prior to data acquisition, the primary ion beam was rastered in a 20 µm × 20 µm area for 30 – 60 s to clean the surface of Au on the mount and implant Cs.

Initially, the coordinates for measurement were set according to the CL images which show the internal growth structure of diamonds. Typically, 2 to 3 points were chosen at both the centre and rim to cover different areas of a diamond. In some diamonds that showed clear growth zoning, up to five points were set on different zones to detect any variations in carbon isotopic composition and nitrogen abundance, which may provide evidence of a diamond growing in temporally distinct events.

During the setting of points, the secondary electron images were viewed to ensure that the points were lying in the designated regions. The points were not set close to the boundary between epoxy and diamond as this may adversely affect the accuracy of the measurement results. Once the coordinates were chosen, each point was milled by the ion beam for about 2 s to ensure that the beam spot was at the desired position, before the coordinates were saved for measurement.

Throughout the analysis, the secondary ions ejected through the bombardment of the diamond surface with the primary ion beam were extracted through a potential of 10 kV to the grounded secondary column, which is the transfer section of the instrument.

2.5.1. Carbon isotopic composition analysis

For carbon isotopes, the collection of secondary ions occurred with an entrance slit width of 110 µm, a field aperture of 5 mm × 5 mm with a 100× field aperture-to-sample magnification, and a fully-open energy slit. Dual Faraday cups, L'2 using $10^{10}\,\Omega$ amplifier and FC2 with $10^{11}\,\Omega$, were utilized for analyzing both $^{12}C^{-}$ and $^{13}C^{-}$ concurrently, at mass resolutions of 2,000 and 2,900, respectively.

Mean count rates were determined over a 75 s counting interval; typically 1.0×10^9 counts/s for $^{12}C^-$ and 1.0×10^7 for $^{13}C^-$ were collected. Measurement time for each spot was 250 s.

The reference material, diamond S0270, was analyzed once every four measurements of unknowns to determine the instrumental mass fractionation, which is the ratio between the measured isotopic ratio and the true isotopic ratio of the sample. S0270 has a $\delta^{13}C$ value of -8.88 ± 0.10 ‰, and the standard deviation of IMF-corrected $\delta^{13}C$ for S0270 was 0.06 ‰ within one session (60 analyses).

The uncertainties of $\delta^{13}C$ analyses are typically ±0.14 ‰ (2σ) per spot, where the propagation of uncertainties includes within-spot, between-spot and between-session errors.

2.5.2. Nitrogen abundance analysis

Nitrogen abundance was measured on the same coordinates set previously for carbon isotopic composition analysis. The collection of secondary ions was performed with an entrance slit width of 40 µm, a field aperture of 3 mm × 3 mm with a 133× field aperture-to-sample magnification, and an energy slit width of 40 eV for the transmission of low-energy ions. A combination of Faraday cup and electron multiplier, L'2 using 10^{10} Ω amplifier and EM axial detector, were utilized for analyzing the molecular ions $[^{12}C^{13}C^-]$ and $[^{13}C^{14}N^-]$ concurrently, at mass resolutions of 6,000 and 5,500, respectively. This experimental condition is adequate to resolve any possible spectral interferences.

The count rate of the electron multiplier signals was corrected for background and deadtime. Electron multiplier background was measured when beam was off, which is typically less than 0.02 cps. The deadtime of the electron multiplier was measured utilizing the reference material, high-nitrogen vitreous carbon S0233A, and was 45.6 ns.

A reference material embedded on a separate epoxy mount, diamond S0280E, which has a nitrogen abundance of 1670 at. ppm with an uncertainty of ±5 ‰ (2σ), was used to determine the sensitivity factor for $[^{13}C^{14}N]^-/[^{12}C^{13}C]^-$. The same procedures as for $\delta^{13}C$ analysis were employed to analyze the $[^{13}C^{14}N]^-/[^{12}C^{13}C]^-$ ratios in unknowns and the reference material S0270. The propagation of uncertainties during the nitrogen abundance analysis includes within-spot error, between-spot error and between-session error. The nitrogen abundance of unknowns was calculated in at. ppm. Measurement time for each spot was 210 s.

3. A case study of yellow diamonds from the Chidliak property

3.1. Introduction

Diamonds in this study were recovered from the CH-7 kimberlite pipe on the Chidliak property – a recently discovered kimberlite field in northeastern Canada, located on the Hall Peninsula of southern Baffin Island. Since the discovery of the first kimberlite in 2008, the Chidliak property is now known to host 74 kimberlite pipes, of which 45 kimberlite pipes are confirmed to be diamondiferous (Fitzgerald et al., 2018). CH-7 is one of the kimberlites with the greatest economic value among all diamondiferous kimberlites in the project area. An assessment on a diamond parcel from the CH-6 kimberlite conducted by WWW International Diamond Consultants Ltd. in 2014 revealed the presence of a subset of smaller sized yellow diamonds (Nowicki et al., 2016), implying that fancy yellow diamonds possibly exist at the Chidliak property. A significant quantity of yellow diamond is also present in CH-7. For my thesis, these diamonds have been systematically analysed to understand the mantle conditions of their formation.

3.2. Geologic background

Previous U-Pb geochronological analyses revealed that the crystallization ages of zircons recovered from gneisses in southern Baffin Island range between 2.92 and 1.85 Ga (Scott, 1999), implying that there is an Archean cratonic basement underlying part of this region (Pell et al., 2013a). As the geology of southern Baffin Island was otherwise not well known, it was selected for diamond exploration by BHP Billiton and Peregrine Diamonds Ltd. in 2005 (Pell et al., 2013a).

The Chidliak kimberlite pipes discovered to date are all situated on the Hall Peninsula block (Pell et al., 2013a), which is located east of the Cumberland batholith and a belt of Paleoproterozoic Lake Harbour group metasedimentary rocks (Scott, 1999) (Fig. 3.1). While the origin of the Hall Peninsula block is not yet well defined, Pell et al. (2013a) summarized three hypotheses: that this area is (i) a portion of the North Atlantic – Nain craton (Scott et al., 2002); (ii) associated with the similar reworked Archean gneisses of the Nagssugtoqidian Orogen in west Greenland (Jackson et al., 1990) and the Trans-Hudson Orogen in Canada (St-Onge et al., 2007); or (iii) the result of a two-phase, three-way collision of the North Atlantic, Rae and Superior cratons at 1.87 to 1.79 Ga (Snyder, 2010). Additionally, From et al. (2014) suggested that the Hall Peninsula block may be (i) a unique and separate microcontinent, or (ii) could be correlated with the surrounding crustal blocks, clockwise from east to north – the Aasiaat domain of central west Greenland (Hollis et al., 2006), the Nain craton (Scott and Campbell, 1993), the Meta Incognita microcontinent (St-Onge et al., 2009) and the Rae craton (Hoffman, 1988).

The result of perovskite U-Pb geochronological analysis for 44 kimberlite bodies at Chidliak showed that they were emplaced between 157.0 and 139.1 Ma, spanning 17.9 Ma during the Jurassic period (Heaman et al., 2015). The mineralogy of the kimberlites (Pell et al., 2013a) and the Sr/Nd isotope composition of kimberlitic perovskites (Heaman et al., 2015) match with the characteristics of Group I kimberlite. Sampling of kimberlite indicator minerals was conducted alongside with diamond exploration. Clinopyroxene (Cr-diopside) was used for geothermobarometry (Nimis and Taylor, 2000) to determine the thermal state of the lithospheric mantle. Results showed that the geotherm underneath the Chidliak project area is colder than that of the Central Slave craton, entering the diamond stability field at around 850 °C, with an inflection at a depth of approximately 190 km (Fig. 3.2) (Pell et al., 2013b).

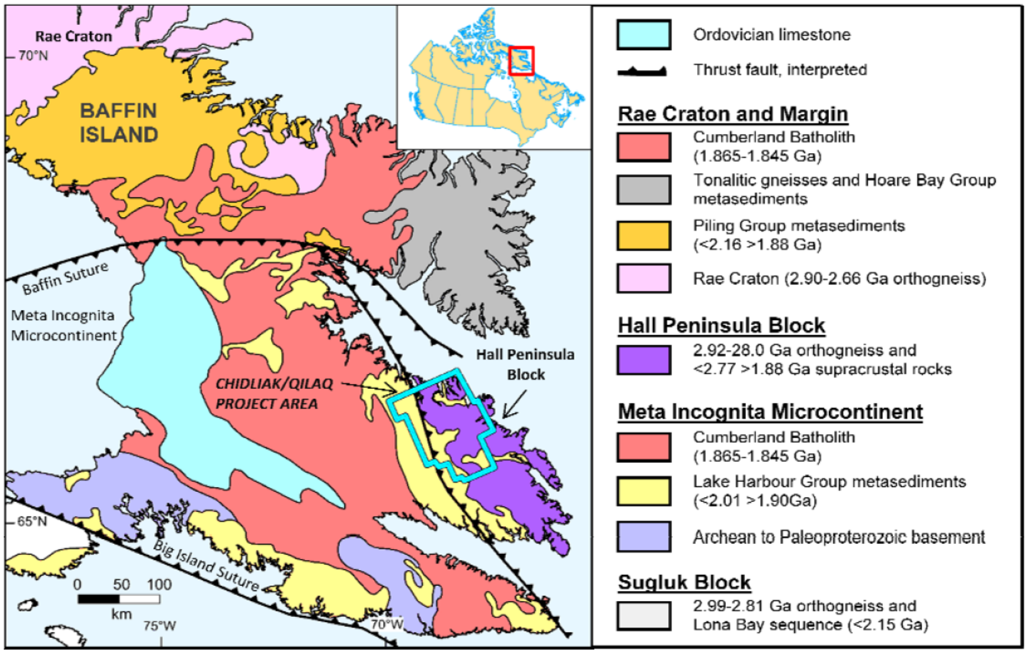

Figure 3.1: A geological map of southern Baffin Island indicating the location of the Chidliak property (taken from Pell et al. (2013a), Fig. 1; after St-Onge et al. (2006) and Whalen et al. (2010)).

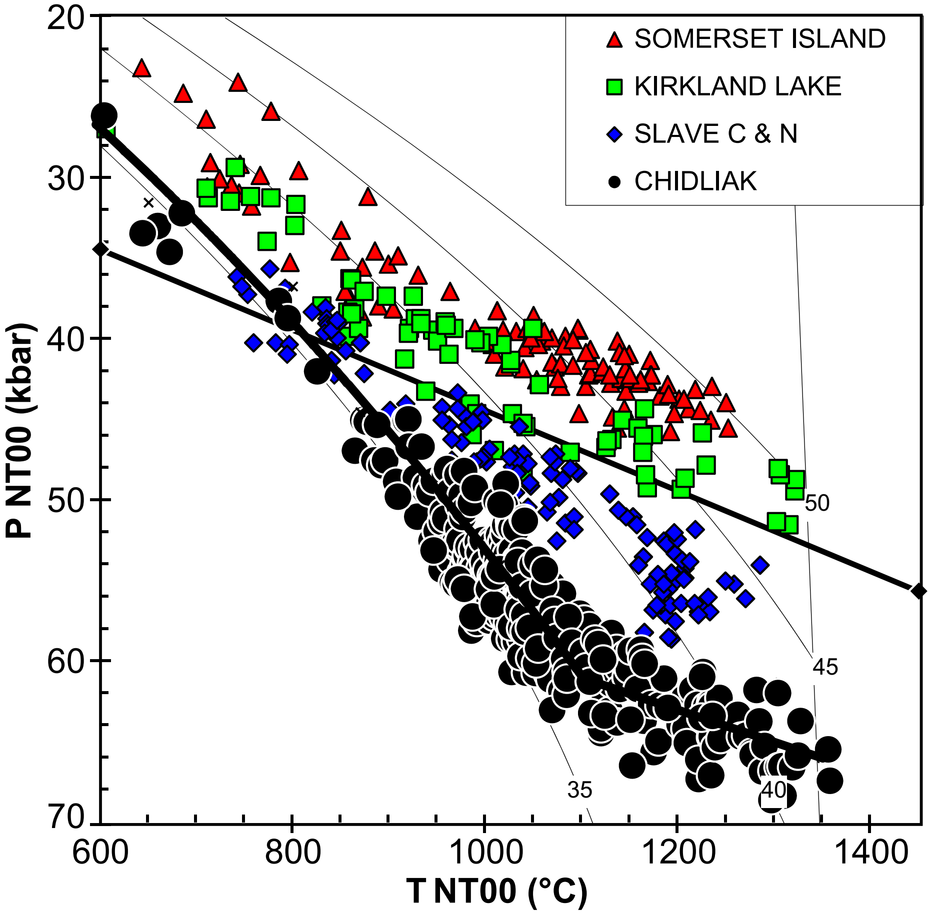

Figure 3.2: Results of Nimis and Taylor (2000) single-grain clinopyroxene geothermobarometry, demonstrating the geotherm underneath the Chidliak property compared to that of other Canadian localities (taken from Pell et al. (2013b), Fig. 2c; after Grütter (2009)).

3.3. Sample description

Diamond parcels containing a total of 2164 diamonds of size < 2 mm were received, from which 147 yellow diamonds were picked for research purposes, making up a proportion of 7 % (Fig. 3.3).

The yellow diamonds, weighing from 0.004 to 0.03 ct, display a wide range of shades, from pale yellow to deep brownish yellow. Pale yellow is the most abundant shade, with a proportion of 35 % among yellows, whereas greenish yellow and brownish yellow are the rarest among all, with proportions of 1 % and 2 % respectively (Fig. 3.4).

Morphology of the yellow diamonds is dominated by fragments (30 %), followed by irregular shapes (defined as diamonds which show less than 50 % of any recognized shape (Harris et al., 1975)) (29 %), and cuboids (24 %) (Fig. 3.5). It has been reported previously in Nowicki et al.

(2016) that a significant proportion of diamond breakage observed at the CH-7 kimberlite pipe was mainly related to the large-diameter RC drilling method during bulk sampling. Fragmentation of diamond can also occur during mantle residence or explosive kimberlite emplacement, often accompanied by resorption afterwards, rounding the edges of the breakage surface. The least common morphology in the sample set is cubo-octahedral (2 %), which is believed to be a consequence of the late stage formation of fibrous overgrowths on octahedral diamond. It was suggested that fibrous overgrowths result from the influx of fluids rich in CO_2 and H_2O into diamondiferous lithospheric mantle, with the fluids being associated with kimberlite magmatism (Boyd et al., 1992). The rugged appearance of fibrous coats is due to rough columnar fibrous growth happening rapidly in diamond forming fluids at high carbon supersaturation (Sunagawa, 1984; Sunagawa, 1990). During the formation of fibrous coats, microscopic inclusions can be trapped within the fibres (Boyd et al., 1992), leading to reduced transparency or sometimes opaqueness (Fig. 3.6). Details of samples are summarized in Table A.1 of Appendix A.

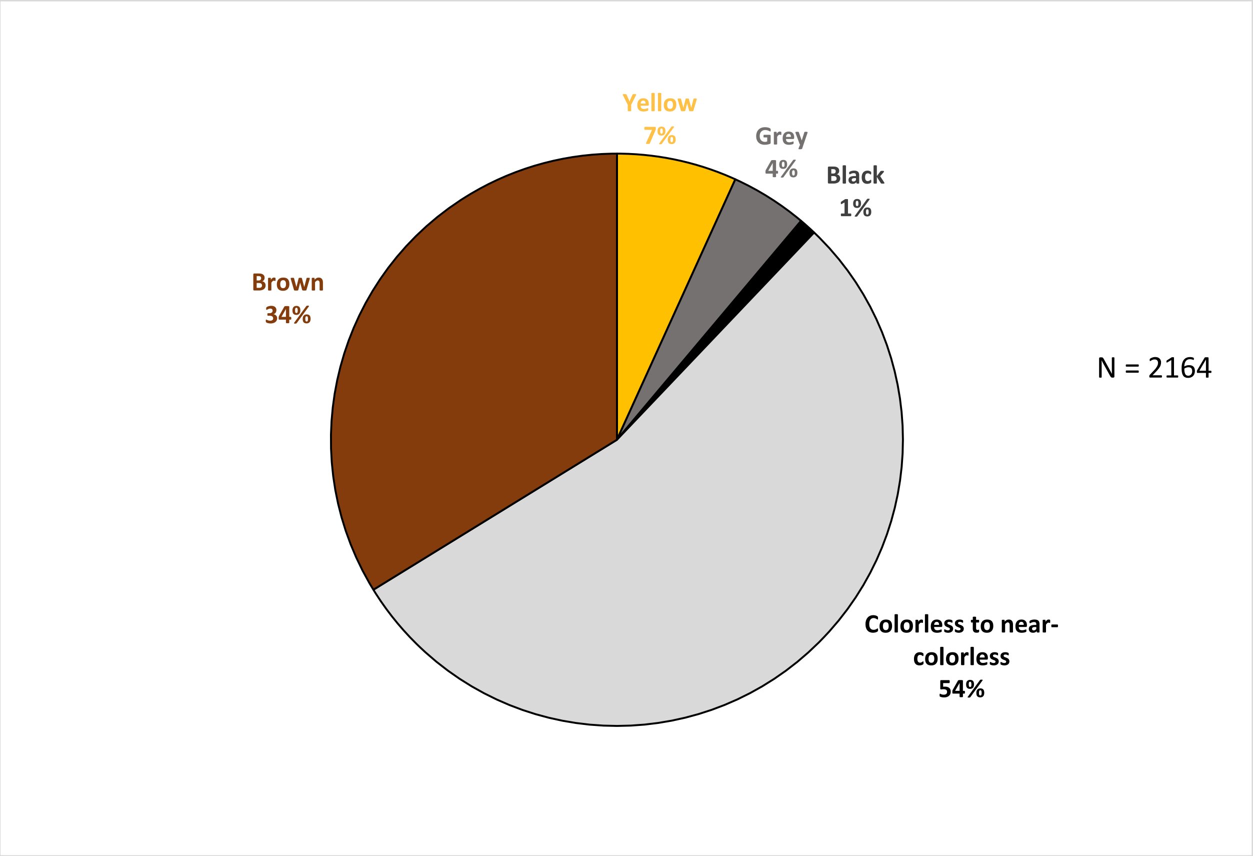

Figure 3.3: Colour distribution of 2164 diamonds recovered from the CH-7 kimberlite.

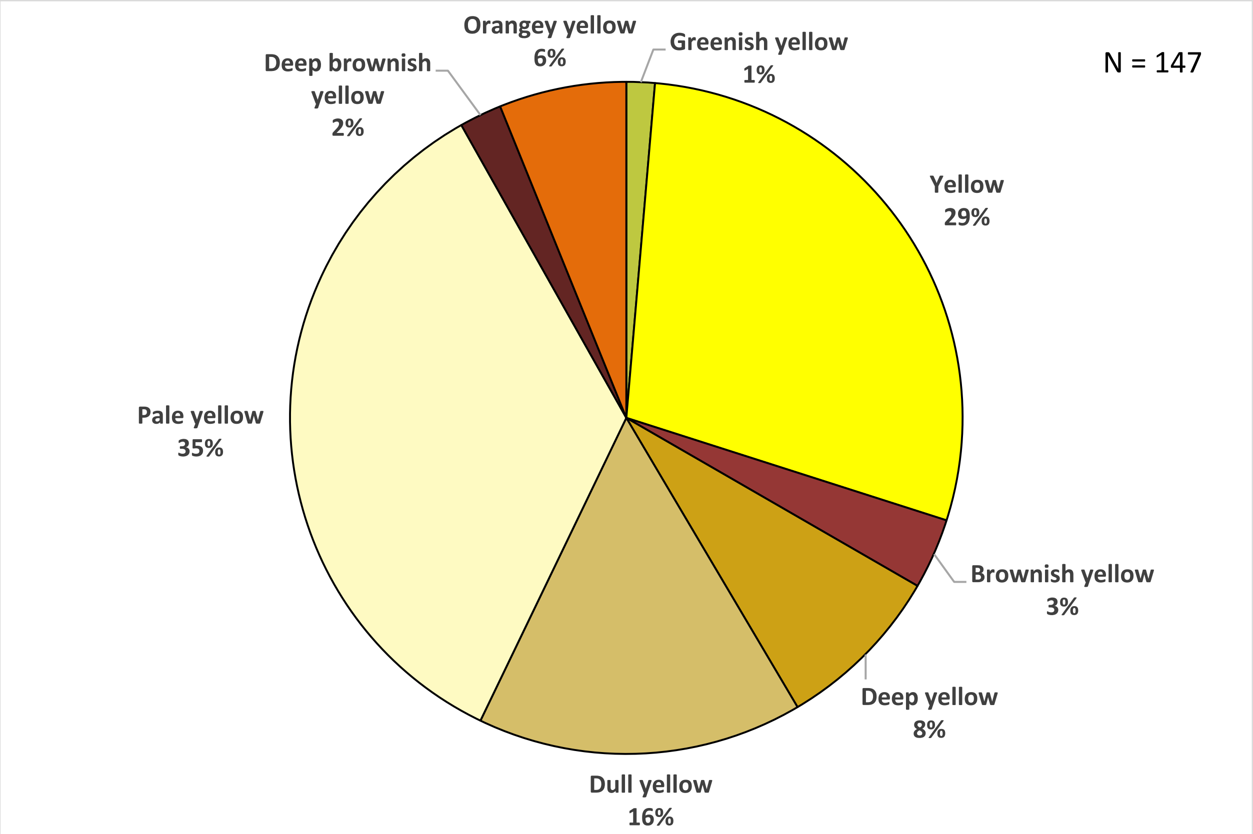

Figure 3.4: Relative proportion of a range of shades among the 147 yellow diamonds.

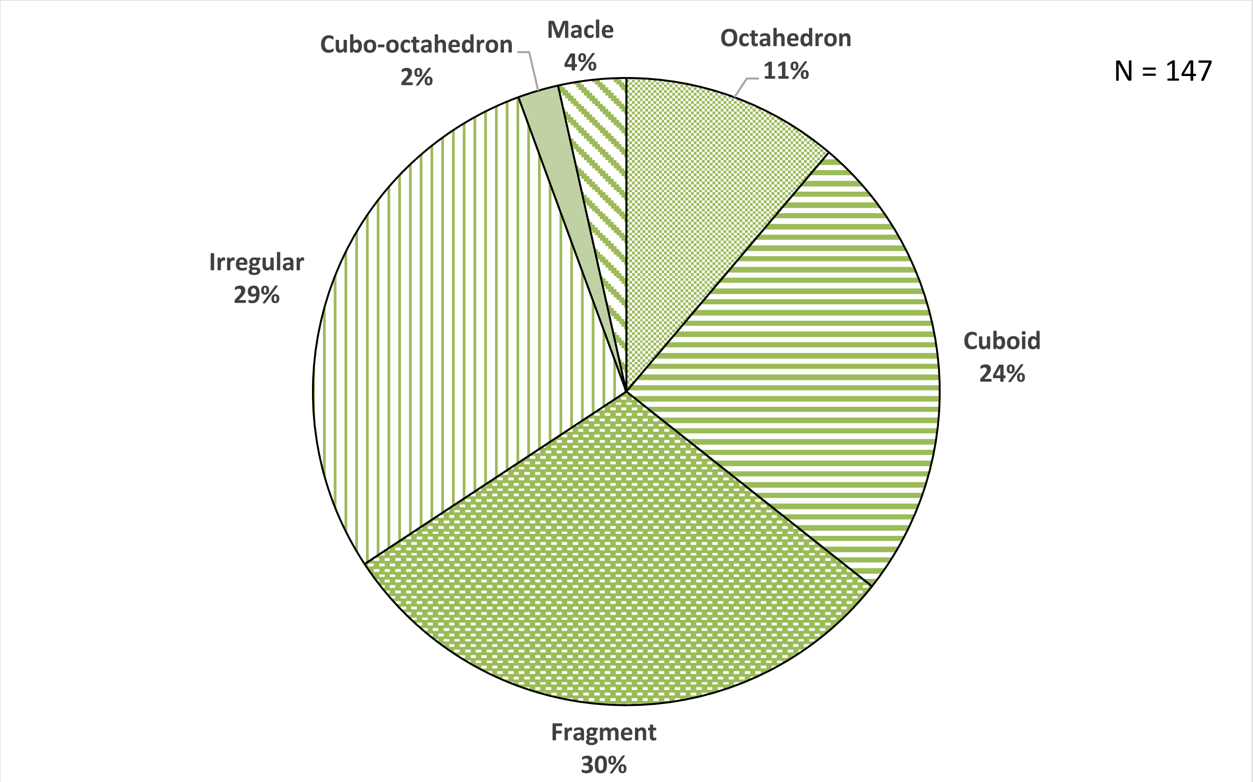

Figure 3.5: Relative proportion of various morphologies among the 147 yellow diamonds.

Figure 3.6: Three cubo-octahedral diamonds from the sample set. From left to right: CH7-S62, CH7-L45 and CH7-L64. CH7-S62 is an intergrowth composed of two cubo-octahedra. CH7-S62 and CH7-L64 still retain the transparency, whereas CH7-L45 (centre) has a cloudy appearance.

It is noticed that numerous yellow diamonds display strong birefringence when viewed between crossed polarizers, correlating to internal strain. Lang (1967) and Howell (2012) classified the causes of birefringence of diamond into five categories: (i) lattice dislocations formed during diamond crystallization; (ii) lattice parameter variations due to unevenly distributed lattice impurities; (iii) radial stress fields within diamond due to expanded inclusions; (iv) internal fractures or external propagated cracks from surface damage; (v) glide planes in the lattice created by plastic deformation. The birefringence is especially obvious when it is surrounding cracks or inclusions in diamonds (Fig. 3.7). These cracks can occasionally lead to thin-film interference and exhibit bright rainbow-like patterns when viewed from certain angles (Koivula et al., 1989).

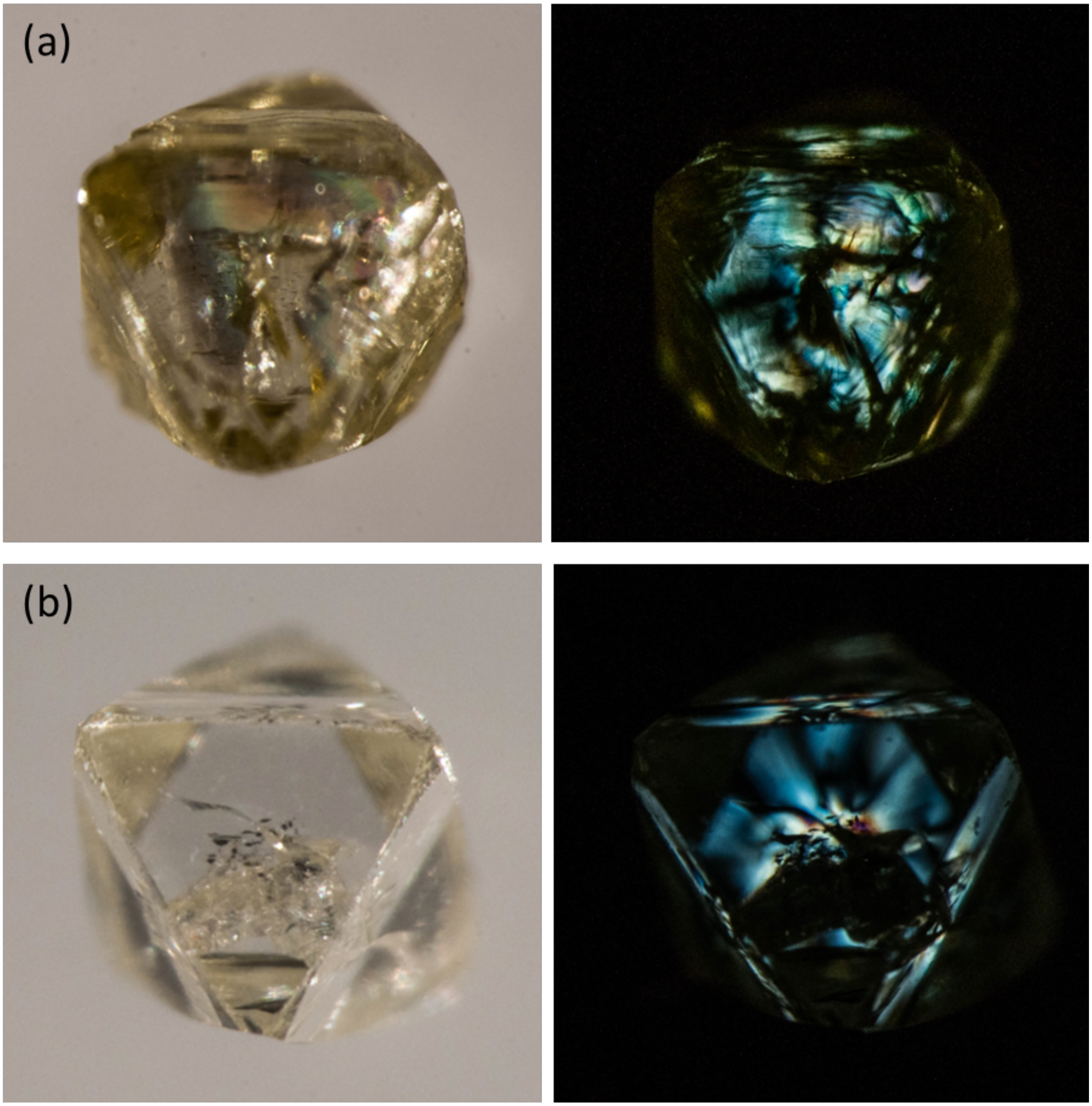

Figure 3.7: CH7-L35 and CH7-L90 displayed strong birefringence correlated to (a) cracks and (b) inclusions, respectively. The cracks in CH7-L35 act as thin films and exhibit rainbow-like interference patterns (top left).

3.4. Results

3.4.1. FTIR spectroscopy

CH-7 yellow diamonds exhibit a broad range of nitrogen concentrations, spanning from 14 to 3782 at. ppm, with a median value of 1228 at. ppm. The vast majority of diamonds (99 diamonds, equating to 67 %) possess nitrogen concentrations over 1000 at. ppm, while 25 diamonds possess very low nitrogen contents (< 200 at. ppm).

None of the yellow diamonds in this sample set belong to pure Type Ib. Instead, 71 diamonds are dominated by A-centres while also exhibiting a discernible C-centre peak at 1344 cm^{-1}, constituting a proportion of 48 %, which is classified as mixed Type Ib/IaA in the rest of the text. The A-centre proportion in the whole sample set is high in general, with a median value of 87 %, where 99 out of 147 diamonds possess an A-centre proportion greater than or equal to 80 %.

Although C-centre absorption is typically linked to the saturated yellow colour of diamond referred to as "canary yellow" (Fritsch, 1998), mixed Type Ib/IaA diamonds in the sample set actually display a wide range of yellow colours (Fig. 3.8). Some of these colours can be confused with so-called "cape yellow" diamonds, with a paler yellow tone caused by N3 and N2 centres (Fritsch, 1998).

Figure 3.8: Mixed Type Ib/IaA diamonds display a wide range of yellow colour. From left to right: CH7-S64 (pale yellow), CH7-S101 (dull yellow), CH7-L24 (yellow), CH7-L28 (orangey yellow), CH7-L67 (deep yellow), CH7-S1 (greenish yellow) and CH7-L10 (brownish yellow).

A number of subtle peaks are detected in all 71 mixed Type Ib/IaA diamonds, located at 1353, 1363 and 1374 cm^{-1} (1387 cm^{-1} is occasionally present) (Fig. 3.8). Aside from these diamonds, subtle peaks in this range are also detected in 23 diamonds which do not show noticeable C-centres.

The platelet peak, detected in 26 diamonds, is known to correlate positively in strength to the N3 and N2 centres (associated with the structure of three substitutional nitrogen atoms surrounding a vacancy), which are by-products formed during the process of nitrogen aggregation from A- to B-centre (Bursill and Glaisher, 1985). The platelet peak, also known as the B′-centre, is located in the range of 1358 to 1378 cm^{-1} (Sobolev et al., 1969). The proposed structure of platelets is a planar aggregation of carbon interstitials (Woods, 1986; Dobrinets et al., 2013). It was observed by Sobolev et al. (1969) and Speich et al. (2017) that the position of B′-centre shifts towards the higher wavenumbers when the size of the platelet decreases.

There are 16 diamonds which contain low nitrogen concentrations, ranging from 14 to 132 at. ppm. Of these, nine exhibit neither a C-centre peak nor a platelet peak, whereas the remaining seven diamonds exhibit very small concentrations of C-centres. Moreover, these nitrogen-poor diamonds usually have anomalous nitrogen absorption in the range of 1000 to 1400 cm^{-1}, which cannot be deconvoluted perfectly (Fig. 3.9). Therefore, these diamonds are not used in the calculation of mantle residence times, discussed in detail below.

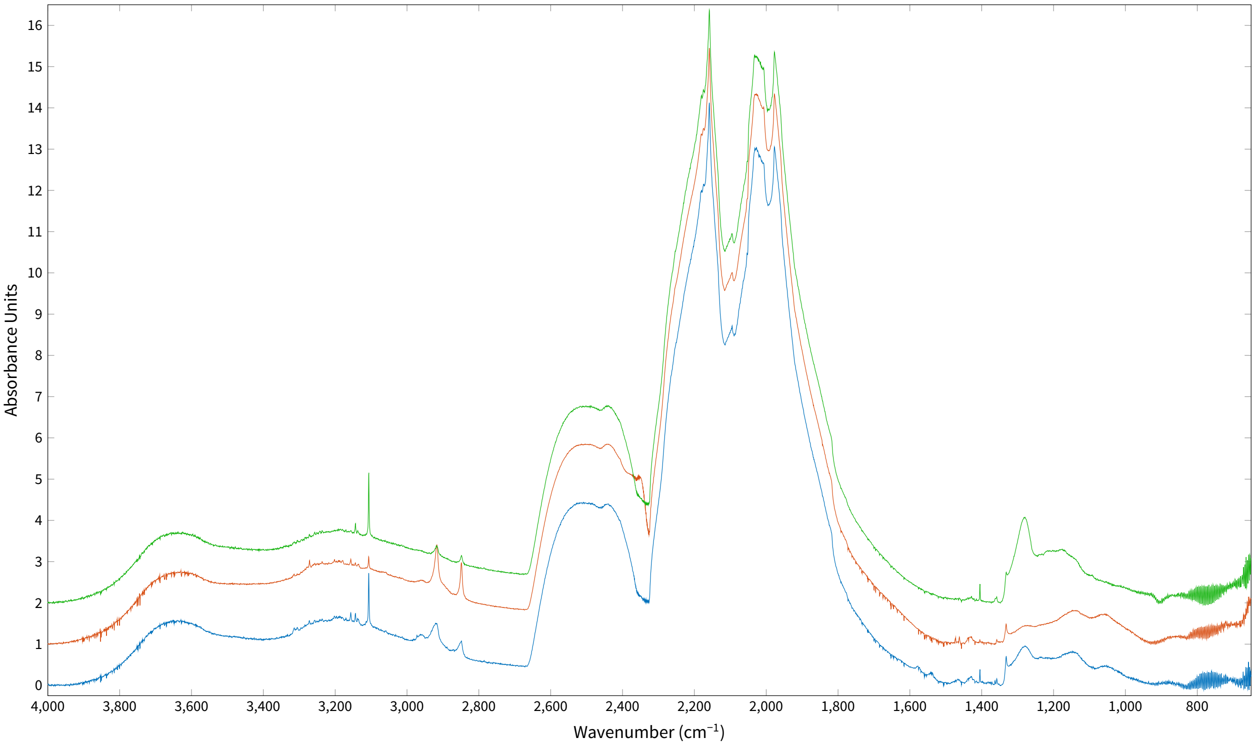

Figure 3.9: Examples of IR spectra collected from CH7-S98 (green), CH7-S99 (blue) and CH7-S100 (orange), exhibiting low nitrogen absorption and anomalous nitrogen absorption bands.

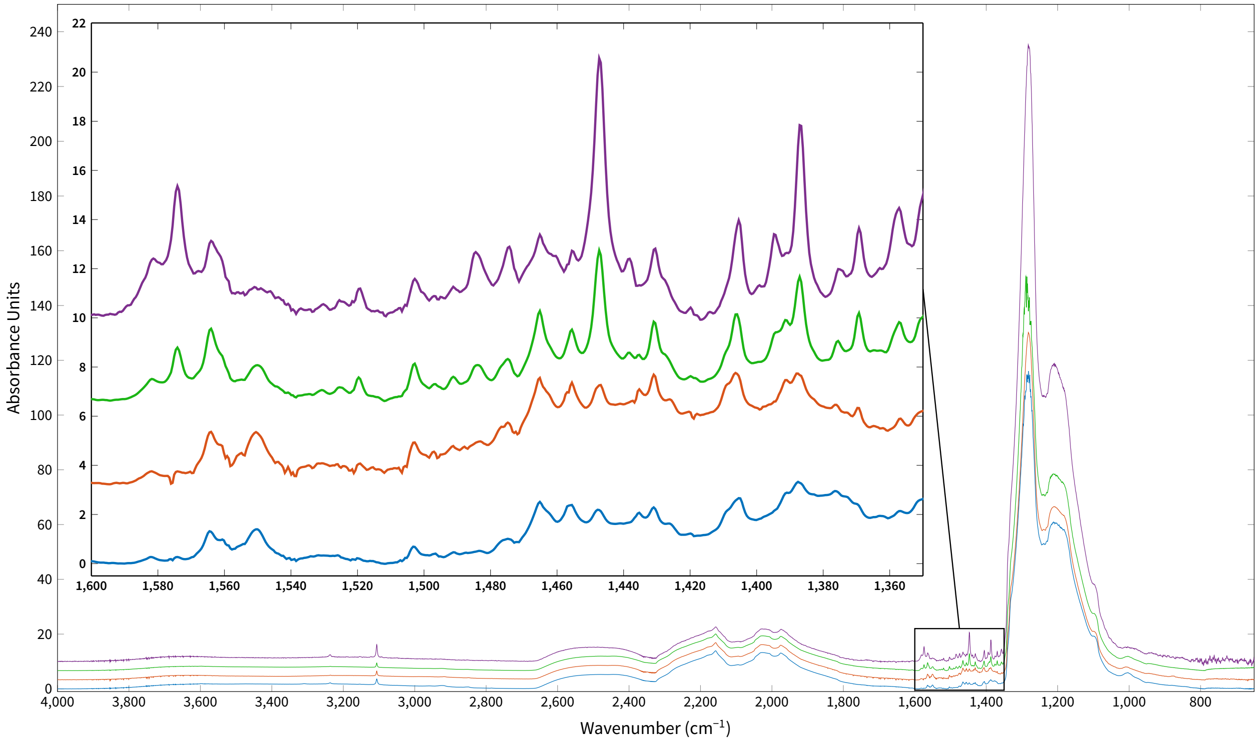

Figure 3.10: Examples of IR spectra collected from CH7-L35 (purple), CH7-L2 (green), CH7-S54 (orange) and CH7-L1 (blue), displaying high nitrogen absorption and numerous peaks in the range of 1350 to 1600 cm^{-1}.

Another set of 14 diamonds, for which their yellow colouration cannot undoubtedly be related to C-centres or platelets, exhibit very intense nitrogen absorption, ranging in concentration from 1568 to 3782 at. ppm. These diamonds display a number of peaks in the range of 1350 to 1600 cm^{-1} (Fig. 3.10), listed in Table 3.1. Here, the peaks frequently observed are categorized as “major” peaks, whereas other peaks which only appear occasionally are categorized as “minor” peaks.

Table 3.1: List of peaks in the range of 1350 to 1600 cm^{-1} observed in 14 diamonds.

	Peak position (cm^{-1})
Major peak	1581, 1574, 1564, 1503, 1474, 1465, 1455, 1447, 1431, 1387, 1375, 1357
Minor peak	1550, 1519, 1491, 1485, 1438, 1435, 1395, 1391, 1369

A dull yellow diamond (CH7-S55) with a grayish tint exhibits unusually intense hydrogen-related absorption at 3107 cm^{-1}, reaching an integrated absorption area of 175 cm^{-2}. This diamond is also nitrogen-rich, reaching a concentration of 2994 at. ppm. A set of absorption peaks is observed which accompanies the major hydrogen-related peak at 3107 cm^{-1} (Fig. 3.11). Table 3.2

lists the peaks observed in the range of 2750 to 3300 cm^{-1}, with most of them being summarized in Fritsch et al. (2007) as hydrogen-related absorptions.

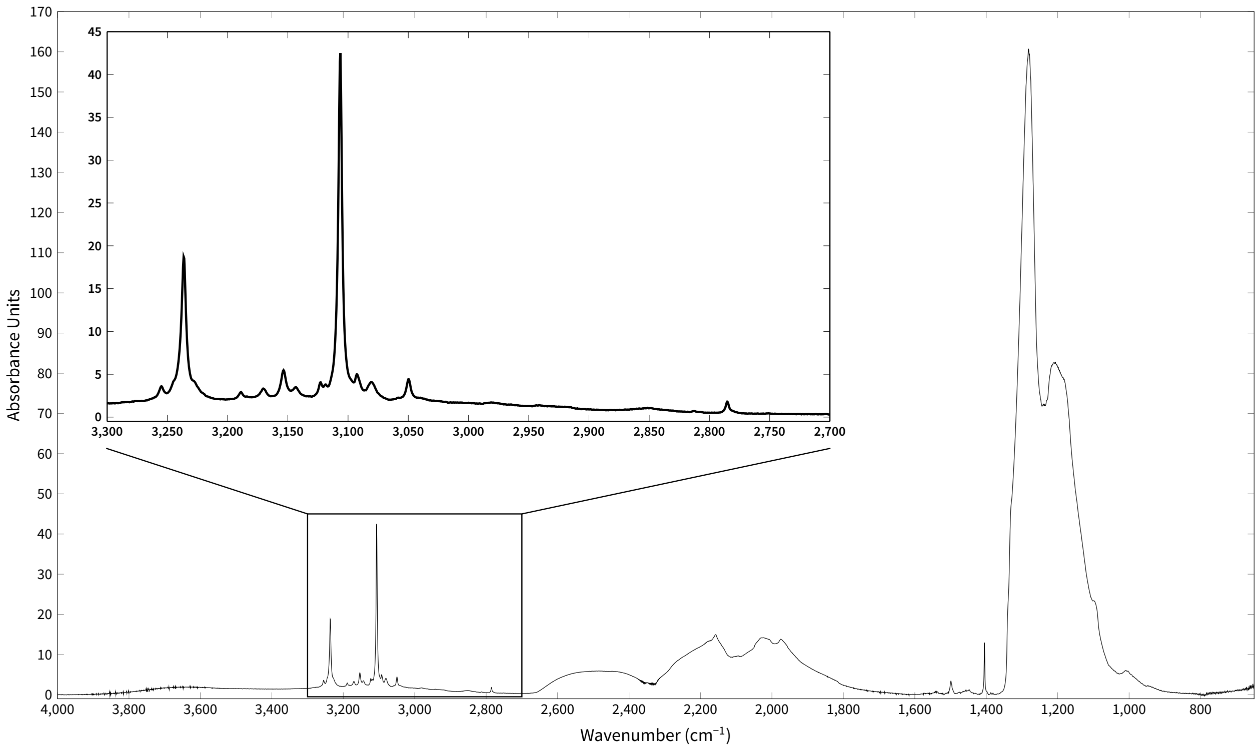

Figure 3.11: IR spectrum of the dull yellow diamond (CH7-S55) with grayish tint that shows high nitrogen content and a set of hydrogen-related peaks.

It was observed that the strength of 3107 cm^{-1} peak corresponds to that of the 1405 cm^{-1} peak, with the former being attributed to the stretching mode and the latter to the bending mode of C-H bond vibration (Woods and Collins, 1983). Plotting the baseline corrected peak area of the 1405 cm^{-1} peak against that of the 3107 cm^{-1} peak for 135 diamonds with discernible hydrogen-related absorption reveals a ratio of approximately 0.19 (Fig. 3.12).

Table 3.2: List of peaks in the range of 2750 to 3300 cm^{-1} observed in 14 diamonds.

Peak position (cm^{-1})	2785, 3050, 3081, 3093, 3107, 3119, 3123, 3143, 3154, 3170, 3189, 3236, 3255

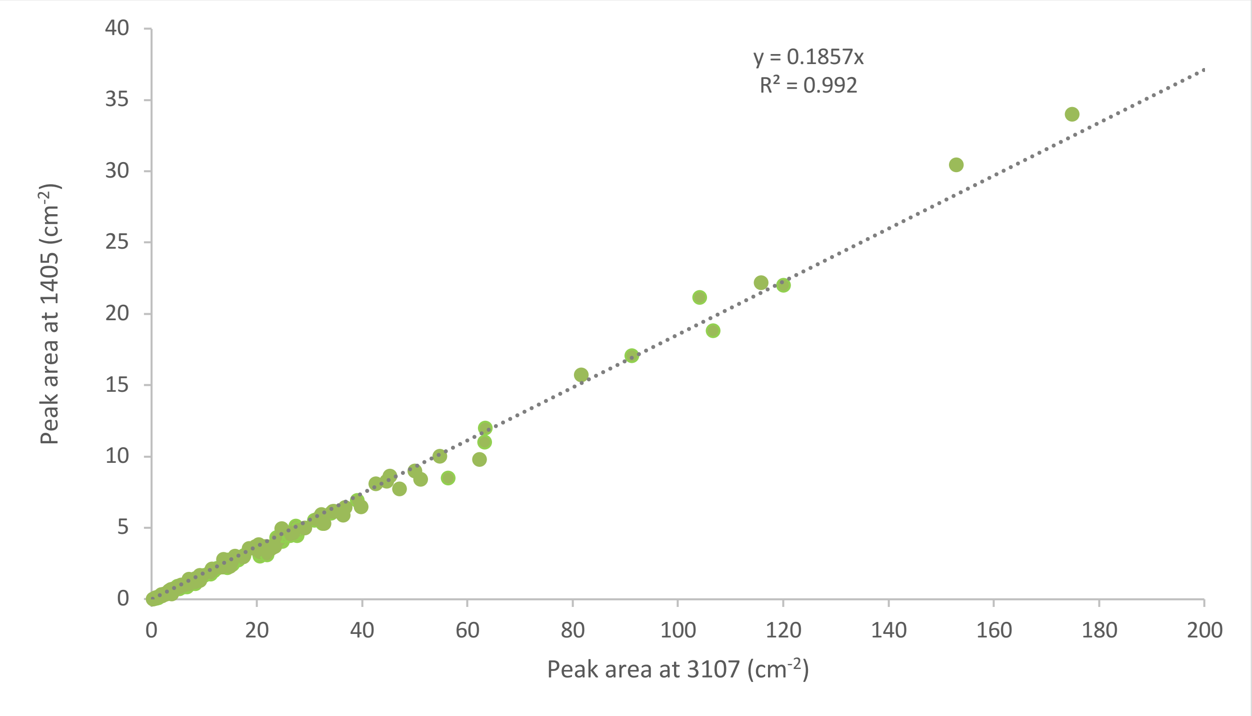

Figure 3.12: Plot of peak area of 1405 cm^{-1} against that of 3107 cm^{-1} for 135 diamonds.

Peaks corresponding to B′- and C-centres were found co-existing in some intact diamonds (Fig. 3.13). As the research progressed, however, a fragment of an octahedron was found to have a distinct yellow rim and a colourless core. As the colourless core was completely exposed, its IR absorption spectrum could be collected separately without any signal contributed by the yellow layer (Fig. 3.14). The B′-centre is found only in the colourless core, which is confirmed to be Type IaAB, with a total nitrogen concentration of 1471 at. ppm and a B-centre proportion of 22 %, while the yellow overgrowth is Type Ib/IaA, with a total nitrogen concentration of 258 at. ppm and a C-centre proportion of 22 %.

In total, 14 diamonds possess B′- and C-centres simultaneously. Within these 14 samples, 10 diamonds were crushed to reveal the colourless cores for separate IR absorption analysis (Fig. 3.15), while the remaining four diamonds could not be crushed due to their morphologies and sizes. Even though these four diamonds could not be broken to reveal the colourless cores, they were then polished for CL imaging and SIMS analysis to verify the existence of the combination of Type IaAB cores and Type Ib/IaA outer layers.

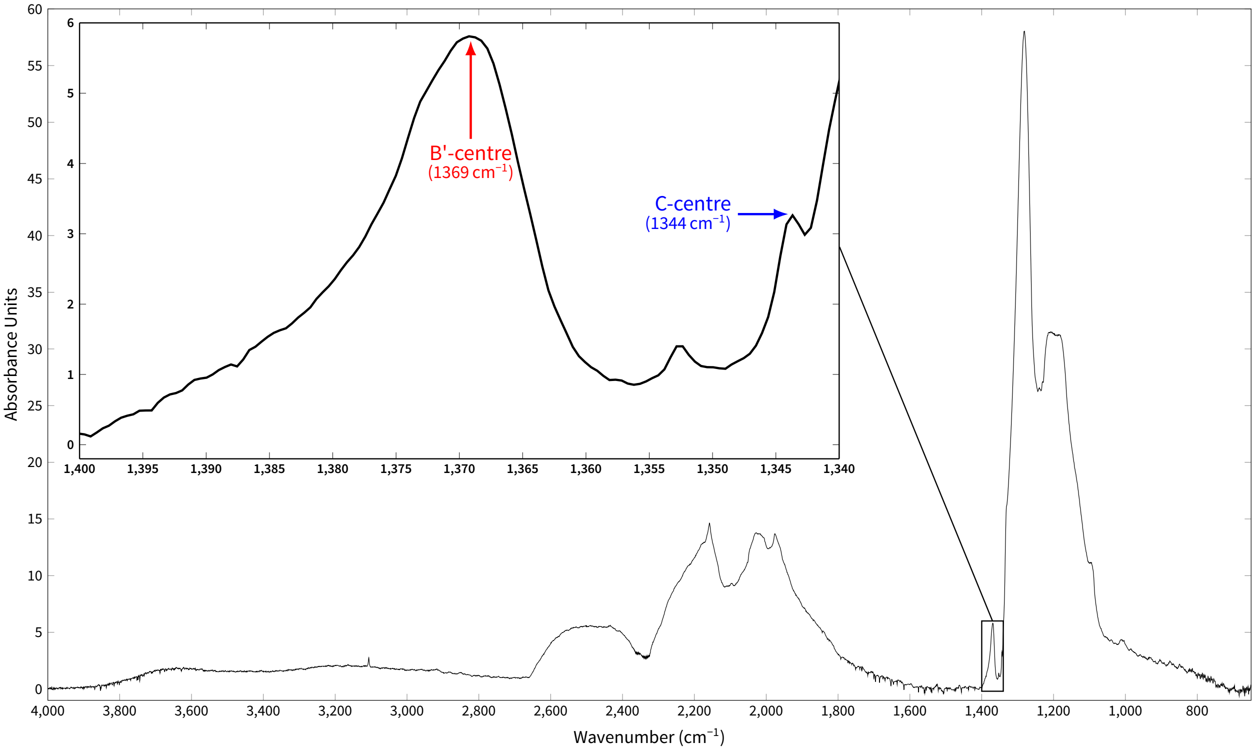

Figure 3.13: IR spectra of CH7-S13 which exhibited both B'- and C-centres.

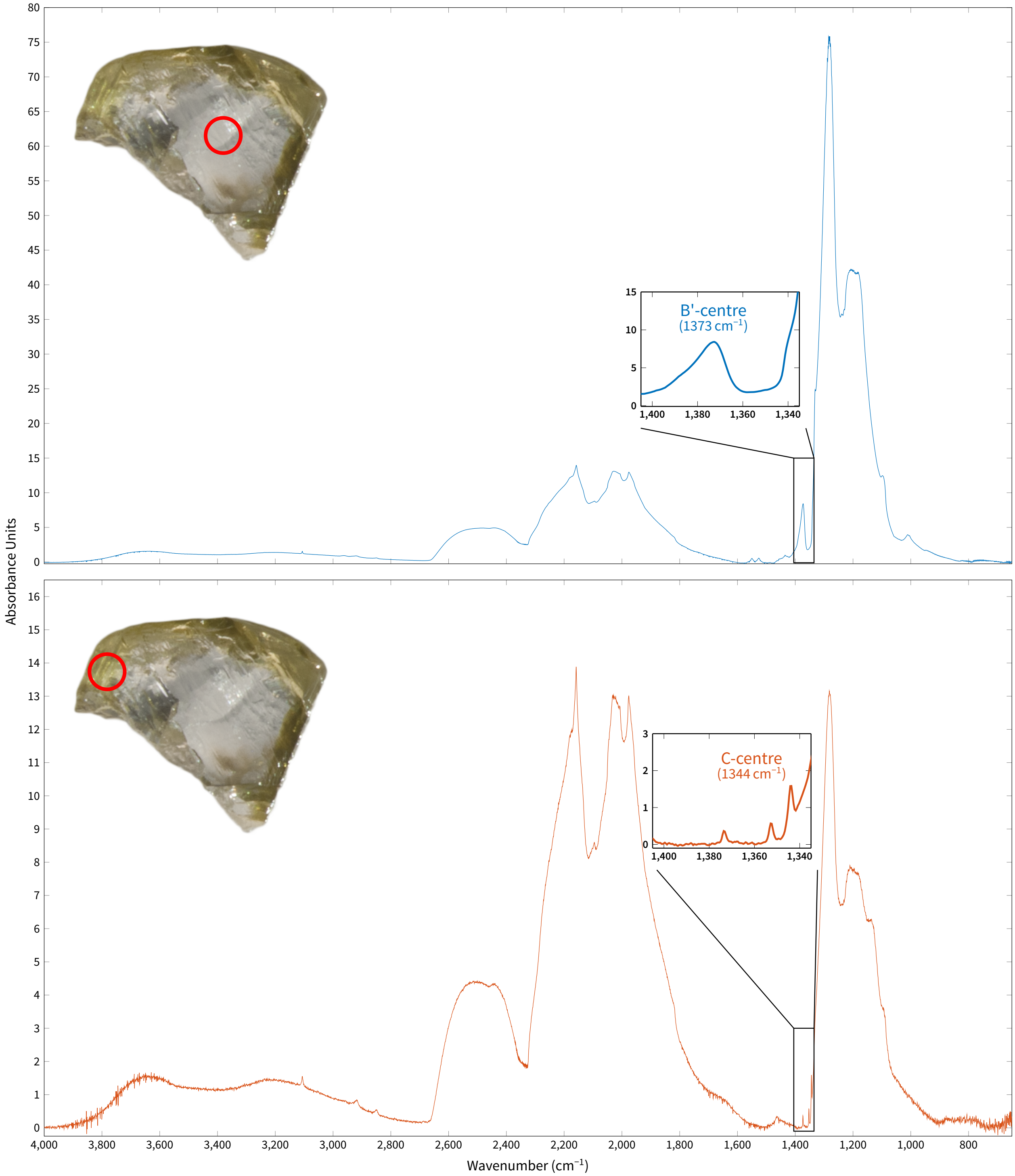

Figure 3.14: IR spectra of colourless core (top) and yellow rim (bottom) of CH7-L65. Red circles in the diagrams indicate the spots of measurement.

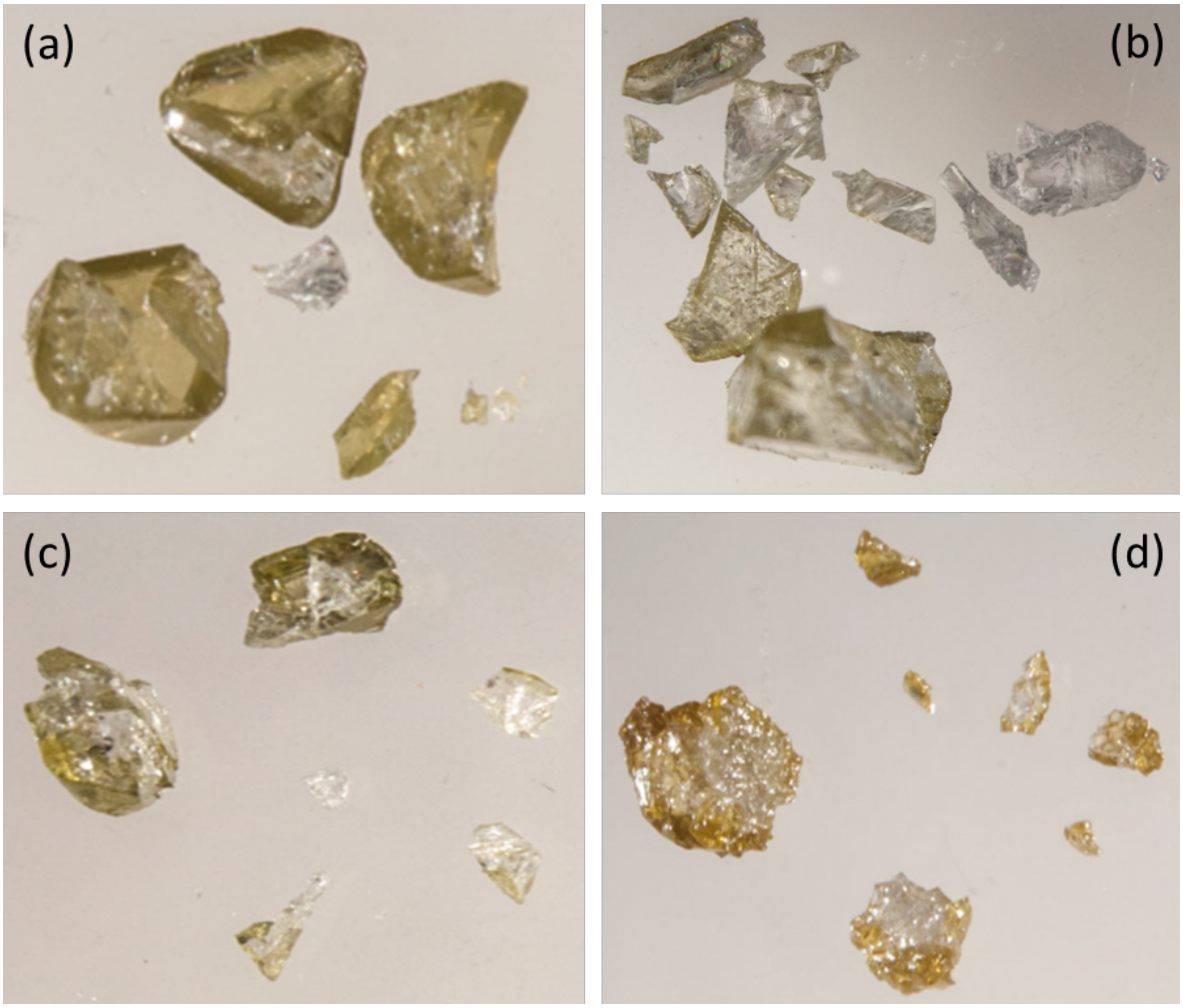

Figure 3.15: Examples of crushed diamonds revealing their colourless cores: (a) CH7-L3, (b) CH7-S13, (c) CH7-L31 and (d) CH7-L40.

3.4.2. Diamond fluorescence by UV light excitation

Forty-three diamonds show obvious fluorescence when excited by LWUV light with a wavelength of 365 nm, where none of which show phosphorescence. Diamonds fluoresce in four different colours in various intensities: 38 are yellow (Fig. 3.16), two are orange, two are green, and one is purple.

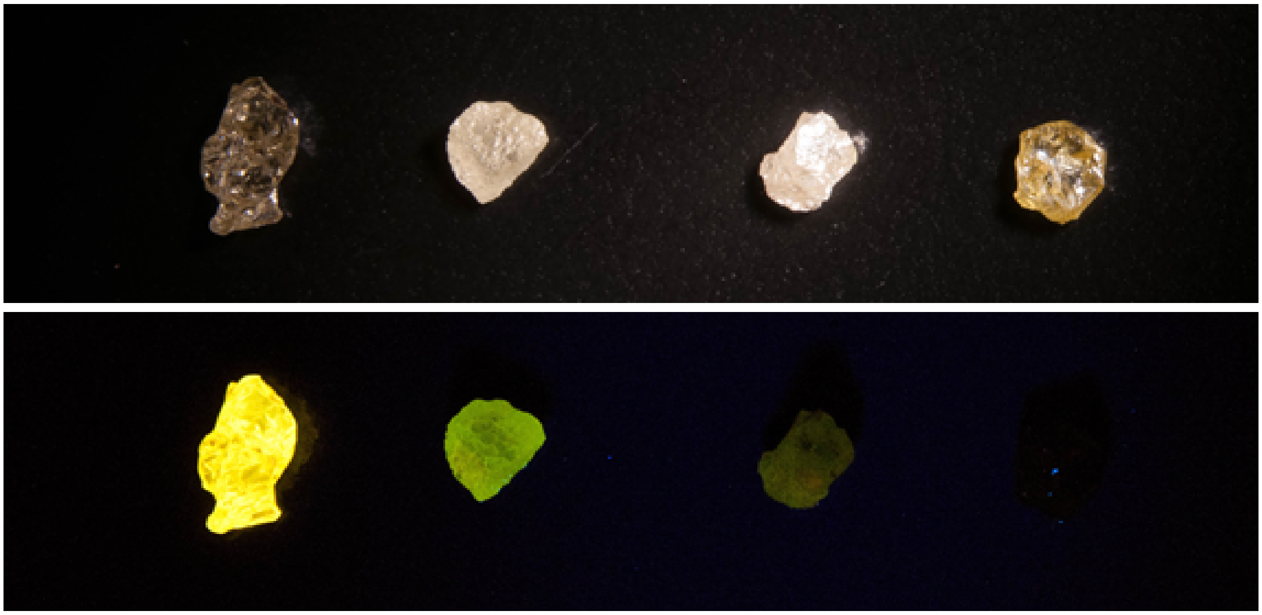

Figure 3.16: Examples of diamonds which exhibit fluorescence compared to a diamond which is inert, excited by LWUV: (Top row) Diamonds under white light illumination. (Bottom row) Diamonds under LWUV excitation. From left to right: CH7-S98 (strong yellow), CH7-S64 (medium greenish yellow), CH7-S70 (weak yellow) and CH7-S83 (inert).

3.4.3. UV-VIS-NIR spectroscopy

Visible absorption spectra of selected diamonds were collected. Mixed Type Ib/IaA diamonds generally display a steady rise of absorption from 700 to 550 nm, and then a steeper slope starting from 550 nm towards the blue end of the visible spectrum (Fig. 3.17 (a)). This absorption continuum is correlated to the C-centre. A reference visible absorption spectrum of a Type Ib yellow diamond is shown in Fig. 3.17 (b) for comparison (Shigley and Breeding, 2015).

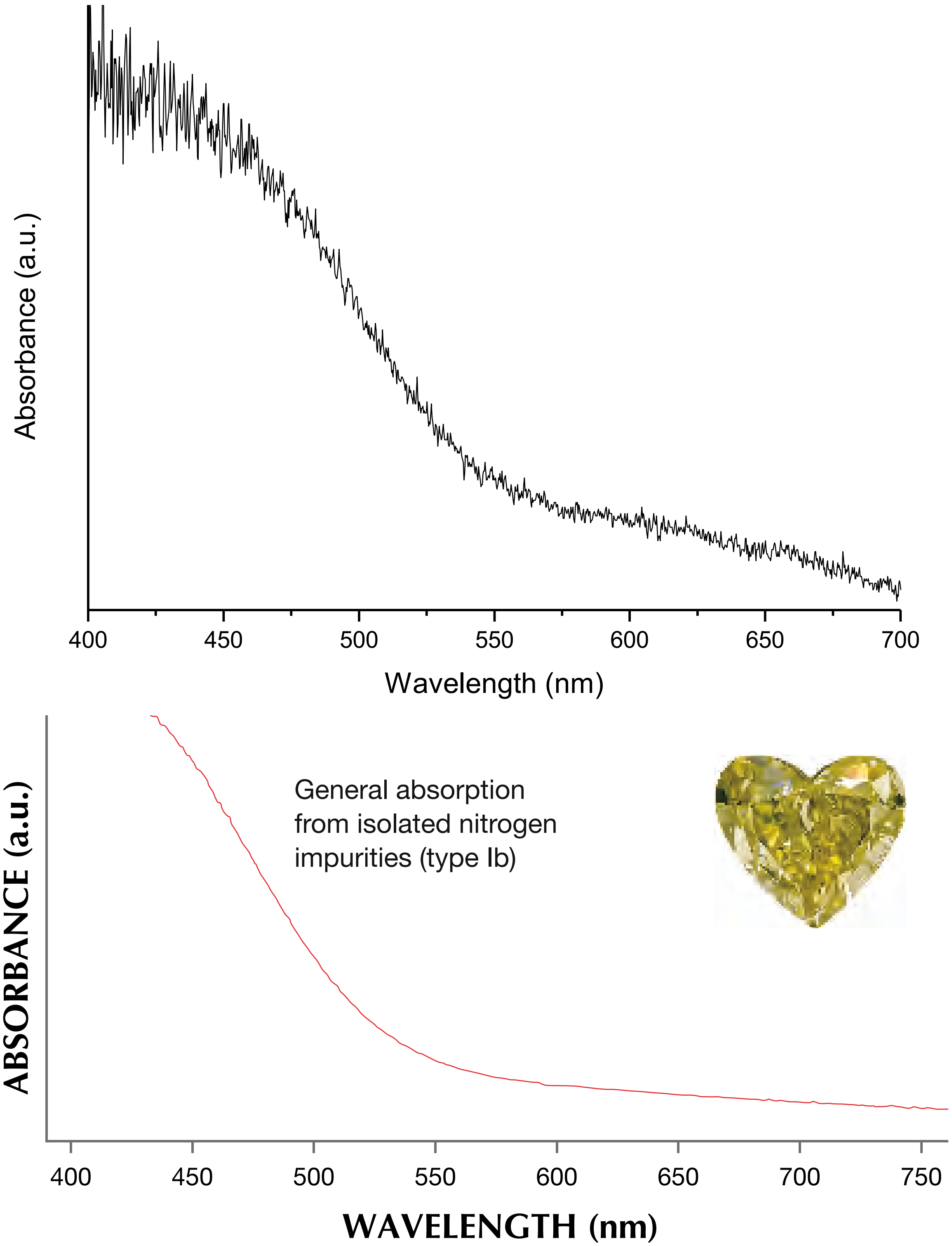

Figure 3.17: Examples of visible absorption spectra (absorbance in arbitrary units). (a) Diamond CH7-L31, which is a mixed Type Ib/IaA diamond, showing an absorption continuum towards the shorter wavelengths. (b) A Type Ib yellow diamond (taken from the chart by Shigley and Breeding (2015)).

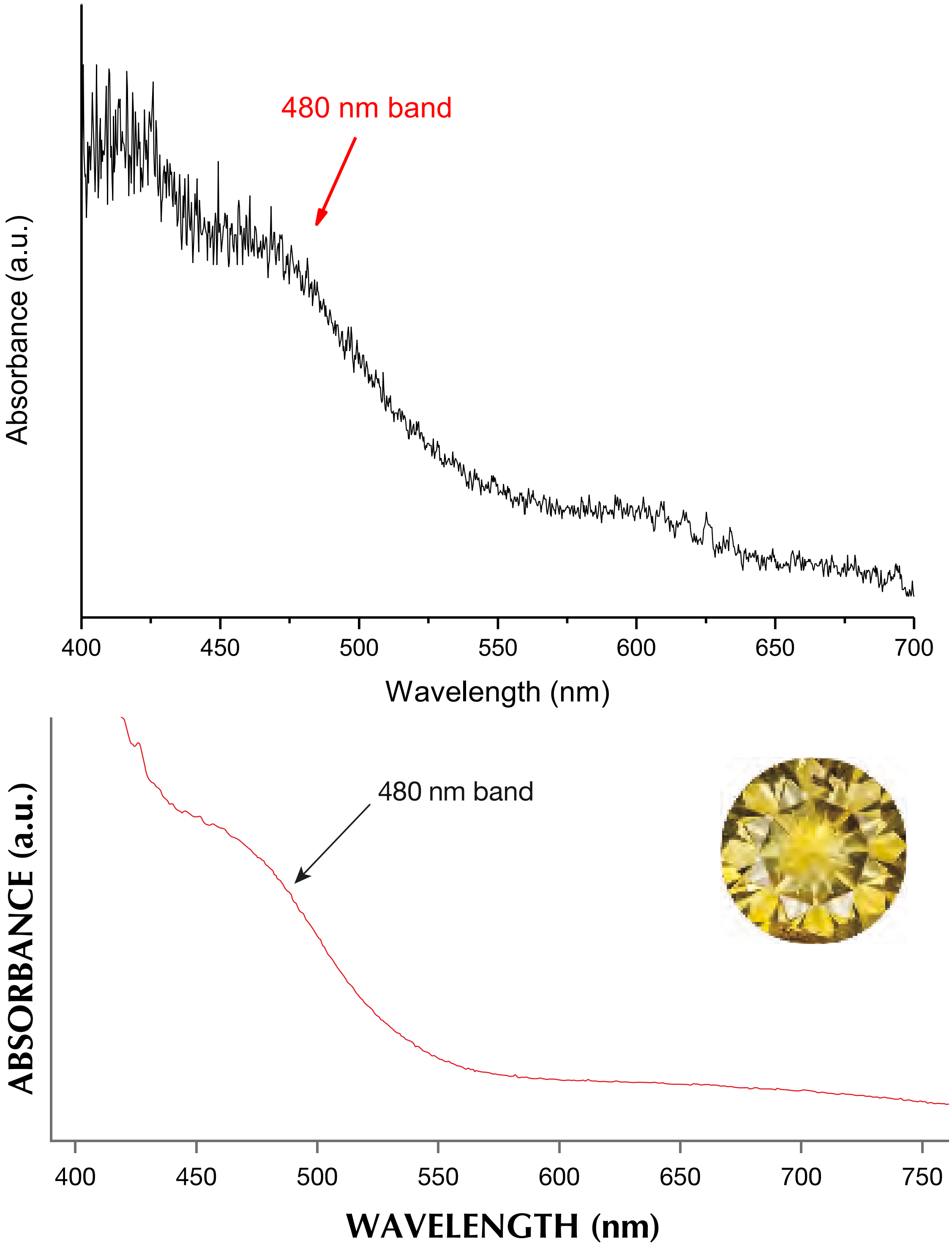

Figure 3.18: Examples of visible absorption spectra (absorbance in arbitrary units). (a) Nitrogen-poor diamond CH7-L75, which possesses C-centres and exhibits strong yellow fluorescence, showing the 480 nm band and a rising absorption towards shorter wavelengths. (b) A yellow diamond with the 480 nm band (taken from the chart by Shigley and Breeding (2015)).

The 480 nm band is observed in diamonds exhibiting intense yellow fluorescence (Fig. 3.18 (a)). These diamonds also show a rising absorption towards the shorter wavelengths. A reference visible absorption spectrum of a diamond with the 480 nm band is shown in Fig. 3.18 (b) for comparison (Shigley and Breeding, 2015).

Although the B′-centre is detected in some diamonds, none of the selected diamonds exhibit the N3 and N2 centres in their visible absorption spectra.

Diamonds which display a number of small peaks in the range of 1350 to 1600 cm^{-1} in their IR absorption spectra exhibit an analogous trend in the visible absorption spectra as the mixed Type Ib/IaA (Fig. 3.19).

Diamonds that exhibit a fairly regular group of peaks in the range of 1353 to 1387 cm^{-1} in IR absorption spectra, also display C-centre like absorption in the visible absorption spectra, with a gentler slope (Fig. 3.20).

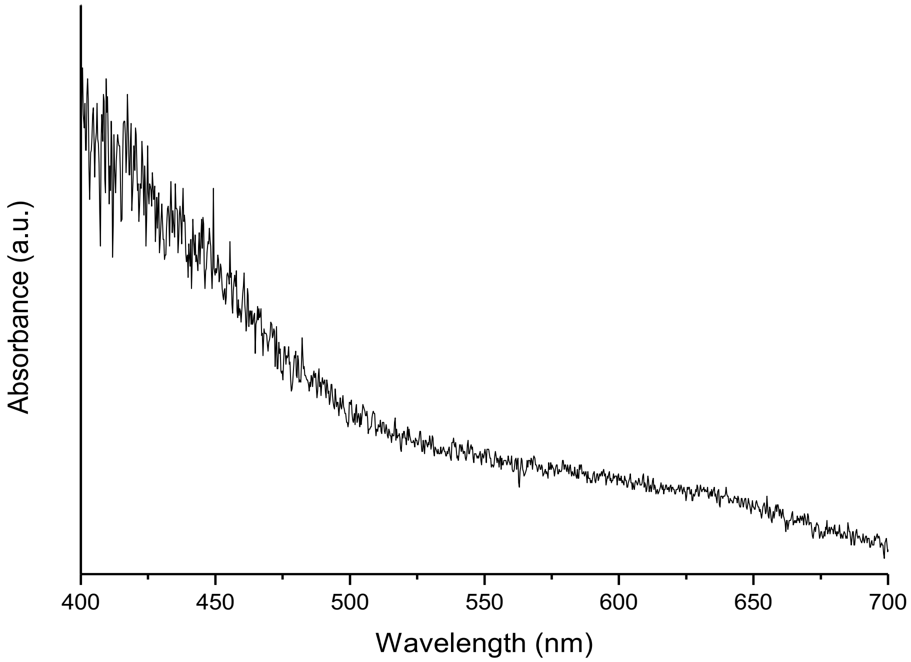

Figure 3.19: Visible absorption spectrum (absorbance in arbitrary units) of diamond CH7-L87, which displays a number of IR absorption peaks in the range of 1350 to 1600 cm^{-1}, showing an absorption continuum towards the shorter wavelengths, similar to the absorption feature related to C-centre.

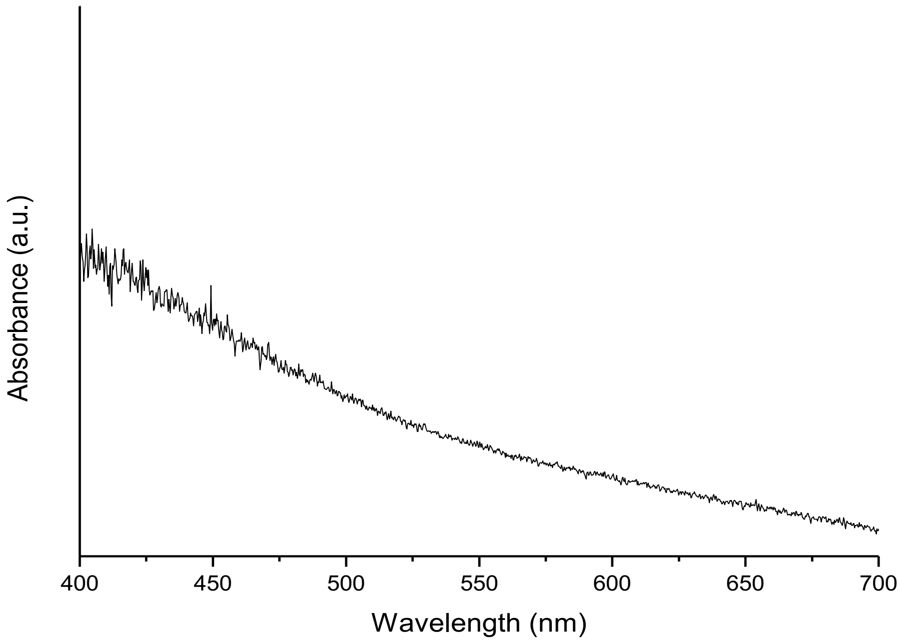

Figure 3.20: Visible absorption spectrum (absorbance in arbitrary units) of diamond CH7-S57, which exhibits IR absorption peaks in the range of 1353 to 1387 cm^{-1}*, showing a similar absorption trend as observed in C-centre bearing diamonds.*

3.4.4. CL imaging and SIMS analysis

According to the IR absorption spectral data, C-centres clearly exist in the vast majority of the CH-7 yellow diamonds. There are some diamonds where presence of C-centres could not be established using FTIR but seem to contain C-centres, based on their visible absorption spectra; however, further analysis was necessary to examine this discrepancy. Thus, selected diamonds were categorized into four groups according to their spectral properties, for CL imaging and SIMS analysis. In the following annotated CL images, the carbon isotopic ratio (δ^{13}C) is presented in the unit ‰ (per mil) and the nitrogen concentration in the unit at. ppm, stated above and below each spot, respectively.

3.4.4.1. Mixed Type Ib/IaA diamonds

Diamonds in this category show dark CL images where no significant growth zoning can be observed (Fig. 3.21). δ^{13}C values are homogeneous within individual diamonds. This diamond category shows a range of δ^{13}C values from –9.0 to –4.0 ‰.

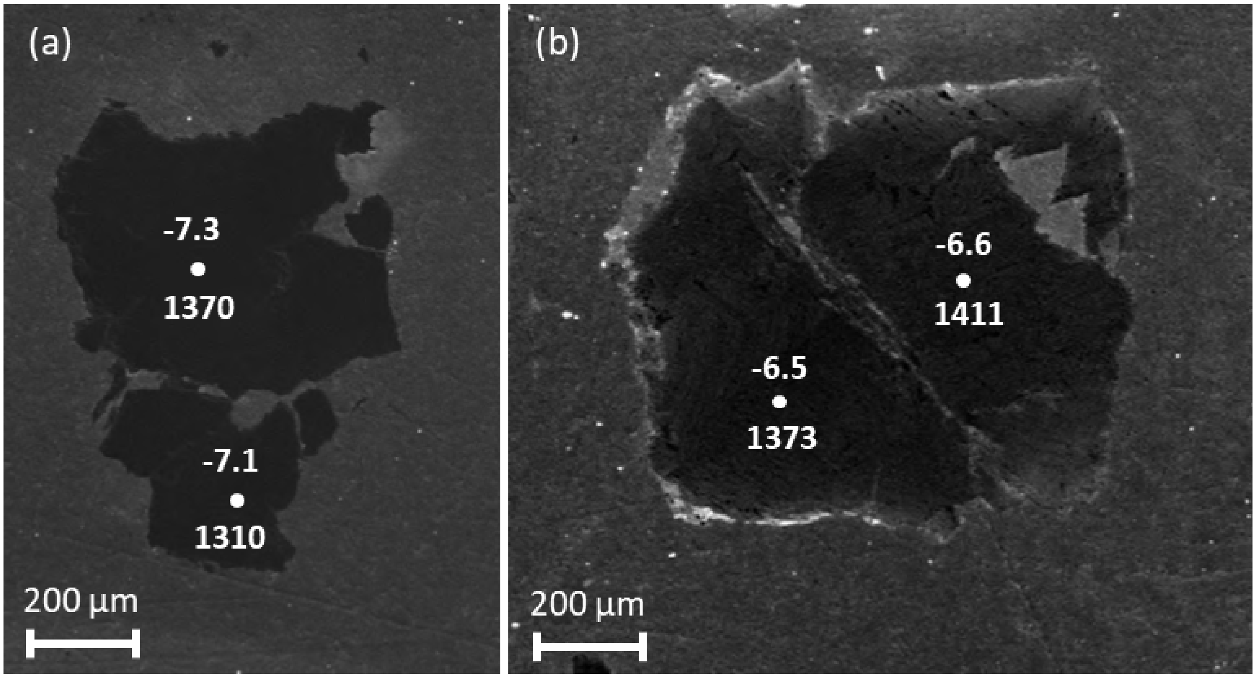

Figure 3.21: Examples of CL images of mixed Type Ib/IaA diamonds: (a) CH7-L43 and (b) CH7-S2.

3.4.4.2. Diamonds with IR absorption peaks in the range of 1350 to 1600 cm^{-1}

From their CL images, it is obvious that the diamonds are surrounded by a very thin dark rim, characterizing an additional growth layer on top of the originally formed diamond core (Fig. 3.22). Diamonds in this category show a range of δ^{13}C between –9.4 and –4.0 ‰.

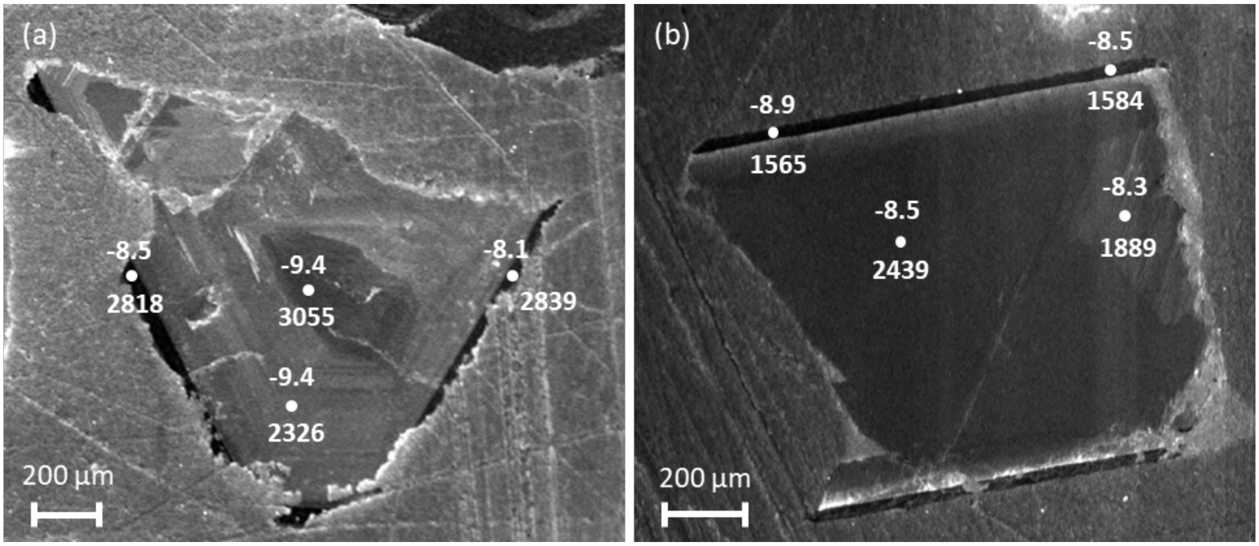

Figure 3.22: Examples of CL images of diamonds with peaks in the range of 1350 to 1600 cm^{-1}: (a) CH7-L1 and (b) CH7-S54.

3.4.4.3. Diamonds with low nitrogen content

Diamonds with low concentrations of nitrogen show irregular areas with bright CL response (Fig. 3.23). $\delta^{13}C$ in this category ranges from –14.5 to –3.6 ‰.

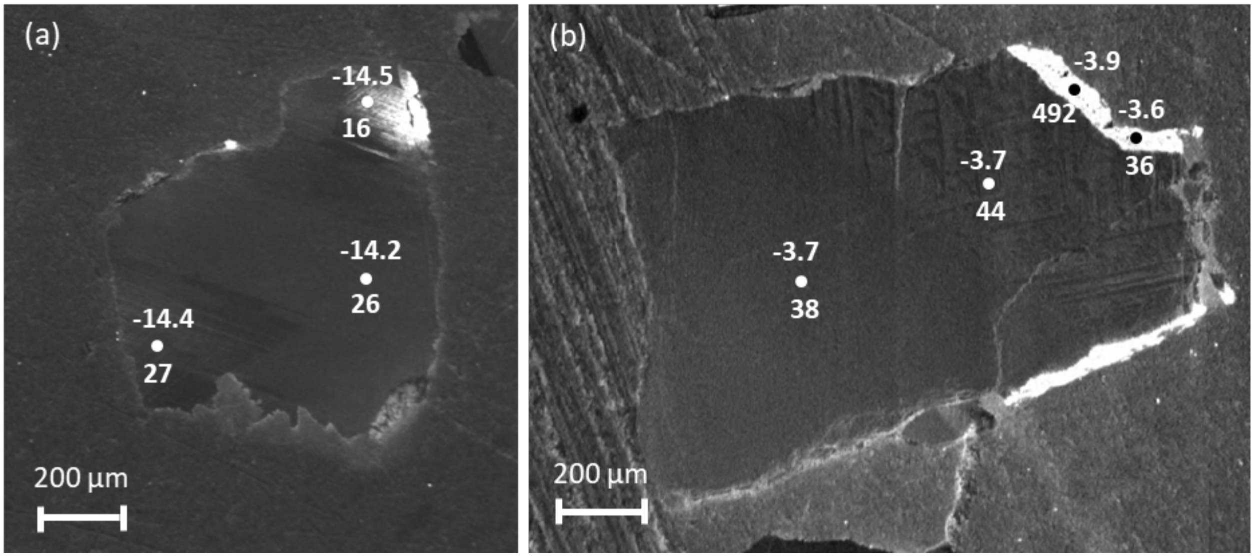

Figure 3.23: Examples of CL images of diamonds with low nitrogen content: (a) CH7-L39 and (b) CH7-S15.

3.4.4.4. Diamonds with co-existing B′- and C-centres

Diamonds in this category have similar internal growth structures to the ones in the second category mentioned above, but with thicker dark outer layers and brighter cores (Fig. 3.24 (a) and (b)). These bright cores emit blue luminescence in colour CL imaging (Fig. 3.24 (c) and (d)). A fibrous textured layer is also observed on top of the dark rim in some of these diamonds (Fig. 3.24 (b)), indicating late stage formation of fibrous overgrowths. The $\delta^{13}C$ signatures are distinct in the cores and rims, with the cores showing stronger ^{13}C depletion (ranging from −18.7 to −8.0 ‰) compared to the rims (ranging from –8.0 to –6.3 ‰). Overall, diamonds in this category display a range of $\delta^{13}C$ from –18.7 to –6.3 ‰.

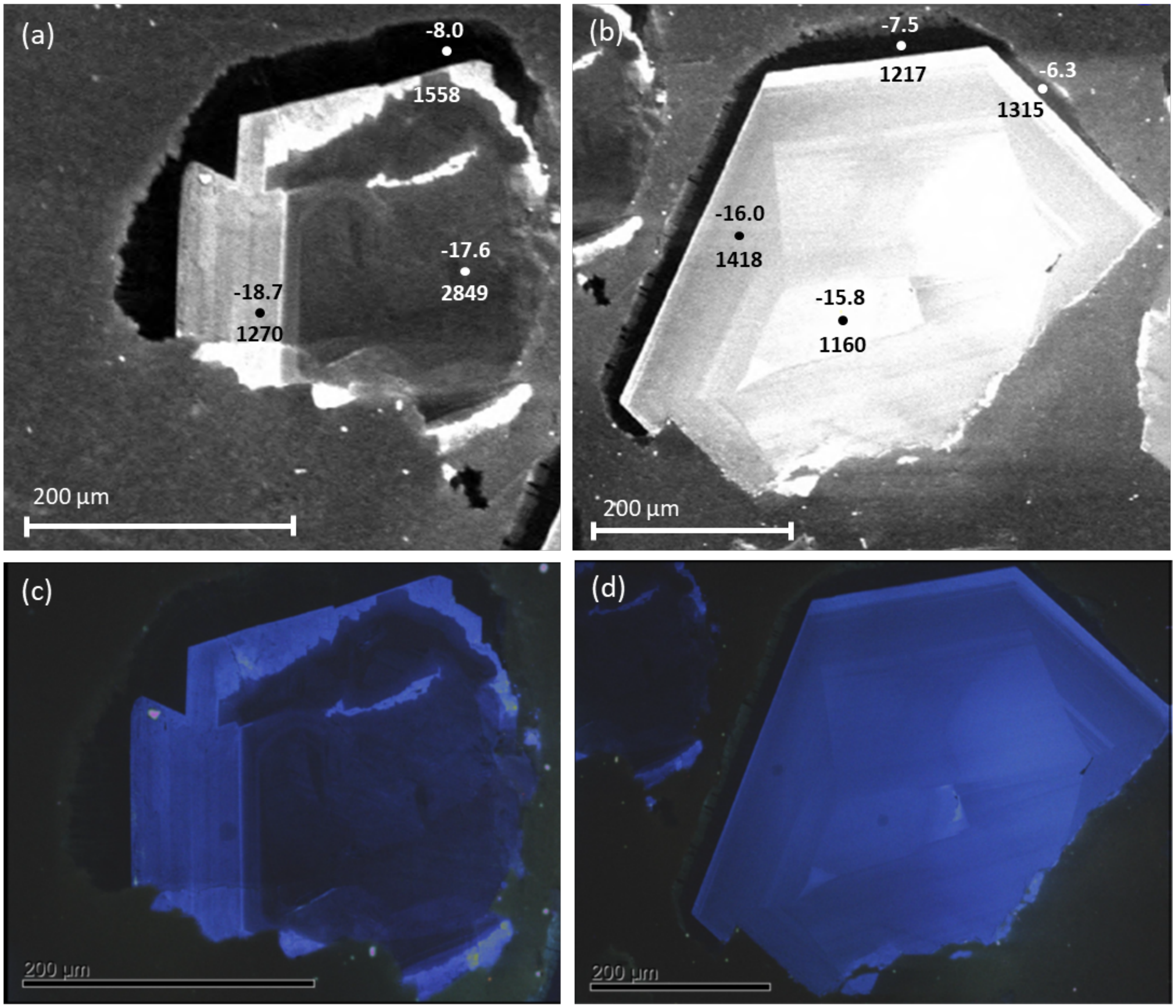

Figure 3.24: Examples of CL images of diamonds with core and rim formed in distinct growth events: (a) CH7-S10 and (b) CH7-S13. The cores show significantly lower ^{13}C compared to the rims. The bright cores appear blue in colour CL imaging, shown in (c) and (d) respectively.

3.5. Discussion

3.5.1. IR absorption features

3.5.1.1. Absence of pure Type Ib diamonds

Pure Type Ib diamond is not observed in the sample set, which is not surprising as the formation of A-centres from C-centres in the diamond lattice occurs rapidly during mantle residence, due to its relatively low activation energy (Taylor et al., 1996). Thus, pure Type Ib diamonds are very scarce in nature and even young diamonds contain measurable concentrations of A-centres instead of possessing solely C-centres (Collins, 2001). This is why all C-centre bearing diamonds studied here are mixed Type Ib/IaA.

3.5.1.2. Subtle peaks in the range of 1353 to 1387 cm^{-1}

These features have previously been reported in studies of C-centre bearing natural yellow diamonds (Hainschwang et al., 2012a and 2013; Titkov et al., 2015), suggesting a correlation between natural mixed Type Ib/IaA yellow diamonds and these peaks. Assuming that these peaks are an indicator of diamonds having C-centre characteristics, a total of 94 (out of 147) yellow diamonds possessing these peaks implies that C-centres are the major cause of yellow colourations in CH-7 diamonds.

3.5.1.3. Relationship between B′- and B-centre

It was proposed by Woods (1986) that B-centre bearing diamonds can be classified into “regular” and “irregular”. “Regular” diamonds exhibit a linear proportional relationship between the strength of the B′ peak and the absorption coefficient at the wavenumber of 1282 cm^{-1} due to B-centres (μ_B). “Irregular” diamonds, in contrast, do not display this linear relationship. This nonlinearity was suggested to be a result of platelet degradation due to extreme temperatures or shear stresses.

As the peak width of the B′-centre is not constant, Woods (1986) suggested that the integrated absorption, i.e. the baseline corrected peak area, should be used instead of peak height to represent the strength of the B′-centre. To verify whether the 26 diamonds which possess the B′-centre are “regular”, their baseline corrected peak areas of the B′ peak are plotted against the concentrations of the B-centre (Fig. 3.25), where “regular” diamonds should fall on the trend line with a gradient of 0.6 deduced from the experimental results of Woods (1986).

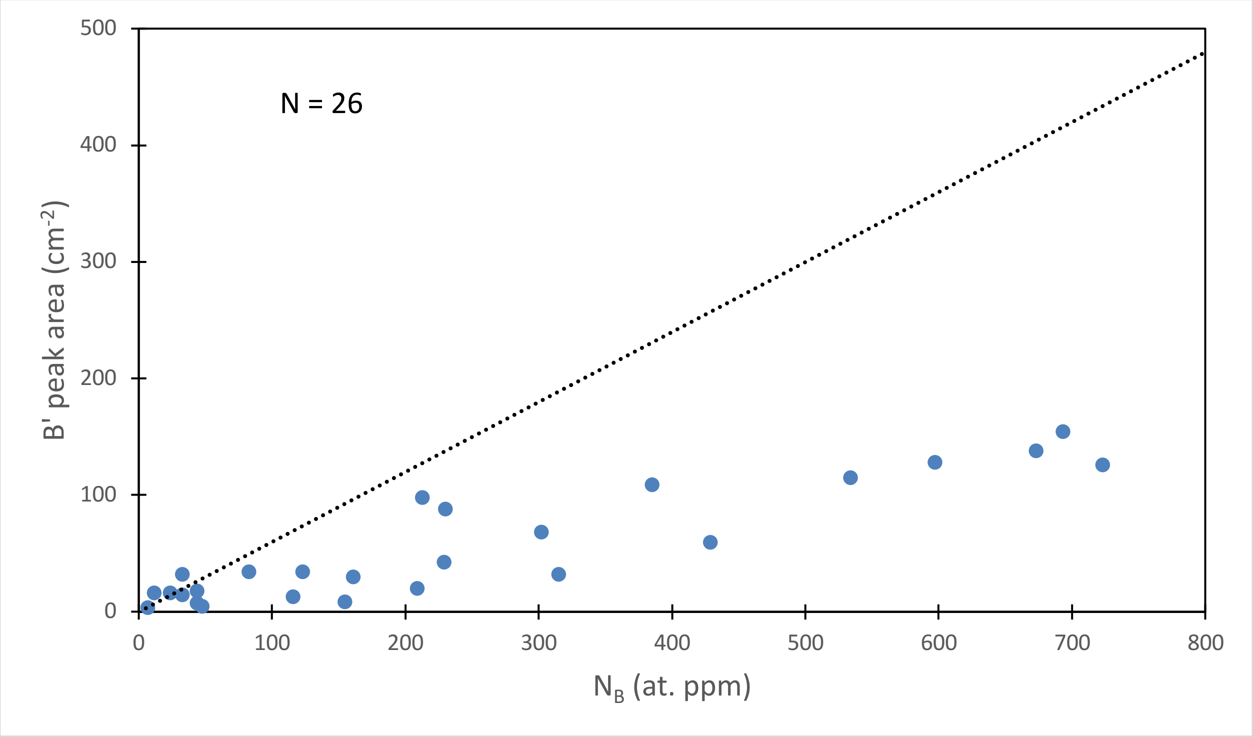

Figure 3.25: Plot of B′ peak area against concentration of B-centre of 26 B′-centre bearing diamonds.

From the graph, only around three out of 26 diamonds follow the proportionality (i.e. plot in close proximity with the trend of Woods (1986)) and thus are categorized as "regular" diamonds. It was observed that "regular" diamonds also demonstrate a linear proportionality between the strength of N3 centre and the integrated absorption of the B′ peak (Woods, 1986). Due to the mostly irregular character of the diamonds, however, it is not possible to estimate the strength of the N3 centre from that of the B′ peak in most of the diamonds. Hence, it cannot be determined whether the yellow colours of the 26 B′-centre bearing diamonds are caused by N3 and N2 centres.

3.5.1.4. Anomalous nitrogen absorption in the one-phonon region

It is likely that one or more new defect centres are needed for complete deconvolution of this region in the 16 nitrogen-poor diamonds. Hainschwang et al. (2012a) noticed that in many natural C-centre bearing diamonds, the typical spectral decomposition method involving A-, B-, C- and X-centres led to a broad residual absorption band. This band, located at about 1145 to 1150 cm^{-1}, which seemed to only appear in mixed Type Ib/IaA or Type Ib diamonds, was coined the Y-centre (Hainschwang et al., 2012a). This implies that these 16 diamonds possibly all possess C-centre characteristics.

3.5.1.5. Numerous peaks detected in the range of 1350 to 1600 cm^{-1}

Although the structure associated with the peaks detected in this range in some nitrogen-rich diamonds is unknown, previously reported experimental results indicated that some of these peaks may correlate to interstitial nitrogen atoms (Goss et al., 2004; Salustro et al., 2018). However, it is unclear whether these peaks have any contribution to the yellow colour of diamonds, or if they only exist in diamonds with high nitrogen concentration.

3.5.1.6. Hydrogen-rich diamond with a grayish tint

Hydrogen impurities can alter the physical properties of diamonds, such as colour and luminescence (Fritsch et al., 2007). Although these impurities could lead to a broad range of colours, hydrogen-rich diamonds were generally linked to grayish colouration (van der Bogert et al., 2009). Fritsch (1998) suggested that hydrogen-related defects are also possible causes of yellow colour in diamonds.

3.5.1.7. Co-existing B′- and C-centres

The occurrence of A-, B- and C-centres in 14 diamonds on first glance suggests the existence of ABC diamonds (diamonds which simultaneously possess A, B and C centres; Hainschwang et al. (2006)). Closer examination of broken fragments of these diamonds, however, reveals that colourless cores (with A-, B- and B′-centres) are surrounded by yellow outer layers (with A- and C-centres). The fact that the cores and outer layers have distinct nitrogen concentrations and levels of nitrogen aggregation suggests that they formed in two episodes of growth, rather than being ABC diamonds.

It is possible that the combination of colourless core and yellow outer layer is more common than the 14 diamonds mentioned above, as the cores may not be observed in some samples due to their small sizes if (i) the core was not aligned with the optical path where IR is transmitted during an FTIR measurement, hence B-centres were not detected even if the diamond did contain a Type IaAB core; (ii) the core inside the diamond was broken into tiny fragments and consequently not observed when the diamond was crushed for further analysis.

3.5.2. Fluorescent properties

Fluorescence properties of diamonds are complementary information to FTIR analysis, to explain some unusual characteristics observed in their IR absorption spectra.

3.5.2.1. Yellow/orange fluorescence

Diamonds with very low nitrogen concentration seem to be correlated to strong fluorescence – besides two diamonds with nitrogen concentrations of 14 and 16 at. ppm, respectively, which exhibit strong orange fluorescence, others display strong yellow fluorescence. These diamonds, as mentioned in the previous section, are suspected to have one or more new optical centres such as the “Y-centre”. Similar observations have been made by Hainschwang et al. (2013), in which the yellow diamonds dominated by the “Y-centre” usually exhibited yellow to orange fluorescence in variable strengths.

It has been observed that intense yellow fluorescence is associated with diamonds possessing an absorption band in the visible absorption spectra at 480 nm (Collins and Mohammed, 1982). In addition, it was suggested that the intensities of the “Y-centre” and the 480 nm band were correlated, based on the observation of 480 nm absorption/680 nm emission in “Y-centre” containing yellow diamonds in the study of Hainschwang et al. (2013). Furthermore, the existence of NV^0 defects in the diamond lattice, which are associated with a vacancy next to a single nitrogen atom in neutral charge state (Mita, 1996), could add an orangey tint to its fluorescence (Shigley and Breeding, 2013).

Other possible causes of yellow fluorescence are nickel-related S1, S2 and S3 centres. These nickel-related defects may as well produce yellowish green to green fluorescence (Fritsch et al., 2007; Dobrinets et al., 2013).

3.5.2.2. Green fluorescence

Green fluorescence observed in some diamonds possibly originates from the H3 centre, associated with a vacancy in between two nitrogen atoms in neutral charge state (Shigley and Breeding, 2013); or from the nickel-related defects mentioned above.

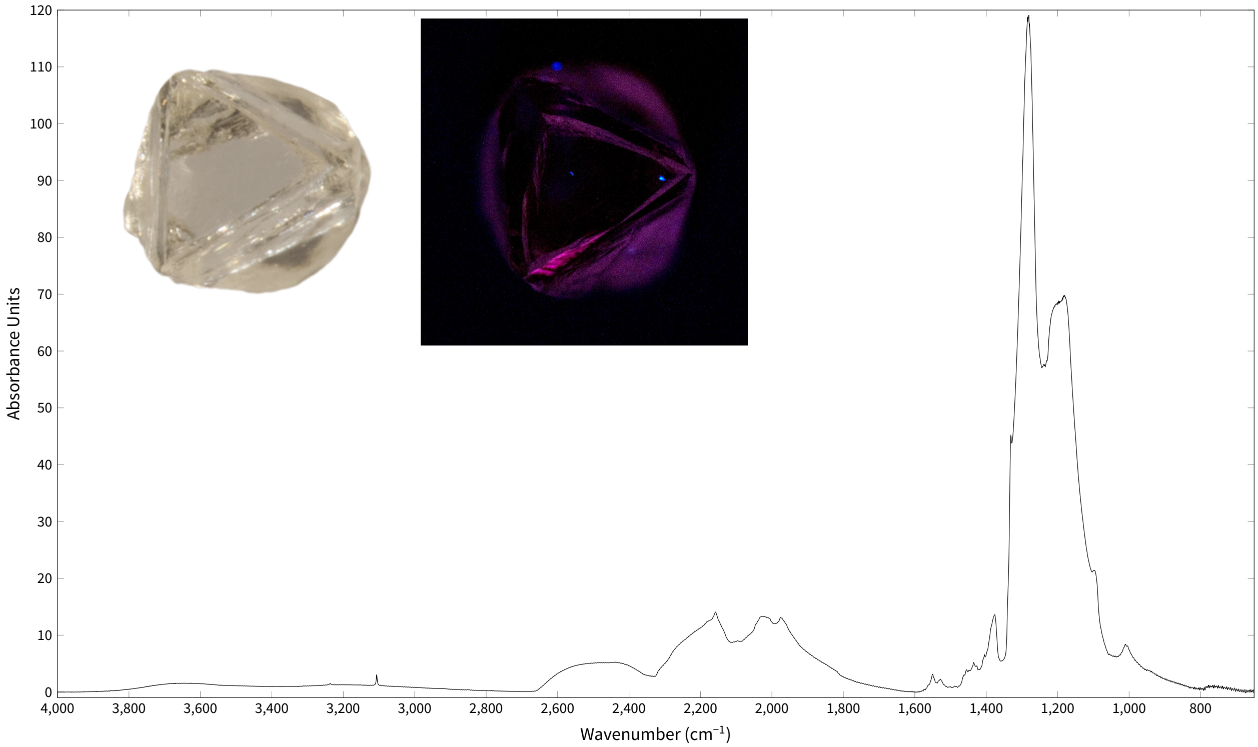

Figure 3.26: CH7-L88, which shows strong B'-centre absorption, exhibits purple fluorescence.

3.5.2.3. Purple fluorescence

Purple fluorescence of the diamond showing a strong B′-centre peak (Fig. 3.26) is thought to be a mixture of blue fluorescence and pink to red fluorescence. The former may originate from N3 centres, while the latter is possibly associated with the NV^- centre (possibly in combination with the NV^0 centre), which has the same structure as NV^0 but in a negatively charged state (Davies and Hamer, 1976; Mita, 1996).

3.5.3. Visible light absorption features

3.5.3.1. Absorption continuum

The absorption continuum is a typical feature for diamonds which possess C-centres as the main cause of their yellow colouration. This feature is observed in all diamonds with concentration of C-centres over 0.1 at. ppm. Even a diamond with very low concentration of C-centres, which is below the detection limit of FTIR, will still display this absorption continuum (Dobrinets et al., 2013). Thus, for those diamonds which do not reveal C-centre peaks in their IR spectra while displaying this absorption continuum, their yellow colour is considered to be originated from C-centre as well.

3.5.3.2. The 480 nm band

The 480 nm absorption band observed in nitrogen-poor diamonds with strong yellow fluorescence is responsible for their yellow colouration. The rising absorption towards the shorter wavelengths may possibly be an absorption feature partially caused by the C-centre. In fact, C-centre is detected with FTIR in some of these diamonds. Thus, it is not rare for diamonds to contain a mixture of several colour-causing optical centres.

3.5.3.3. Absence of N3 and N2 centres

It was shown previously in Section 3.5.1.3 that most of the B′-centre containing diamonds are "irregular", so it is not possible to establish a relationship between the strength of B′-centre and that of N3 centre. This signifies that diamonds with strong B′-centres do not necessarily have intense N3 centres. In this case, either the N3 centre in these diamonds is too weak to be detectable with the low signal-to-noise ratio of the visible absorption spectra obtained for the small diamonds studied here, or the diamonds do not possess N3 centres.

3.5.4. Cathodoluminescence (CL) features

3.5.4.1. Homogeneous CL

Dark CL without growth zoning is the common feature observed in most of the mixed Type Ib/IaA diamonds, meaning a lack of defects which produce emission, which explains why these diamonds are inert under LWUV excitation.

3.5.4.2. Irregular areas with bright CL response

It is not certain which defects are associated with this bright CL response. However, it can be observed in some nitrogen-poor diamonds with deformation lines. Bright CL concentrated around these deformation lines is possibly attributed to the A-band, with a luminescent wavelength at 435 nm (Zaitsev, 2001). The A-band is associated with lattice dislocations as a result of plastic deformation, and it is usually intense in nitrogen-poor diamonds (Sumida and Lang, 1981). It was suggested that the intensity of luminescence caused by the A-band decreases with nitrogen content (Yokota et al., 1992).

3.5.4.3. Combination of dark rim and brighter core

(i) Diamonds without detectable C-centre peaks

These diamonds display the C-centre related absorption continuum in visible absorption spectra. It is possible that the dark rims in the CL images are thin layers of C-centre bearing overgrowths and they are responsible for the yellow colouration of diamonds in this category, explaining the fact that these diamonds exhibit similar colours and visible absorption spectra as those of Type Ib/IaA diamonds. The reason why C-centres are not detected in the IR absorption spectra is likely due to the fact that the concentration of C-centres in the very thin outer layers is low; this low signal is then further diluted by the A-centre rich core, given that the diamonds in this category have very intense nitrogen absorption dominated by the A-centre. As a consequence, the C-centre related absorption is below detection in these zoned diamonds.

(ii) Diamonds with Type Ib/IaA outer layers and Type IaAB cores

CL imaging and SIMS analysis further consolidate the hypothesis that these diamonds formed in at least two temporally distinct growth events. The dark rims are where C-centres are located. The bright cores which contain B′-centres, emit blue luminescence in colour CL imaging, which is thought to be attributed to the N3 centre (Zaitsev, 2001).

3.5.5. Nitrogen aggregation state and mantle residence time

Ninety-four diamonds are classified as Type Ib/IaA. The aggregation states of these Type Ib/IaA diamonds are represented by their A-centre proportion ranging from 36 to 98 %A (Fig. 3.27). Forty-three diamonds belong to Type IaAB and are A-centre dominated (up to 48 %B; Fig. 3.28). Ten diamonds have an A-centre proportion > 90 %A (< 10 %B; Fig. 3.28) and hence are categorized as Type IaA.

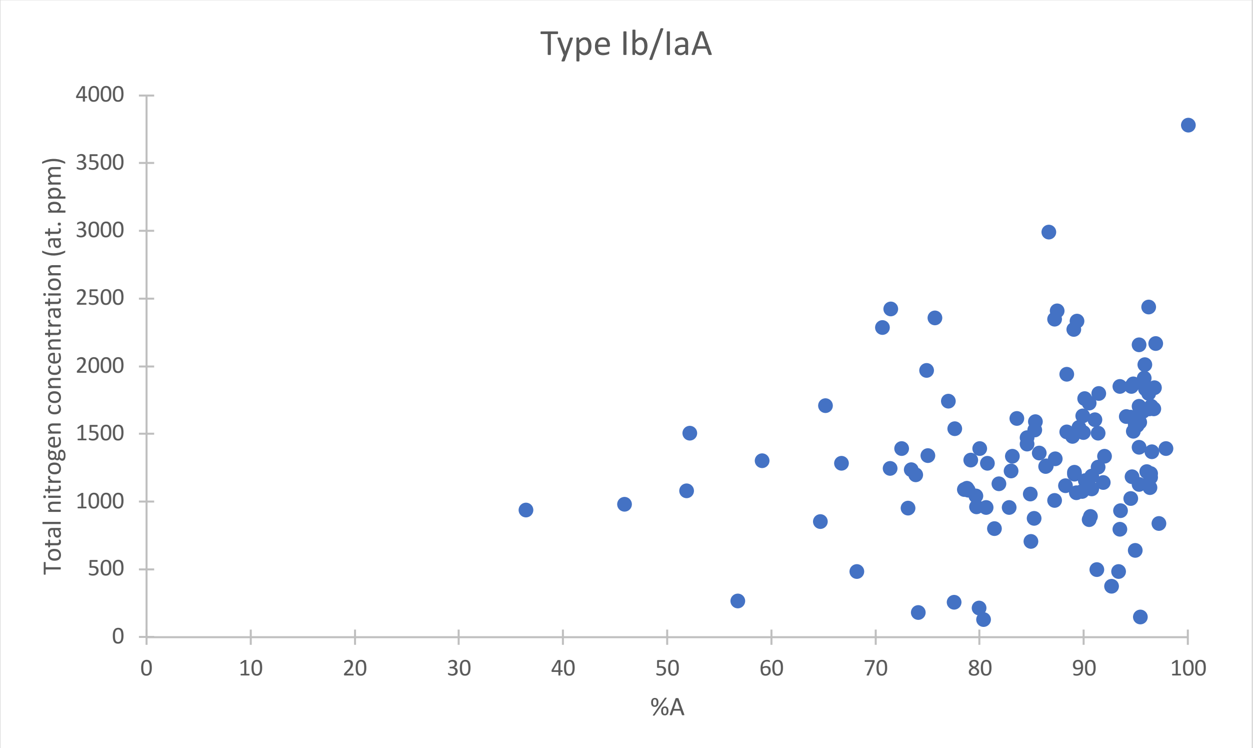

Figure 3.27: Plot of total nitrogen concentration (at. ppm) of Type Ib/IaA diamonds against their aggregation state, represented by %A.

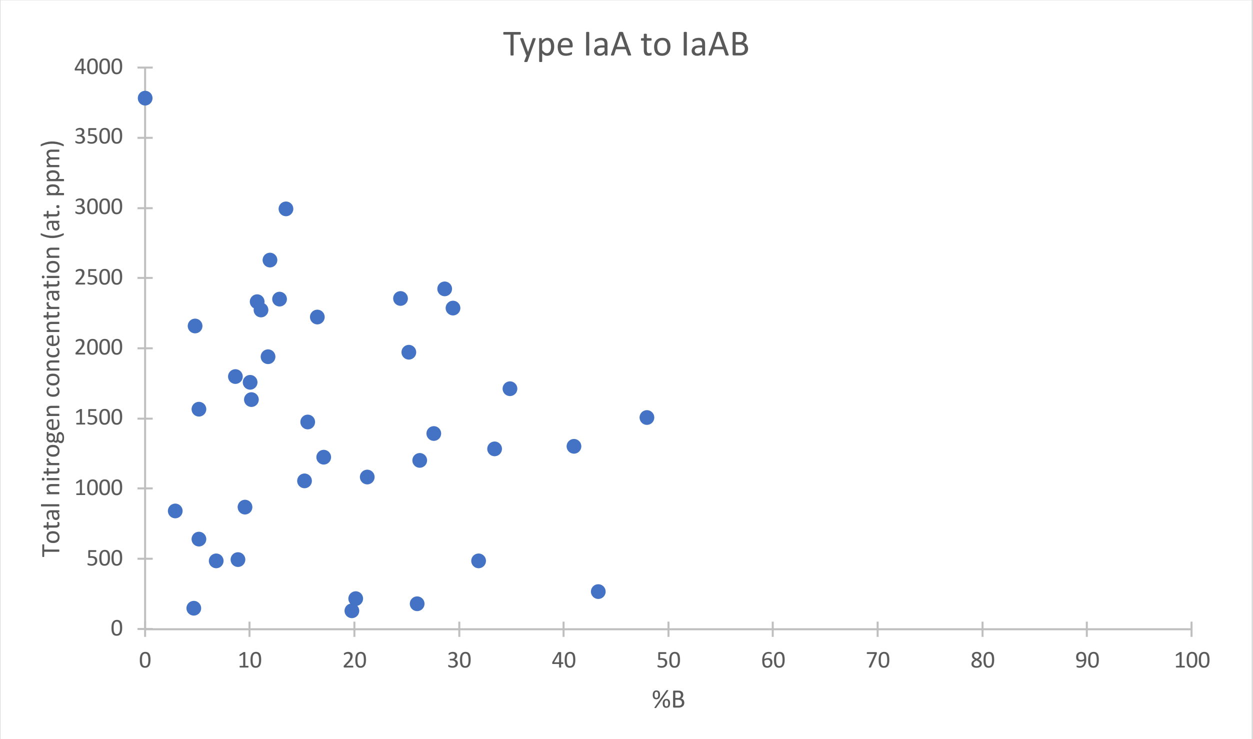

Figure 3.28: Plot of total nitrogen concentration (at. ppm) of Type IaA and Type IaAB diamonds against their aggregation state, represented by %B.

The total nitrogen concentration and the C- and A-centre proportions (for Type Ib/IaA diamonds) or the A- and B-centre proportions (for Type Ia diamonds) are necessary parameters for estimating the mantle residence time of diamonds (Taylor et al., 1990 and 1996; Leahy and Taylor, 1997). Nitrogen-poor diamonds, which cannot be deconvoluted perfectly, were not included in the calculation. Irregular shaped diamonds were only included in the calculation if they showed surface features related to cubic or octahedral faces, such as tetragons or trigons. This is because the aggregation rate from C- to A-centres depends on the diamond morphology, with octahedral sectors requiring a lower activation energy than cubic sectors (Taylor et al., 1996). A time-averaged mantle residence temperature of 1100 °C is adopted in the calculation, based on the results of a previous study on Chidliak diamonds, in which 80 % of the diamonds fell in the range of 1050 to 1150 °C and the average value was approximately 1090 °C (Hogberg et al., 2016).

The mantle residence times calculated are categorized into three groups according to the diamond types: (i) Type IaA and Type IaAB; (ii) Type Ib/IaA and (iii) Type Ib/IaA outer layer with Type IaAB core. Diamonds in the first group span a range in mantle residence times of approximately 0.1 to 1.8 Ga, with a median and an average of 0.6 and 0.7 Ga respectively; the second category ranges from about seven years to 49,000 years, with a median and an average of 9,800 and 14,000 years respectively; the last group has an age range for the outer layers from five to 34 years, with a median and an average of 12 and 16 years respectively, whereas the cores span a range of 0.2 to 1.1 Ga, median and average are both 0.8 Ga.

The Type IaA and Type IaAB diamonds in the first group and the Type IaAB cores in the last group share a similar mantle residence time range, which implies that they may have crystallized at about the same period of time and thus have the same origin. The relatively broad range in mantle residence time in these diamonds is probably due to the fact that they formed at different depths in the mantle, i.e. experienced different residence temperatures. For example, if a diamond with particular nitrogen characteristics had resided at a depth with a time-averaged mantle temperature of 1100 °C, this would have resulted in a mantle residence time of about 0.1 Ga; if the same diamond had resided at slightly shallower depth corresponding to 1050 °C, a mantle residence time of approximately 1 Ga would be deduced.

Five diamonds in the second group had resided in the mantle for about seven to 28 years, which is different from the rest of the group, where mantle residence times are thousands of years.

This implies that a small population of diamonds in this group might have formed together with the Type Ib/IaA overgrowth layers in the third group, as both of them show a similar range of mantle residence times. For these decades old diamonds to have mantle residence times raised to thousands of years, a decrease in residence temperature to 950 °C or lower is needed.

3.5.6. Source paragenesis

The overall range of $\delta^{13}C$ values in CH-7 diamonds is between –18.7 and –3.6 ‰, with a mode at −6.3 ‰. The distribution pattern is similar to the one observed from eclogitic (and websteritic) diamonds worldwide, which has a wider spread of $\delta^{13}C$ compared to that of peridotitic diamonds worldwide (Fig. 3.29). Moreover, the results agree with a previous study on Chidliak CH-6 and CH-7 diamonds, which also indicated the existence of an eclogitic (or websteritic) paragenesis (Hogberg et al., 2016). The ^{13}C depleted CH-7 diamonds, with $\delta^{13}C$ values below −10 ‰, are likely related to former organic matter transported into the lithospheric mantle through the subduction of oceanic crust (e.g. Kirkley et al., (1991)). However, care should be taken in interpreting the isotopic data without having the additional information on the mineralogy of diamond substrates provided by an inclusion study; the possibility that peridotitic diamonds exist in the sample sets consequently cannot be ruled out, as the $\delta^{13}C$ ranges for peridotitic, ecologitic and websteritic diamonds partially overlap (Cartigny et al., 2014).

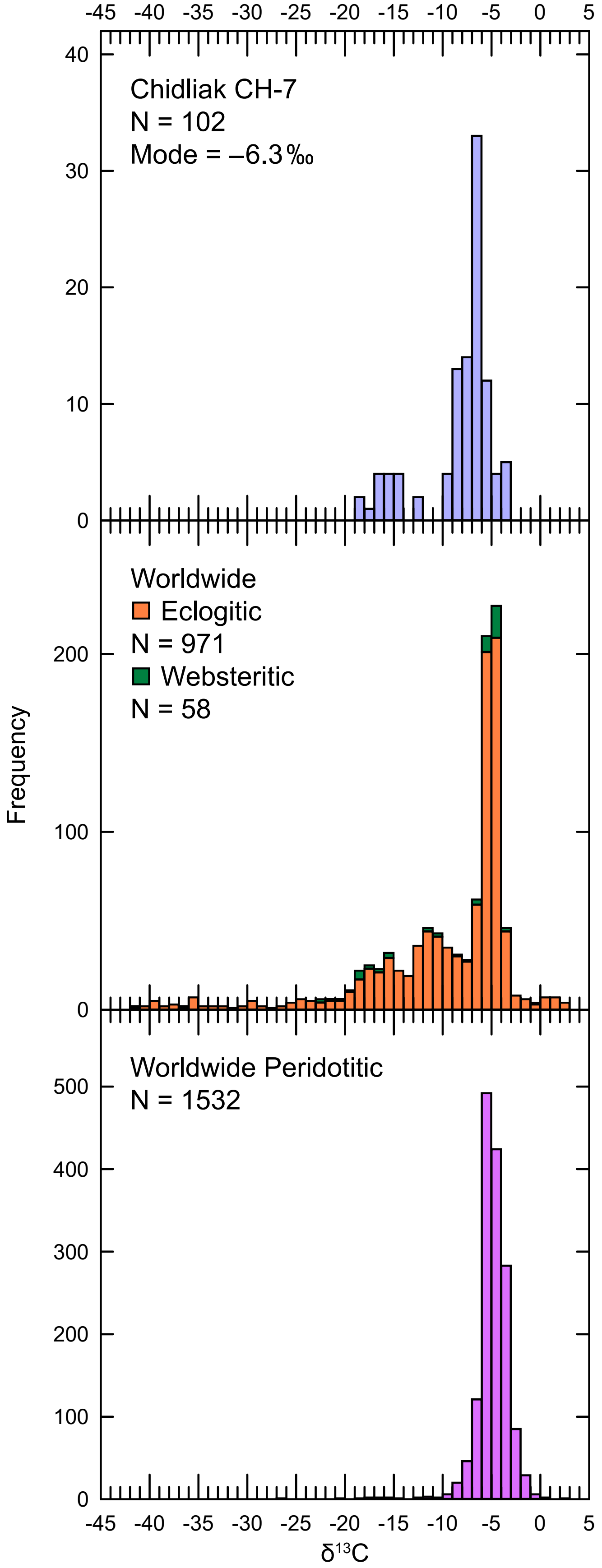

Figure 3.29: Distribution of $\delta^{13}C$ in yellow CH-7 diamonds, compared to eclogitic, websteritic and peridotitic diamonds worldwide (from the database of Stachel et al., 2017). The mode of $\delta^{13}C$ in CH-7 diamonds is calculated using Isoplot (Ludwig, 1999).

3.6. Conclusions

Summarizing the data collected from various analyses, 71 diamonds exhibit an obvious C-centre peak at 1344 cm^{-1} in their IR absorption spectra; an additional 23 diamonds show C-centre related IR absorption features in the spectral region of 1353 – 1387 cm^{-1}; 14 diamonds display visible absorption spectra and CL images analogous to those of C-centre containing diamonds; hence, in total 108 diamonds (73 % of all yellow diamond samples) are believed to have C-centre characteristics, suggesting that the presence of C-centres is the major factor responsible for the yellow colouration of diamonds from the Chidliak CH-7 kimberlite.

Carbon isotope analyses show a wide spread of $\delta^{13}C$ in diamonds, indicating the presence of an eclogitic (or webseritic) paragenesis of Chidliak CH-7 yellow diamonds, which agrees with the results from a previous study on Chidliak CH-6 and CH-7 diamonds. It can, however, not be ruled out that some diamonds in the sample sets have a peridotitic origin. Strongly ^{13}C depleted diamond carbon ($\delta^{13}C$ between –18.7 and –12.1 ‰) is probably related to former organic matter recycled into the mantle during the subduction of oceanic crust.

The discovery of co-existing B′- and C-centres in 14 diamonds (10 % of the sample set), associated with evidence for separate growth zones with distinct carbon isotope compositions and large differences in the mantle residence time between the colourless Type IaAB cores and yellow Type Ib/IaA outer layers, imply that these diamonds formed during (at least) two temporally distinct growth events. An additional 14 diamonds exhibit very thin dark rims in CL images and these rims are suspected to be C-centre bearing, again involving episodic growth. If they are counted towards the group of episodic growth diamonds, the proportion of this group in the yellow sample set increases to approximately 20 %. Given that similar observations were also made at Qilalugaq (Banas et al., 2017), episodic diamond growth may be a common feature for yellow diamonds from Canada’s eastern Arctic, or perhaps even worldwide.

3.7. Future work

To confirm the source paragenesis of diamonds, mineral inclusion data should be collected. Defects of diamonds can be further analyzed by collection of their photoluminescence (PL) spectra to reveal the emission peaks related to impurities or vacancies, utilizing various laser excitations.

Furthermore, PL and FTIR mapping will provide more information on the distribution of defects in these diamonds to better understand their growth structures. CL spectra along with coloured CL images can be obtained to confirm the origins of the optical centres which cause the luminescence.

4. A case study of yellow diamonds from the Ekati Diamond Mine

4.1. Introduction

The Ekati Diamond Mine is the first surface and underground diamond mine in Canada. It is located in the Lac de Gras area of the Northwest Territories. It is well-known for a high quality production of diamonds. The first diamondiferous kimberlite pipe at Ekati was discovered in 1991. The Ekati Diamond Mine hosts a total of 150 kimberlite pipes to date, of which approximately 10 % are known to be economically significant (Carlson et al., 2016). The Misery kimberlite complex is one of the actively mined sites on the property, and is also known to frequently produce high value fancy yellow diamonds. The 30.54 ct "Arctic Sun" diamond, cut and polished from a 65.93 ct rough yellow diamond recovered from the Misery Main pipe in 2016, is by far the largest fancy yellow diamond found in North America. This project was motivated by a recently increased recovery of yellow diamonds from the Ekati Diamond Mine, the Chidliak property (Chapter 3) and Qilalugaq Kimberlite Field (Banas et al., 2017). Diamonds in this project were recovered from the Misery Southwest Extension of the Ekati Diamond Mine, in order to understand the conditions of yellow diamond formation in the mantle.

4.2. Geologic background

The Ekati project area is located it the central Slave Province (Fig. 4.1), which is an exposed part of the Archean Slave craton grown by tectonic plate accretion onto a pre-3 Ga nucleus. Kimberlites in the Lac de Gras area exhibit typical geochemical and petrographic features of Group I kimberlites (Nowicki et al., 2004). Clinopyroxene thermobarometry data indicate a cold conductive geotherm in the lithospheric mantle beneath Ekati (Grütter, 2009), which is a feature favourable for diamond crystallization and preservation.

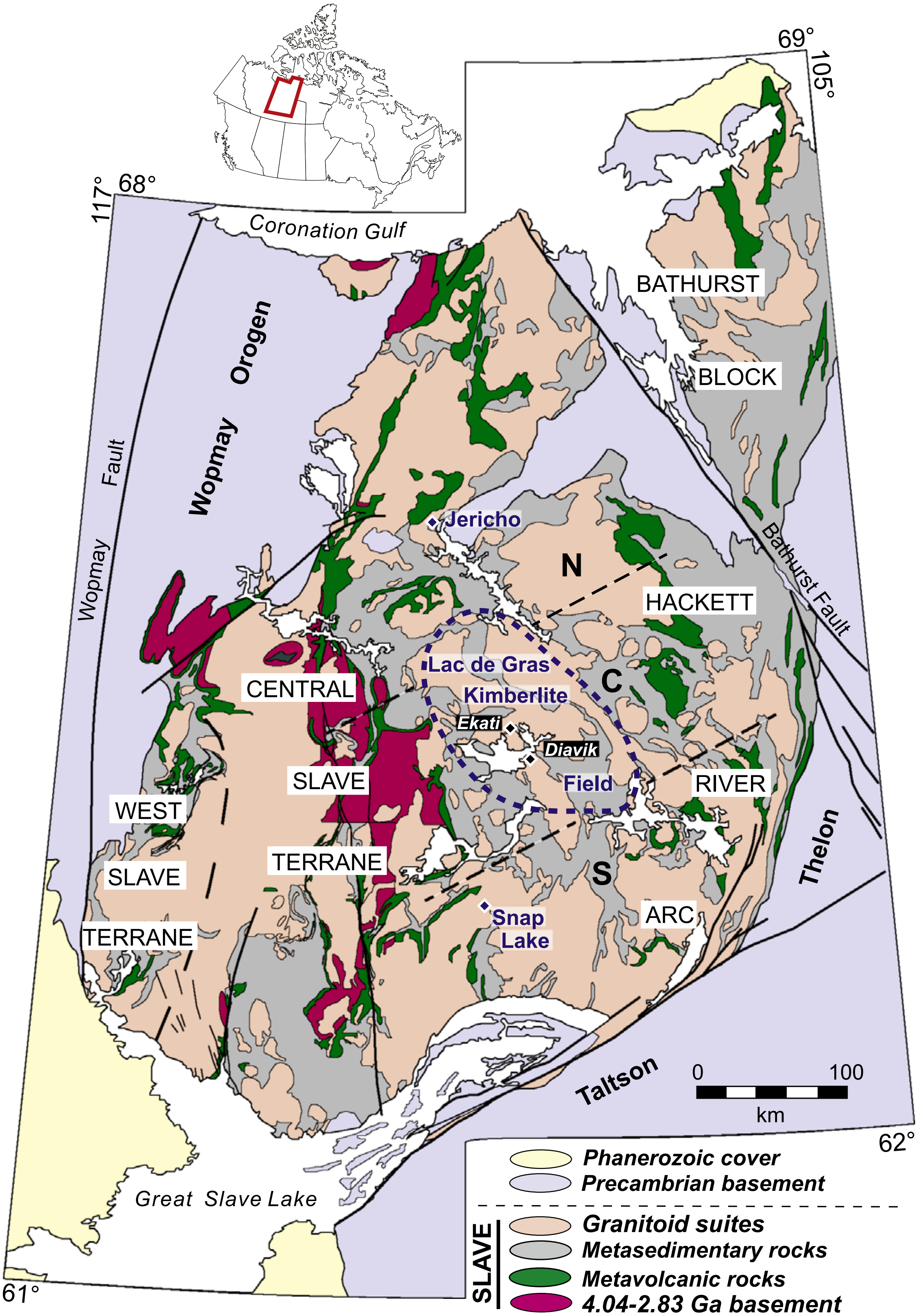

Figure 4.1: Geologic map of the Slave craton (after (Bleeker, 2003)) showing the location of the Ekati diamond mine in the Lac de Gras Kimberlite Field of the Northwest Territories (taken from Fig.1 of Tappe et al. (2013)).

The results of U-Pb and Rb-Sr geochronological analysis of kimberlite bodies at Ekati showed that they were emplaced in at least five temporally distinct phases of kimberlite magmatism between 75 and 45 Ma, spanning approximately 30 Ma during the Late Cretaceous and Eocene periods (Creaser et al., 2004; Lockhart et al., 2004; Sarkar et al., 2015). Correlating the diamond potential at Ekati with the age of kimberlite eruption, more recently emplaced kimberlites throughout the Eocene period from 56 to 45 Ma tend to have higher diamond contents (Heaman et al., 2003; Creaser et al., 2004; Lockhart et al., 2004).

The Misery kimberlite complex is located in the southeastern part of the Ekati Mine. The complex pipe morphology distinguishes Misery from other kimberlites at Ekati, which mostly are single pipe intrusions while the Misery pipes form a cluster (Nowicki et al., 2004). The cluster comprises six main kimberlite bodies, where the Main pipe at the centre of the cluster is the largest, followed by Southwest Extension and the South pipe (Fig. 4.2).

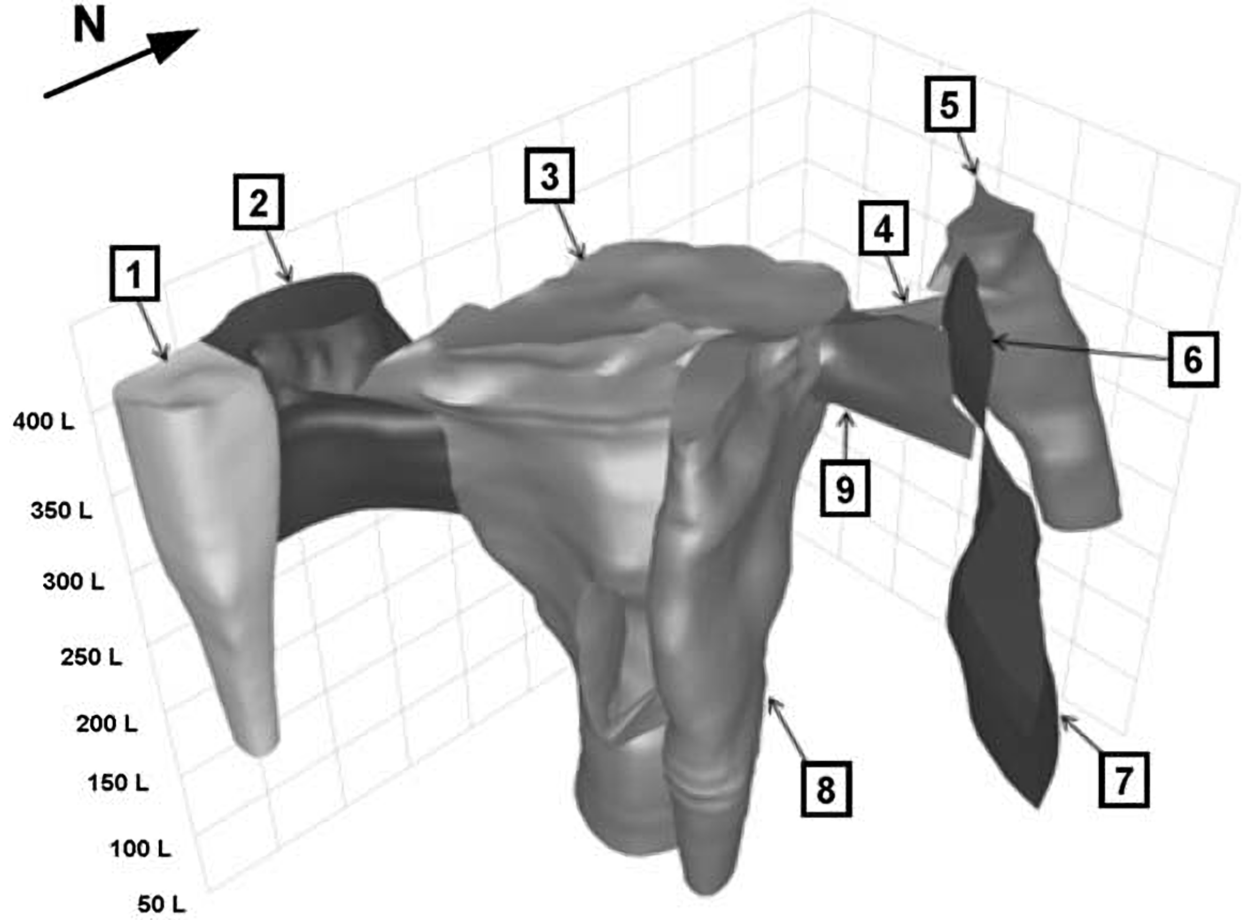

Figure 4.2: Misery kimberlite complex showing (1) South pipe, (2) Southwest Extension, (3) Main pipe, and other intrusive bodies (4-9) (taken from Fig. 4 of Nowicki et al. (2004)).

4.3. Sample description

A diamond parcel from Misery Southwest Extension containing 1324 diamonds with size < 3 mm was received, from which 51 yellow diamonds were picked for this study, comprising a proportion of 4 % (Fig. 4.3). An additional 20 yellow diamonds, with a size range of 3 – 5 mm, were received as the project progressed to allow comparison with the diamonds in the smaller size group; they were recovered from both the Misery Main pipe and Southwest Extension.

Diamonds in the smaller size group and the larger size group weighed from 0.02 to 0.08 ct and 0.10 to 0.42 ct, respectively. As the 20 larger diamonds were selected for specific properties, they are not included in the statistics displaying the distribution of morphology and colour in the sample set. Four shades of yellow colour are observed in the sample set – yellow (35 %), orangey yellow (33 %), pale yellow (24 %) and dull yellow (8 %) (Fig. 4.4). Diamonds have high transparency in general, as fibrous overgrowth is not common in the sample set, and inclusions are only occasionally observed.

Over half (51 %) of the diamonds in the sample set have irregular shapes, followed by cuboids (31 %) (Fig. 4.5). These two types of morphology seem to always dominate the population of yellow diamonds, as a similar trend was also observed in Chapter 3 for Chidliak CH-7 yellow diamonds. Dodecahedra, derived from resorption of octahedral diamonds, are present, making up a proportion of 8 %. Aggregated diamonds and octahedra are less common, each of them constituting 4 %. Fragmented diamonds, which show smooth breakage surfaces, are rare in the sample set, comprising only 2 %. Details of samples are summarized in Table B.1 of Appendix B.

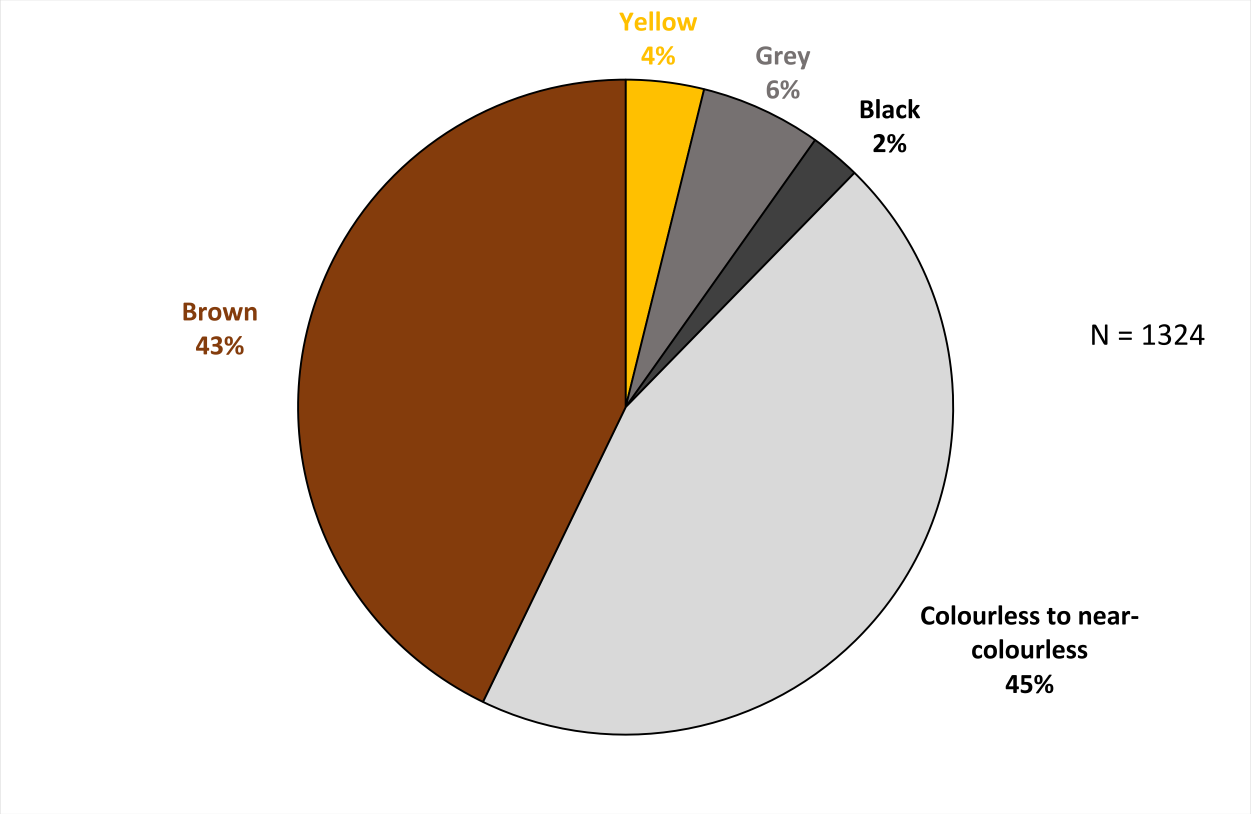

Figure 4.3: Diamond colour distribution of 1324 diamonds recovered from Misery Southwest Extension.

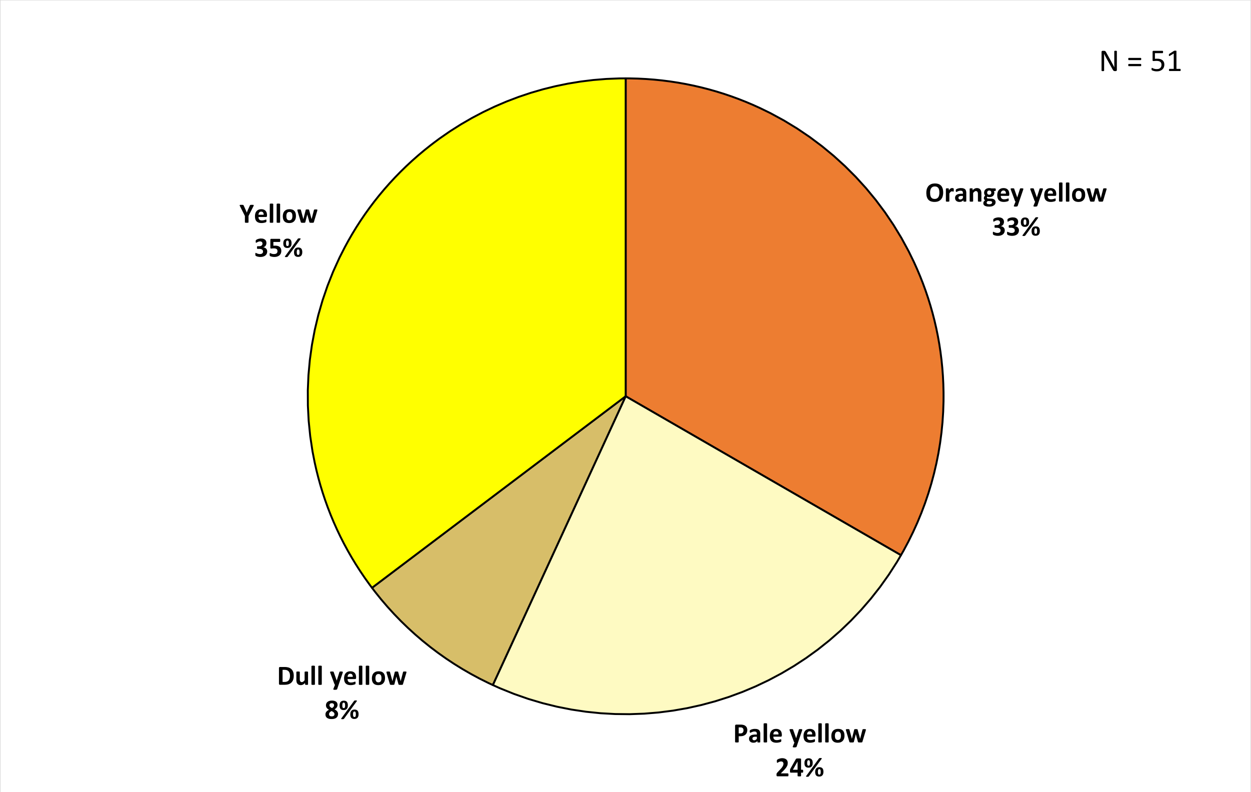

Figure 4.4: Relative proportion of a range of shades among 51 yellow diamonds.

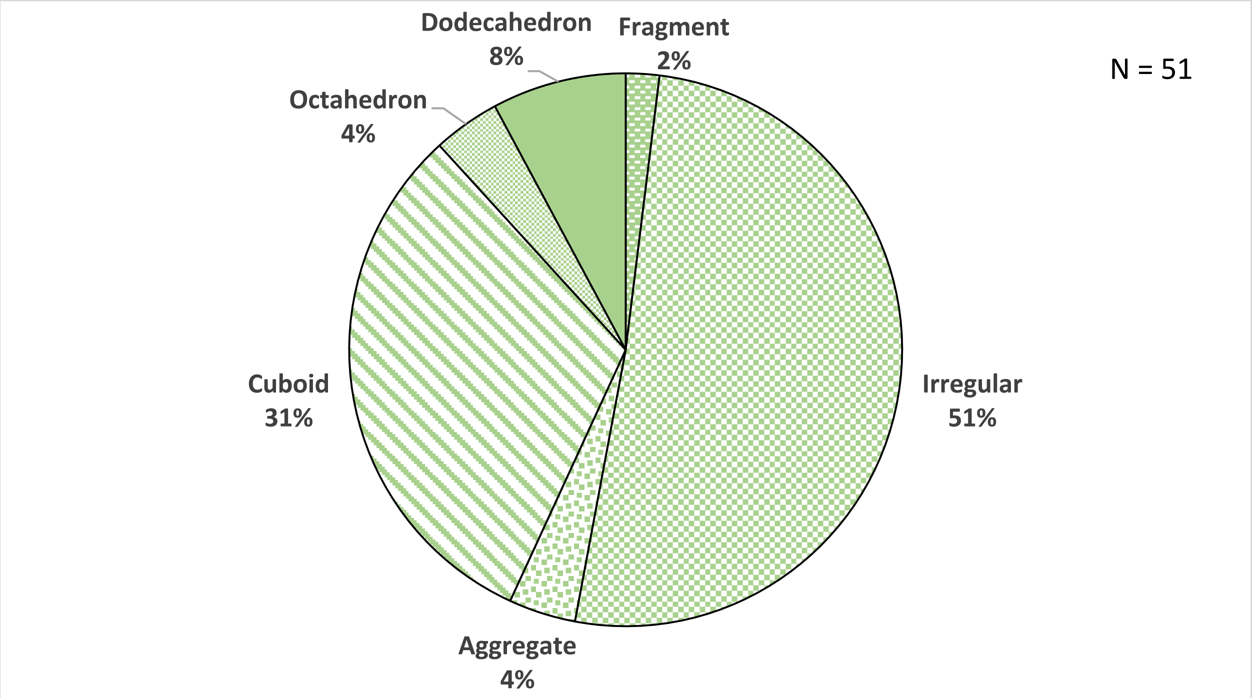

Figure 4.5: Relative proportion of various morphologies among 51 yellow diamonds.

4.4. Results

4.4.1. FTIR spectroscopy

Nitrogen concentrations of Misery yellow diamonds with a size < 3 mm range from 685 to 1490 at. ppm, with a median value of 1031 at. ppm. Diamonds in the larger size group (3 – 5 mm) display a range slightly shifted towards higher nitrogen contents, spanning from 960 to 2351 at. ppm, with a median value of 1129 at. ppm. Diamonds in both groups are generally rich in nitrogen, where 47 out of a total of 71 diamonds (66 %) contain nitrogen in concentrations above 1000 at. ppm.

Similar to Chidliak yellow diamonds (Chapter 3), Misery yellow diamonds also possess a high concentration of A-centres, where 67 diamonds (94 %) exhibit an A-centre proportion ≥ 80 %, with a median value of 92 %.

It is observed that 62 diamonds (87 %) contained C-centres (see Section 2.1 in Chapter 2 for diagnostic peaks in IR absorption spectra). These diamonds are all dominated by A-centres and thus classify as mixed Type Ib/IaA. A group of subtle peaks, located at 1353, 1363 and 1374 cm^{-1} (1369 and 1387 cm^{-1} are occasionally present), always accompany the C-centre peak in these diamonds.

Misery mixed Type Ib/IaA diamonds of the two size groups display a range of yellow colour from pale yellow to deep yellow (Fig. 4.6), suggesting that C-centre bearing diamonds do not necessarily display a saturated “canary yellow” colour. Pale yellow diamonds with fairly low concentrations of C-centres, can sometimes be very difficult to discriminate from the so-called “cape yellow” diamonds (yellow colour caused by N3 and N2 centres (Fritsch, 1998)) without instrumentation.

Figure 4.6: Mixed Type Ib/IaA diamonds display a range of yellow colour. From left to right: MS-S23 (pale yellow), MS-S48 (dull yellow), MS-L16 (yellow), MS-L4 (orangey yellow) and MS-L19 (deep yellow).

The rest of the diamonds in the two sample sets (9 diamonds, equating to a proportion of 13 %) exhibit platelets peak (also known as B′-centre), which is a by-product formed alongside with the N3 centre in the progression of nitrogen aggregation from A- to B-centres (Bursill and Glaisher, 1985). B′-centres are found in the spectral range of 1358 to 1378 cm^{-1}, with the exact position depending on the size of the platelets in the diamond lattice, where larger platelets lead to a peak shift towards the smaller wavenumber (Sobolev et al., 1969; Speich et al., 2017).

A hydrogen-related peak at 3107 cm^{-1} is detected in all studied yellow diamonds. The integrated peak area of the 3107 cm^{-1} absorption peak ranges from 4 to 62 cm^{-2} for diamonds in the smaller size group, with a median value of 37 cm^{-2}; and from 2 to 152 cm^{-2} for diamonds in the larger size group, with a median value of 31 cm^{-2}.

Experimental data show that the strength of the peak at 3107 cm^{-1} does not necessarily reflect the total hydrogen concentration in the diamond lattice, as hydrogen can be present in the form of IR inactive defects (Sweeney et al., 1999). Even so, the peak intensity can still loosely indicate whether a diamond is rich in hydrogen. It was suggested that the 3107 cm^{-1} absorption is attributed to the stretching mode of C-H bond vibrations, where it is always accompanied by the 1405 cm^{-1} absorption corresponding to the bending mode of the same bond vibration (Woods and Collins, 1983). It is observed from 70 diamonds with discernible hydrogen-related absorption at 3107 and 1405 cm^{-1} that the ratio between the baseline corrected peak areas of these two peaks is approximately 0.17, which is in good agreement with the ratio deduced from Chidliak diamonds in Chapter 3 (Fig. 4.7).

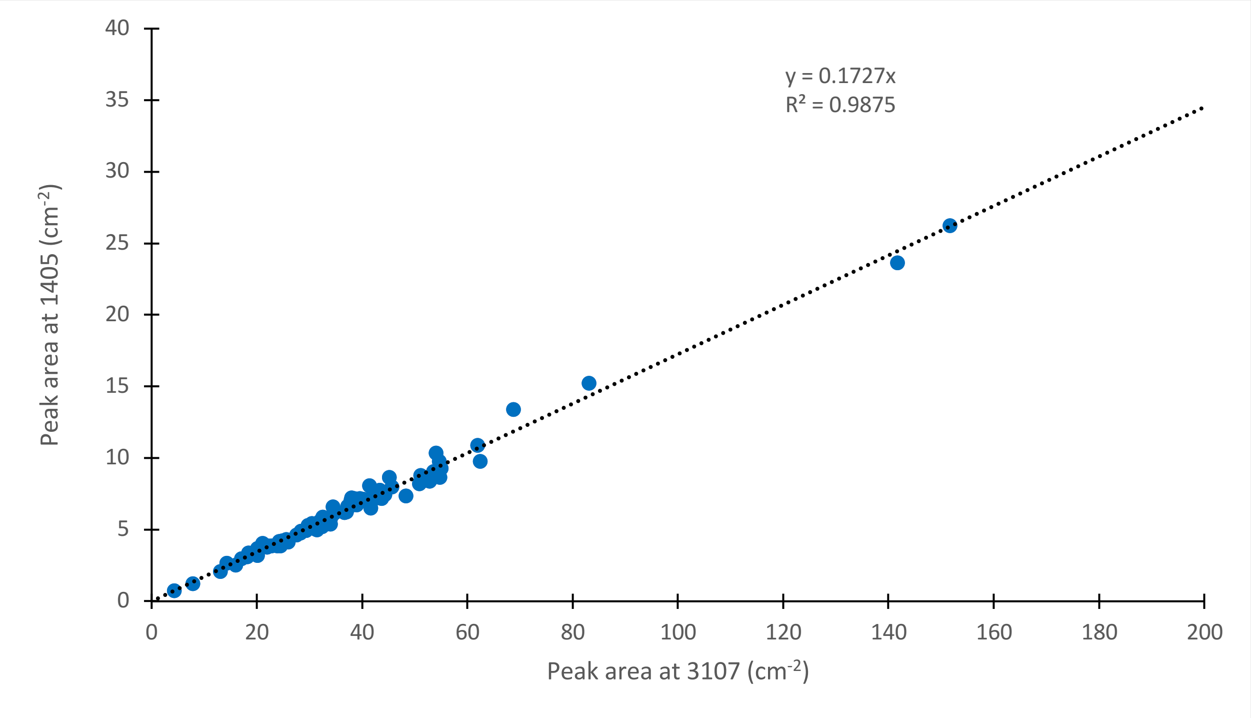

Figure 4.7: Plot of the peak area at 1405 cm^{-1} against that at 3107 cm^{-1} for 70 diamonds.

A fragment was found to have a combination of a colourless core and a yellow outer layer. This fragment, with a single breakage surface, exhibited B′-centres and weak C-centres accompanied by the subtle peaks at 1353, 1363 and 1387 cm^{-1} (Fig. 4.8). Based on the previous observation of Chidliak diamonds with Type Ia cores and Type Ib/IaA rims, the B′-centres may be located in the colourless core, whereas the C-centres exist in the yellow periphery. To verify this hypothesis, this fragment was further broken to separate the colourless core and yellow outer layer for individual FTIR analyses.

It was observed that B′-centres (~ 4 %B) can only be found in the colourless core, classifying the colourless core as Type IaA (refer to Section 2.1 in Chapter 2 for diamond Type classification). The yellow periphery is a mixed Type Ib/IaA, containing a C-centre proportion of 28 % (Fig. 4.9). Apparently co-existing B′- and C-centres are also observed in three diamonds in the larger size group (3 – 5 mm) (Fig. 4.10).

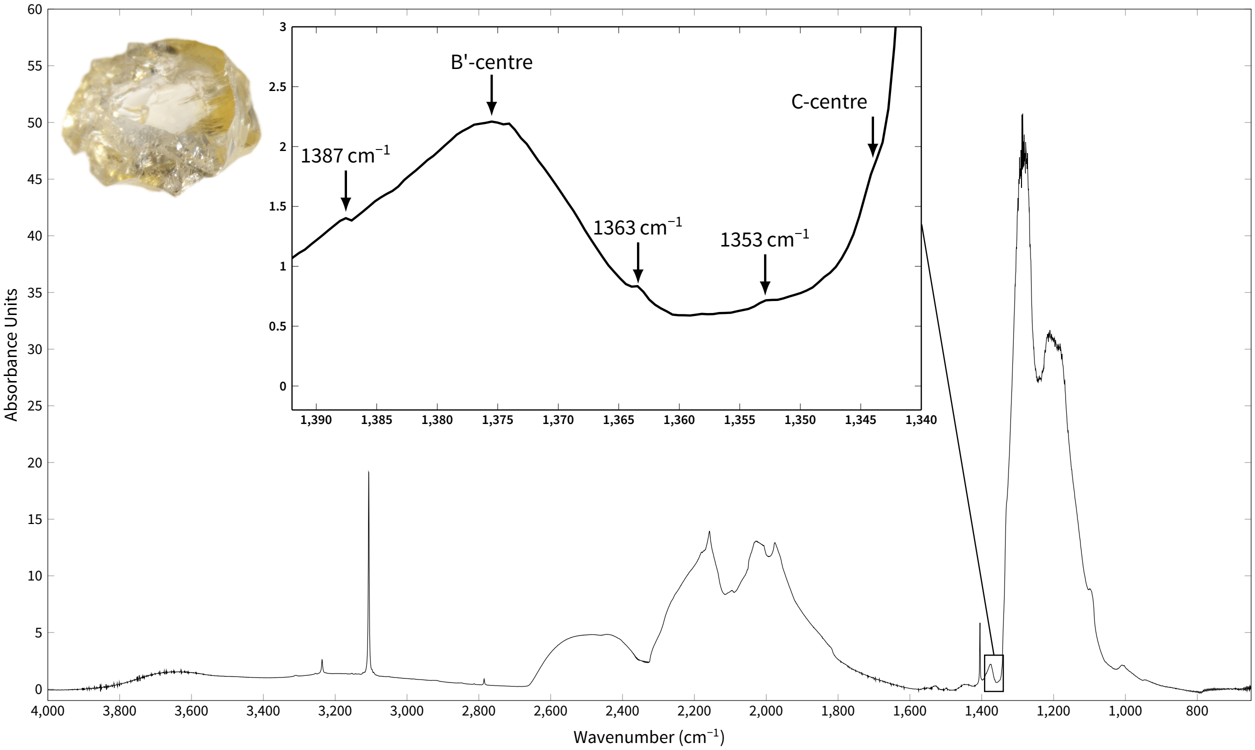

Figure 4.8: IR spectra of MS-S50 which exhibited both B'- and C-centres.

In addition, three diamonds in the smaller size group and three diamonds in the larger size group revealed colourless cores during crushing for sample preparation for CL imaging and SIMS analysis. However, their colourless cores do not exhibit B′-centres. Among the three diamonds in the larger size group, one diamond has a Type IIa (i.e. nitrogen content below the detection limit of FTIR spectrometer) core (Fig. 4.11). Apart from this exceptional sample, the colourless cores of all other diamonds belong to pure Type IaA, with an A-centre proportion of 100 %.

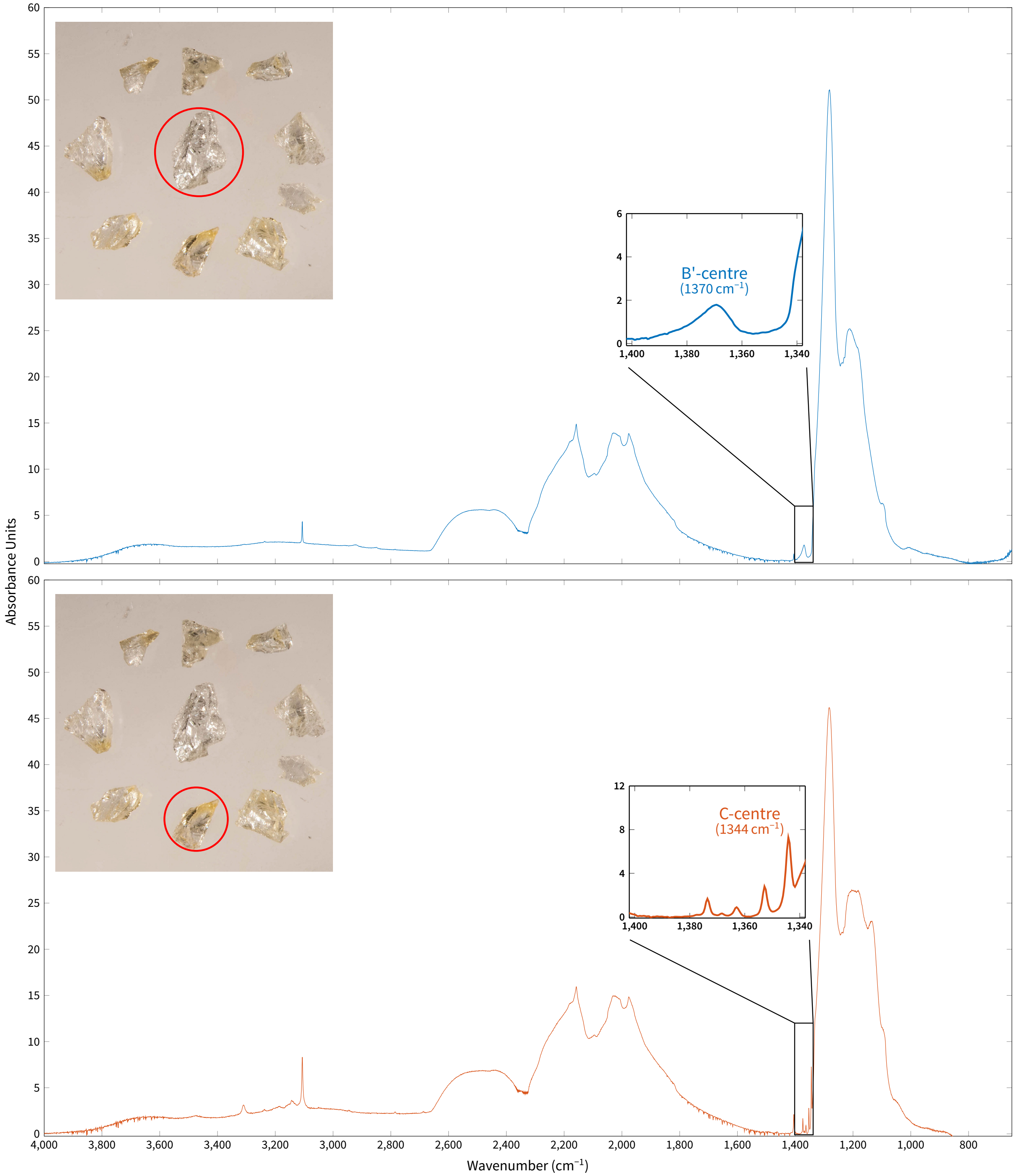

Figure 4.9: IR spectra of colourless core (top) and yellow periphery (bottom) of MS-S50.

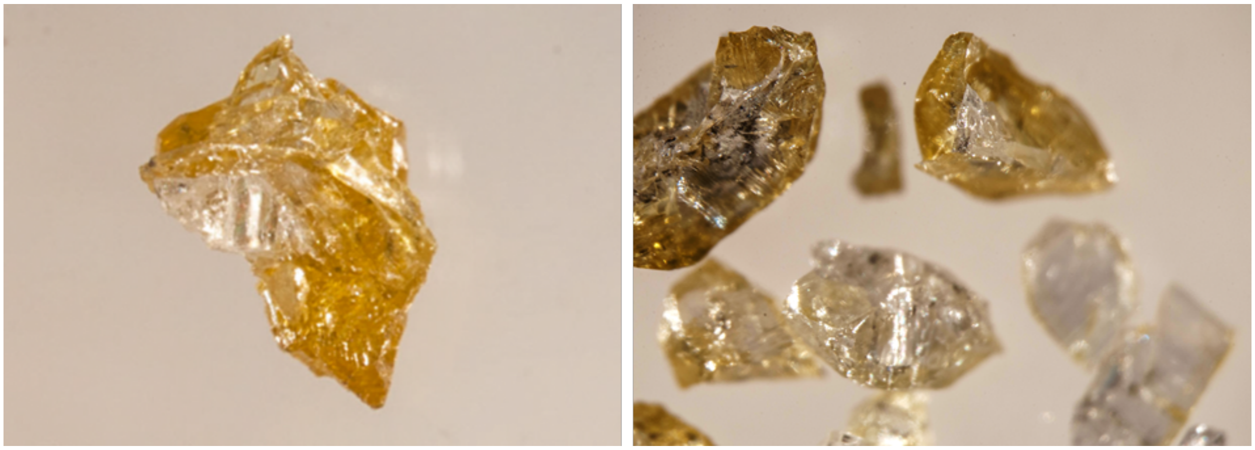

Figure 4.10: Examples of crushed diamonds in the larger size group (3 – 5 mm) revealing their colourless cores: (left) MS-L10 and (right) MS-L14. Co-existing B'- and C-centres were observed.

4.4.2. Diamond fluorescence by UV light excitation

Forty-two out of 71 diamonds (59 %) display observable fluorescence in three colours – yellow (93 %), greenish yellow (5 %) and purple (2 %), when excited by LWUV light with a wavelength of 365 nm. No phosphorescence was observed. Diamonds fluoresce with various intensities, however, none of them exhibit a strong level of fluorescence; the majority show medium intensities at most, with some exhibiting weak fluorescence.

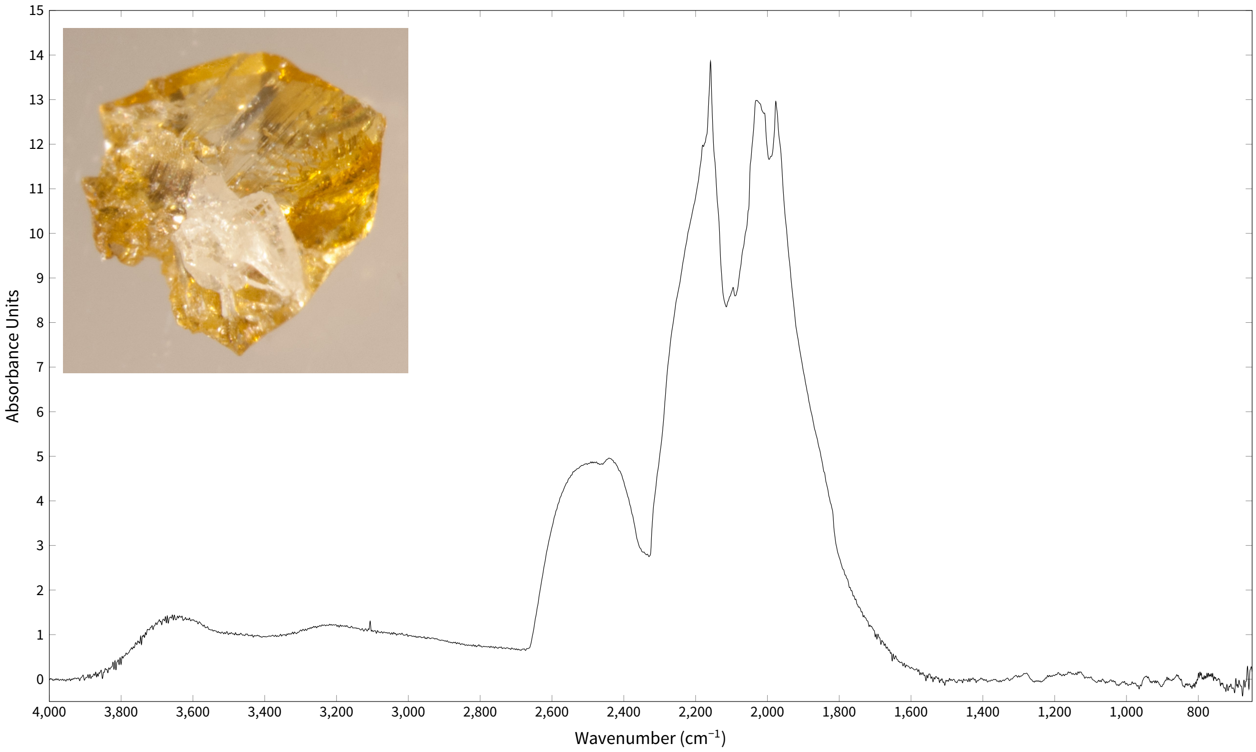

Figure 4.11: The colourless core of MS-L19 as exposed after crushing. IR spectrum shows that the core is Type IIa.

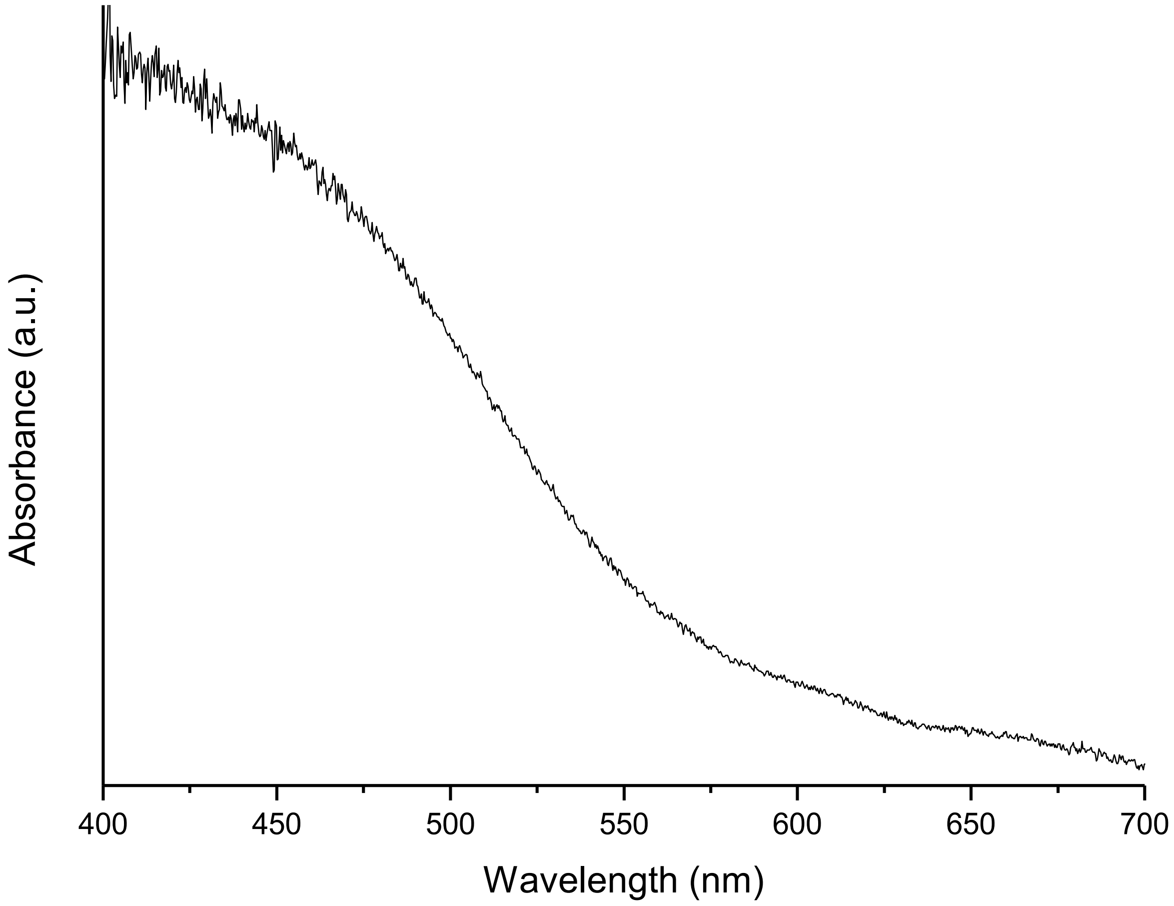

Figure 4.12: The visible absorption spectrum of MS-S5, which is a mixed Type Ib/IaA diamond, showing an absorption continuum towards the shorter wavelengths.

4.4.3. UV-VIS-NIR spectroscopy

Visible absorption spectra of selected diamonds from the smaller size group show that all mixed Type Ib/IaA diamonds display a similar absorption feature – a continuous rise from near-IR towards the shorter wavelengths of the visible spectrum (Fig. 4.12).

4.4.4. CL imaging and SIMS analysis

To further investigate the internal growth structures and growth histories of the diamonds, they were selected based on their IR absorption spectra for additional CL imaging and SIMS analysis. The carbon isotopic ratio ($\delta^{13}C$ in ‰) and the nitrogen concentration (at. ppm) are indicated above and underneath each spot, respectively, in the following annotated CL images. The CL images are categorized into four main groups (and three sub-groups) according to the spectral features and growth patterns displayed.

4.4.4.1. Mixed Type Ib/IaA diamonds

(i) Homogeneous CL

Diamonds in this group with homogeneously dark CL images display a range of δ^{13}C from −5.8 to −3.6 ‰, with median and average values of −4.9 and −4.8 ‰ respectively (Fig. 4.13). There is no significant variation in the carbon isotope compositions and nitrogen contents between different spots on individual diamonds.

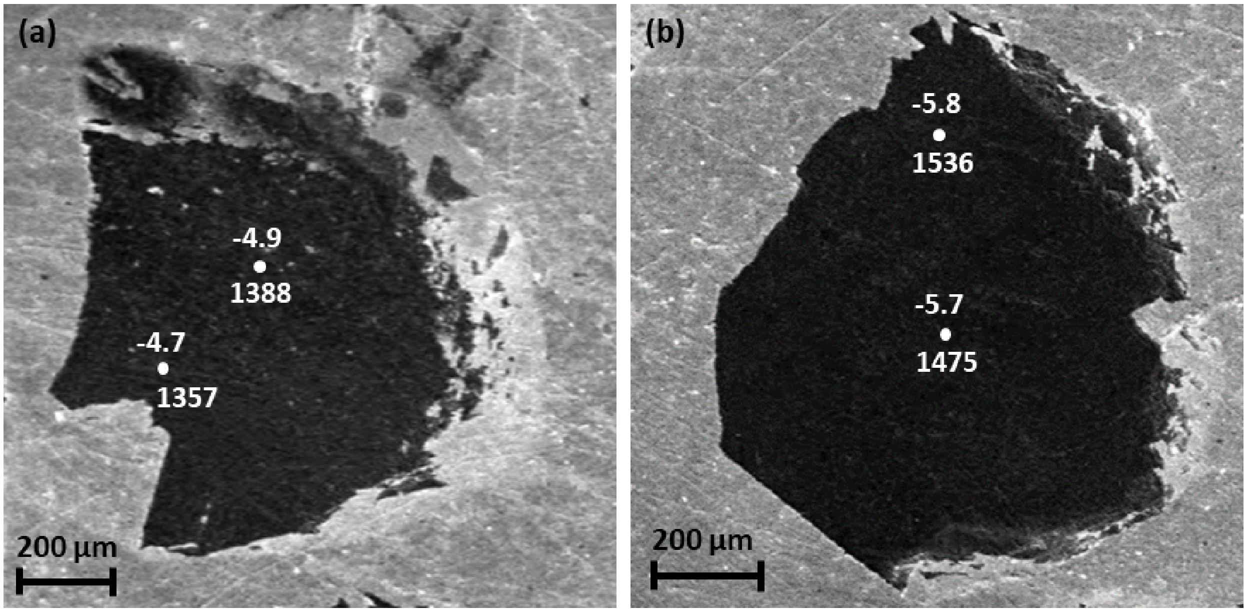

Figure 4.13: Examples of C-centre bearing diamonds that show homogeneous CL: (a) MS-S41 and (b) MS-S3.

(ii) Growth zoning

Growth zones of alternating brightness levels can be observed in some diamonds, but the CL images are dark overall (Fig. 4.14). δ^{13}C ranges from −5.5 to −3.2 ‰, with median and average values of −4.9 and −4.7 ‰ respectively. These carbon isotope compositions are similar to those of diamonds with homogeneous CL.

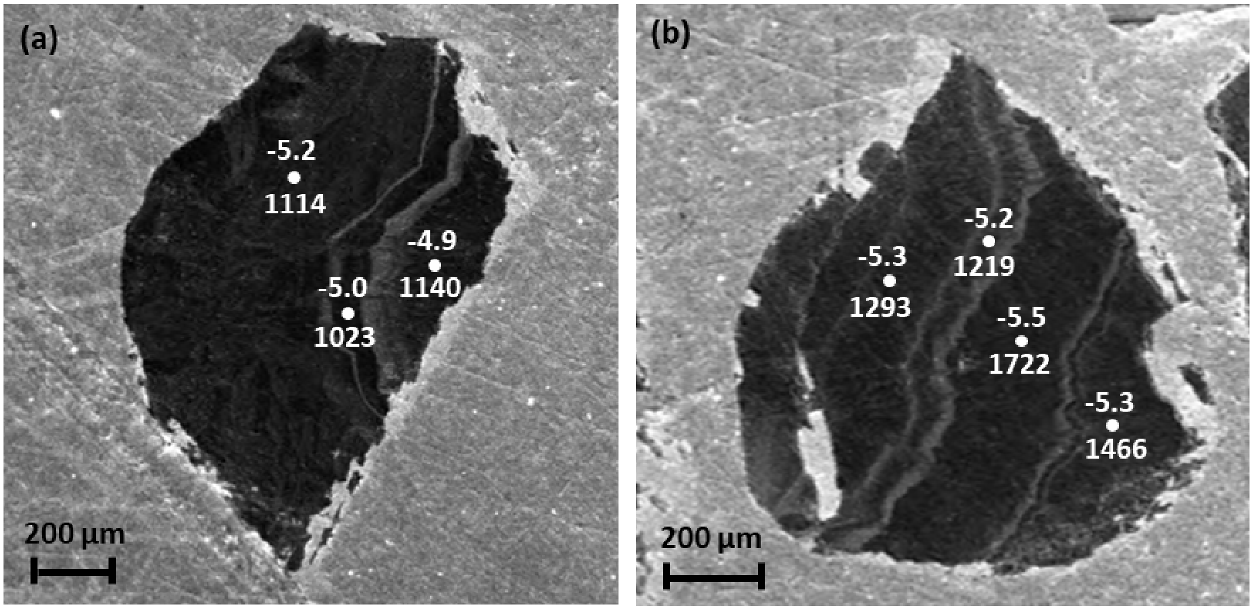

Figure 4.14: Examples of C-centre bearing diamonds that show growth zoning: (a) MS-S2 and (b) MS-S4.

(iii) Combination of brighter core and dark rim

Diamonds in this group possess colourless cores (Type IaA) enclosed by yellow outer layers (mixed Type Ib/IaA). The range of δ^{13}C is slightly larger than that in the above sub-groups, spanning from −6.3 to −2.9 ‰, with median and average values of −4.2 and −4.4 ‰ respectively. All diamonds in this group display variations in nitrogen contents between their brighter cores and dark rims, where the difference is up to 3341 at. ppm (Fig. 4.15).

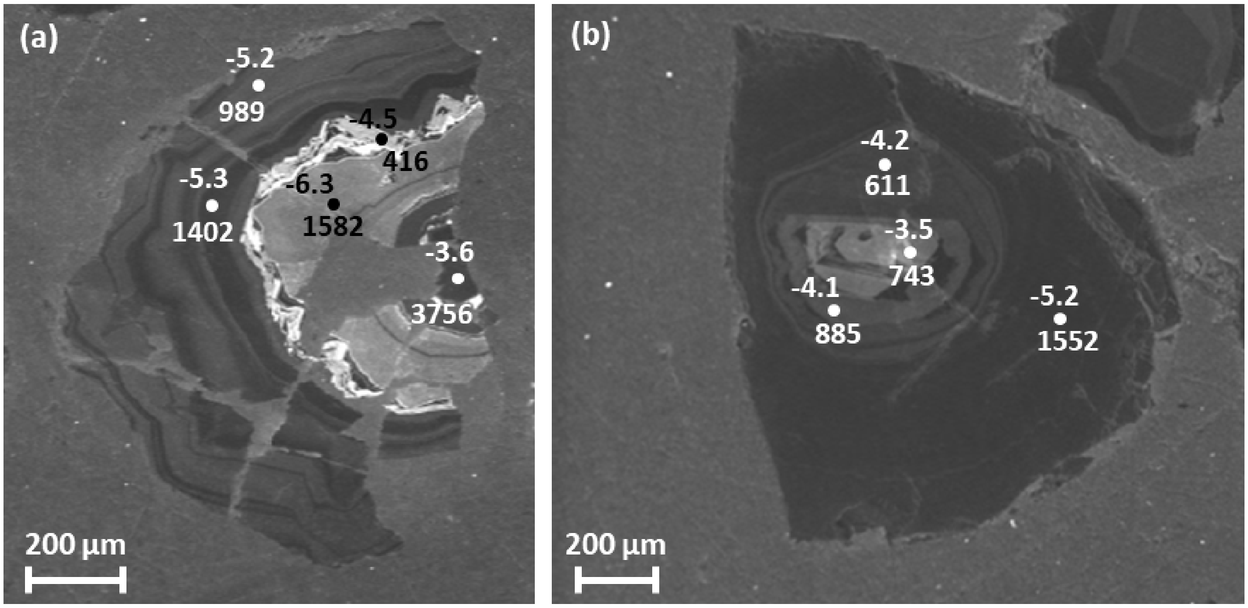

Figure 4.15: Examples of C-centre bearing diamonds that show cores with brighter CL: (a) MS-S56 and (b) MS-S7.

4.4.4.2. Diamonds with co-existing B′- and C-centres

Bright cores and dark rims are observed in all diamonds in this category (Fig. 4.16). $\delta^{13}C$ ranges from −5.4 to −3.9 ‰, with median and average values of −4.9 and −4.8 ‰ respectively. Although the variation of $\delta^{13}C$ between the bright core and dark rim of individual diamond is not significant, distinct total nitrogen concentration (differences up to 753 at. ppm) between different growth zones are observed on all diamonds in this group.

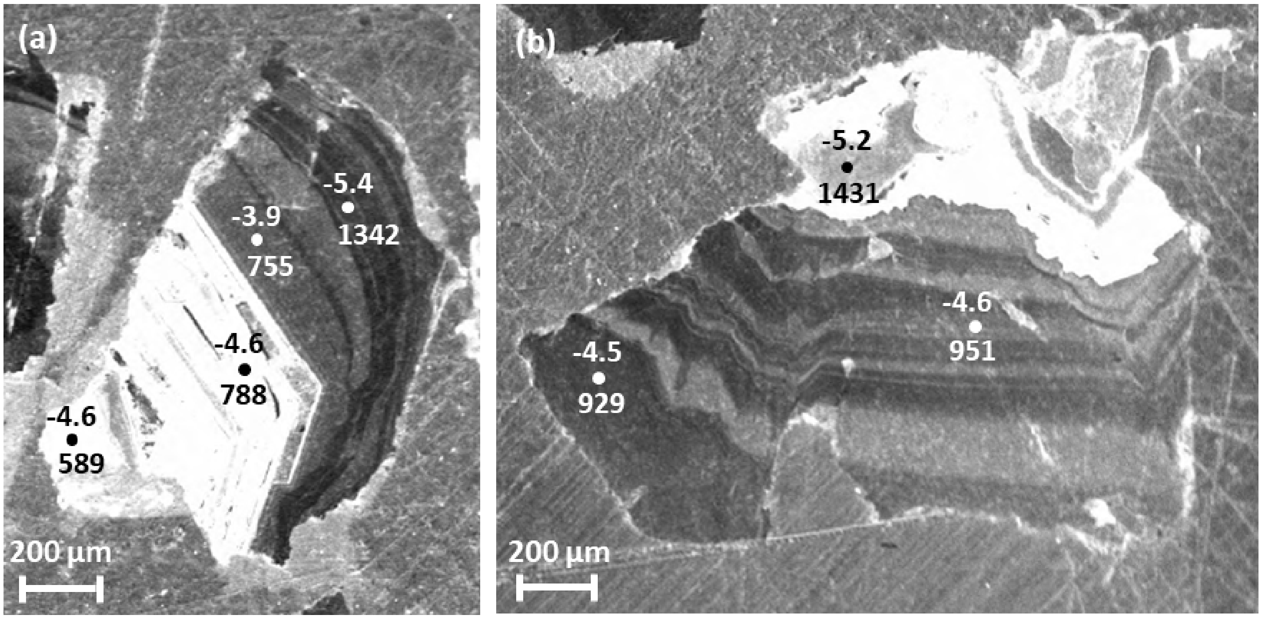

Figure 4.16: Examples of diamonds with co-existing B'- and C-centres, that show bright cores and darker rims: (a) MS-L14 and (b) MS-L18.

4.4.4.3. B′-centre containing diamonds with growth zones

Some B′-centre bearing Type Ia diamonds show concentric growth bands with contrasting brightness levels. The brightness decreases from the core to the outer growth zones (Fig. 4.17). $\delta^{13}C$ ranges from –4.9 to –3.0 ‰, with median and average values of –4.3 and –4.1 ‰ respectively.

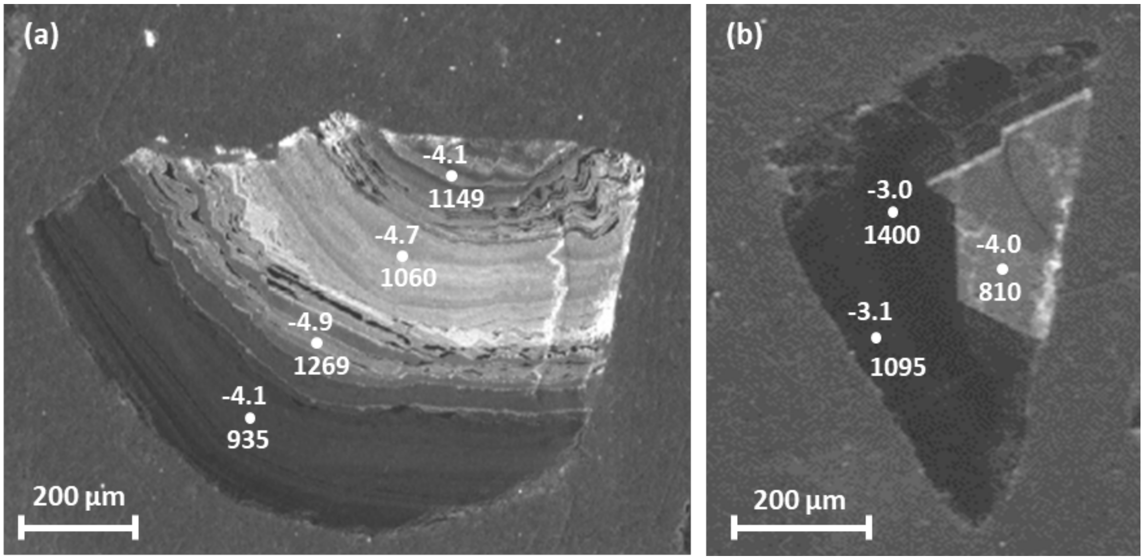

Figure 4.17: Examples of B'-centre containing Type Ia diamonds that show concentric growth bands with contrasting brightness levels: (a) MS-S18 and (b) MS-S20.

4.4.4.4. An unusual C-centre containing diamond with a Type IIa core

One diamond (MS-L19) shows a colourless Type IIa core surrounded by a mixed Type Ib/IaA yellow outer layer. Before crushing, this diamond had a tetrahexahedral external morphology (resorbed cuboid) while the internal structure shows that the core is octahedral, indicating a switch in growth habit. The distinct growth zones display huge difference between their carbon isotope compositions (Fig. 4.18(a)). The core has an average δ^{13}C value of –26.2 ‰ while δ^{13}C of the outer growth zone is −5.0 ‰. A dislocation-related CL pattern is observed in the Type IIa core, along with blue luminescence in colour CL imaging (Fig. 4.18(b)).

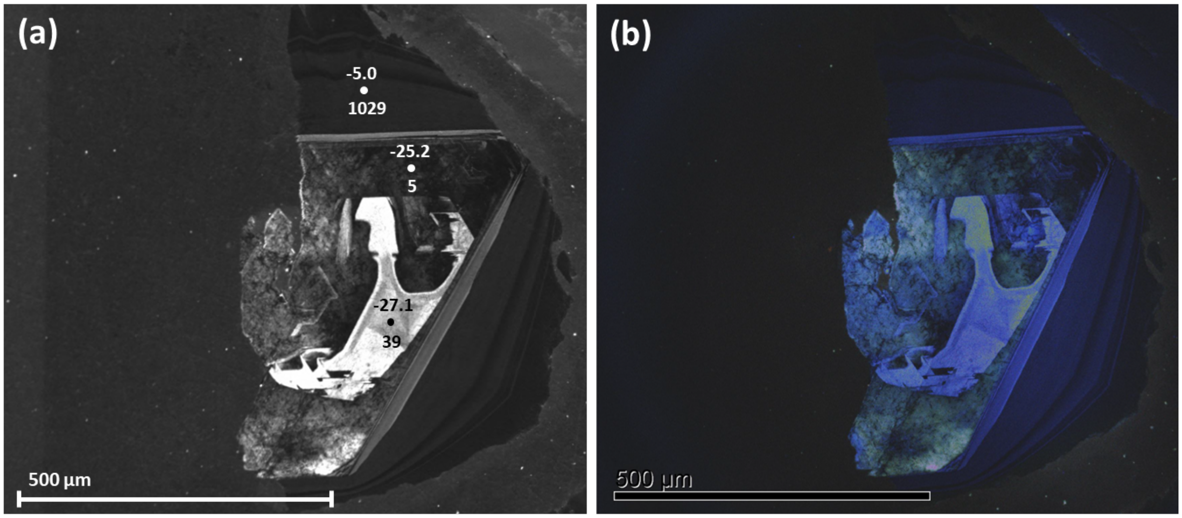

Figure 4.18: CL images of MS-L19 that possesses a colourless Type IIa core: (a) annotated grayscale image and (b) colour image.

4.5. Discussion

4.5.1. IR absorption features

4.5.1.1. Peaks observed in C-centre bearing diamonds

The group of subtle peaks in the range of 1353 to 1387 cm^{-1} is found always accompanying the C-centre peaks in yellow diamonds from Misery. An identical observation was also reported in Chapter 3 for diamonds from CH-7 at Chidliak, linking this feature to natural, mixed Type Ib/IaA yellow diamonds.

4.5.1.2. Relationship between B′- and B-centres in Type Ia diamonds

In "regular" diamonds, the integrated absorption of the B′ peak and the concentration of nitrogen in B-centres demonstrate a linear proportionality (Woods, 1986; refer to Section 3.4.1 in Chapter 3 for a detailed explanation of "regular" and "irregular" diamonds). Thus, a plot of the baseline corrected peak areas of the B′ peak (cm^{-2}) against the concentration of nitrogen in B-centres (at. ppm) is used to verify whether this linear proportionality can be established for Misery diamonds (Fig. 4.19). From this plot, it can be observed that only two diamonds fall on the trend line, suggesting that the diamonds experienced platelet degradation as a result of transient heating and/or shear stresses during mantle residence, and can be categorized as "irregular" diamonds (Woods, 1986). The results agree with a previous study conducted on Misery diamonds, in which the vast majority of diamonds did not show a correlation between the integrated absorption of B′-centre and concentration of nitrogen in B-centres (Krebs et al., 2016). As a consequence of widespread platelet degradation, the integrated absorption strength of the N3 centre in the visible absorption spectra cannot link to that of the B′-centre in these diamonds (Woods, 1986).

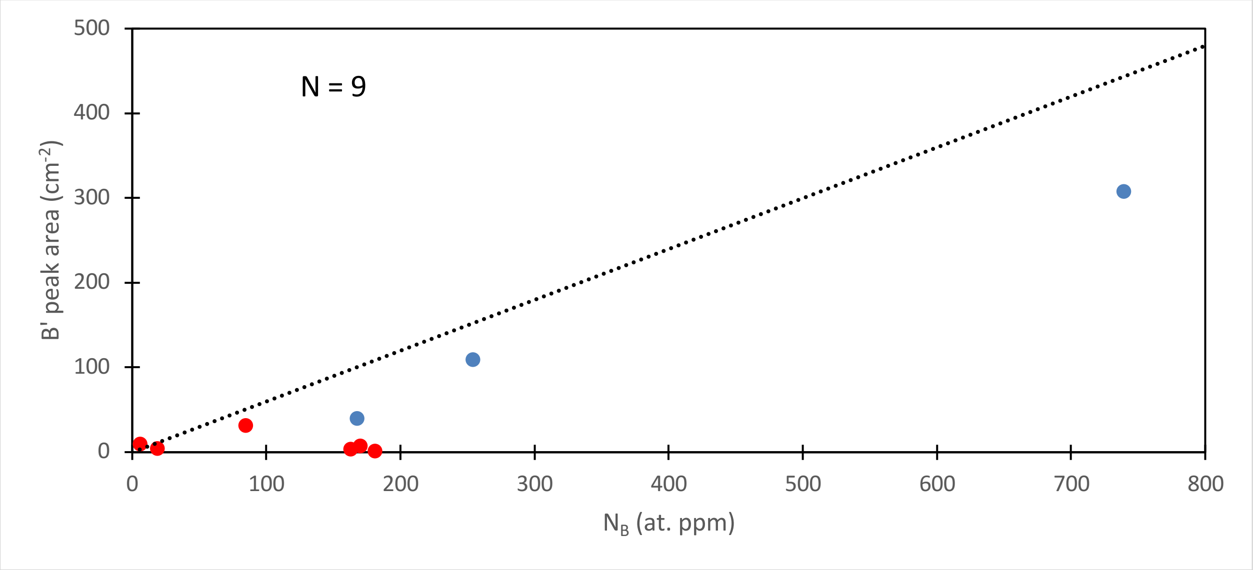

Figure 4.19: Plot of B' peak area against concentration of nitrogen in B-centres (N_B) of nine B'-centre bearing diamonds. Red dots represent diamonds in the smaller size group, while blue dots represent diamonds in the larger size group. The trend line with a slope of 0.6 represents the linear proportionality between the integrated absorption of the B' peak and concentration of nitrogen in B-centres, deduced from the experimental results of Woods (1986).

4.5.1.3. Relationship between 3107 cm^{-1} absorption and nitrogen concentration

It has been suggested that the peak at 3107 cm^{-1} is related to nitrogen impurities (Fritsch et al., 2007; Goss et al., 2014), especially the presence of B-centres (Dobrinets et al., 2013). Plotting the baseline corrected peak area of the 3107 cm^{-1} absorption peak against total nitrogen concentration (Fig. 4.20) and B-centre concentration (Fig. 4.21) for Misery yellow diamonds, however, does not indicate such a correlation.

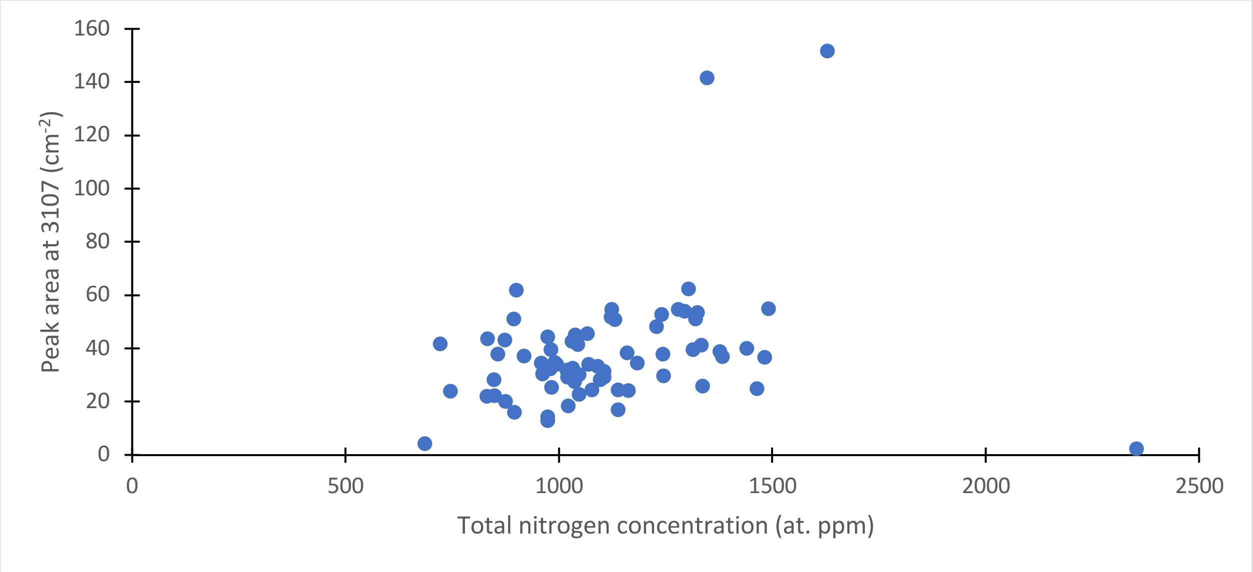

Figure 4.20: Plot of peak area at 3107 cm^{-1} against total nitrogen concentration for 71 diamonds.

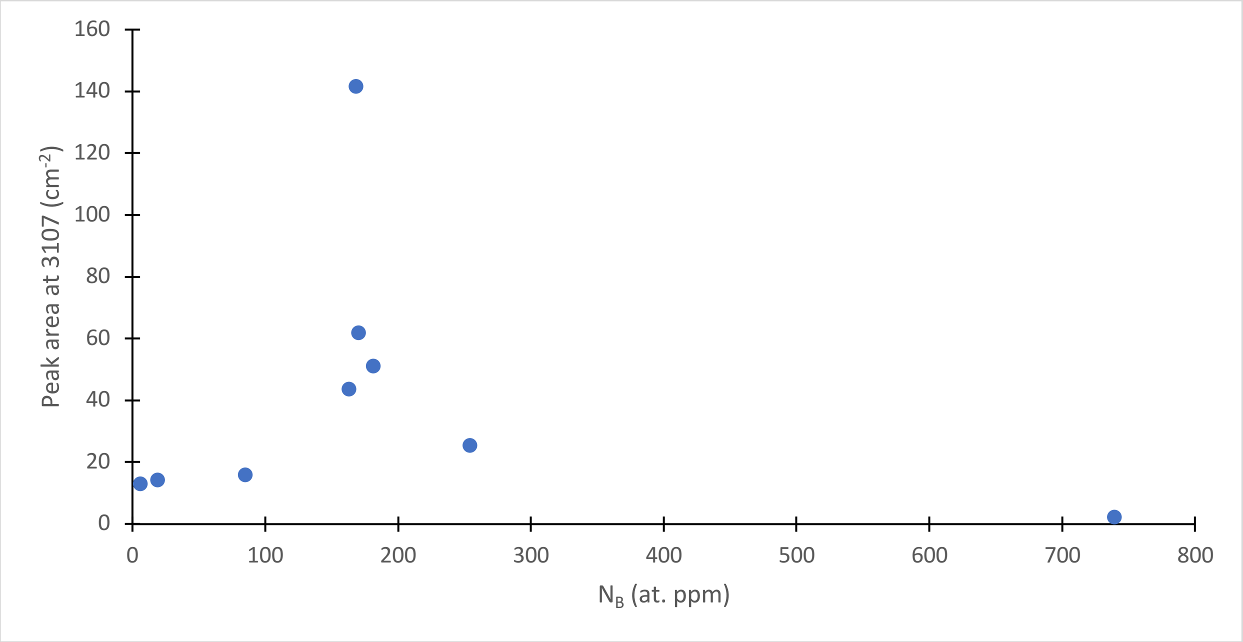

Figure 4.21: Plot of peak area at 3107 cm^{-1} against concentration of nitrogen in B-centres (N_B) for nine diamonds.

4.5.1.4. Co-existing B′- and C-centres

The combination of colourless cores (with A-, B- and B′-centres) and yellow outer layers (with A- and C-centres) found in Misery yellow diamonds suggests that they have undergone temporally distinct growth events similar to the two growth stages reported for Chidliak diamonds (Chapter 3). The fact that the same observation is also made on diamonds from the larger size group (3 – 5 mm) implies that episodic growth is not just a feature limited to small diamonds.

4.5.2. Fluorescence properties

Fluorescence properties provide additional information on the causes of body colours of diamonds, as it is common for diamonds to possess a mixture of colour-causing optical centres and many of these centres cannot be detected with FTIR.

4.5.2.1. Yellow and green fluorescence

Yellow and greenish yellow fluorescence colours were the most common colours observed in C-centre bearing diamonds in the study of Hainschwang et al. (2013). Yellow fluorescence can be caused by several defects, such as the 480 nm band (Collins and Mohammed, 1982; Dobrinets et al., 2013) and nickel-related S1, S2 and S3 centres. These nickel-related defects can also produce yellowish green to green fluorescence (Fritsch et al., 2007; Dobrinets et al., 2013). Additionally, green fluorescence can probably originate from the H3 centre (a vacancy between two substitutional nitrogen atoms in a neutral charged state) (Shigley and Breeding, 2013). These centres were previously detected in some yellow diamonds with Type Ib characteristics (Hainschwang et al., 2013).

4.5.2.2. Purple fluorescence

Purple fluorescence is observed in a Type IaAB diamond (MS-L1) with strong B′-centre related absorption (peak area of 308 cm^{-2}) in the larger size group. It is known that the B′-centre is associated with N3 centre. Although their intensities cannot be directly linked for "irregular" diamonds (refer to Section 4.5.1.2), it cannot be ruled out that N3 centre exists in these diamonds. The N3 centre is responsible for blue fluorescence and it can combine with one or more optical centres to form purple fluorescence, such as the NV^{-} centre, that gives pink to red fluorescence, or the NV^{0} centre, that produces an orangey fluorescence.

4.5.3. Visible light absorption features

C-centres are effective in visible light absorption, so mixed Type Ib/IaA diamonds with concentration of C-centres over 0.1 at. ppm display a similar absorption continuum increasing from long to short wavelengths, which is the main cause of their yellow body colour.

The 480 nm band does not exist in any of the spectra, meaning that it is not related to the yellow fluorescence nor the body colour of those diamonds. Unlike the 480 nm band, which appears as a recognisable broad absorption band (refer to Section 3.4.3 in Chapter 3), other defects mentioned in the previous section appear as sharp peaks, which are only detectable by UV-VIS-NIR spectroscopy when the concentrations of such defects are sufficiently high (Hainschwang et al., 2013). Thus, the absence of these peaks in the visible absorption spectra of diamonds with yellow to greenish yellow fluorescence is probably due to low concentrations of the respective centres and overall weak signals detected from small diamonds that make the low absorption of these defects unidentifiable.

4.5.4. Cathodoluminescence (CL) features

4.5.4.1. Ordinary mixed Type Ib/IaA diamonds

Many of these diamonds show homogeneous dark CL. Occasionally, wavy growth bands with slightly brighter CL are also observed. Homogeneous dark CL is a typical feature for mixed Type

Ib/IaA diamonds which do not possess defects that allow for emission in the visible light spectrum. This is the reason why these diamonds do not show fluorescence under LWUV excitation either (only 59 % among all yellow diamonds in this study show observable fluorescence; refer to Section 4.4.2).

4.5.4.2. Combination of dark rim and brighter core

(i) Mixed Type Ib/IaA diamonds with Type IaA or Type IaAB cores

A bright core and dark rim observed in CL images of individual diamonds and significant differences in nitrogen content between separate growth layers provide evidence that these diamonds have multi-stage growth histories. The N3 centres are likely the cause of the bright CL of the cores, and the dark outer layers result from CL inactive C-centres.

(ii) Type IaAB diamonds

Concentric growth bands with decreasing CL brightness levels from core to rim indicate that these diamonds also have undergone multiple growth events, with stages of resorption occurring in between. The older cores acted as seeds for further crystallization. As the cores have resided in the mantle for a much longer amount of time, they possess more aggregated nitrogen (and B′- and N3 centres) compared to the rims, explaining the decreasing brightness levels in the rims.

(iii) Mixed Type Ib/IaA diamond with a Type IIa core

A strongly ^{13}C depleted core and mantle-like δ^{13}C in the outer layer are strong evidence that this diamond precipitated from more than one diamond forming fluid. The bright area of the Type IIa core is likely associated with the A-band, which is related to lattice dislocations as a result of plastic deformation, and its luminescence is particularly intense in regions of low nitrogen content (Zaitsev, 2001).

The dislocation-related CL pattern in the Type IIa core is similar to the ones reported previously, which was described as “mosaic” (Sumida and Lang, 1981) or “fish-scale” patterns (Gaillou et al., 2012) and likely form due to interactions of different strain directions. Lattice dislocations are especially common in Type IIa diamonds, as the presence of A- and B-centres hardens the diamond lattice and restricts plastic deformation (Nailer et al., 2007).

4.5.5. Nitrogen aggregation state and mantle residence time

Sixty-two diamonds contain 3 to 28 % of C-centres (equivalent to 72 to 97 %A) and thus are Type Ib/IaA. Of these, four diamonds are found to have colourless cores with B′-centres (Fig. 4.22).

Nine diamonds exhibit B′-centres, of these six diamonds classify as Type IaAB and three diamonds have a B-centre proportion < 10 % and hence are categorized as Type IaA. The aggregation states of the Type IaA and Type IaAB diamonds range from 1 to 31 %B (Fig. 4.23).

The mantle residence time of diamonds is calculated by inserting the total nitrogen concentration and the A- (for C- to A-centre aggregation) or B- (for A- to B-centre aggregation) centre proportions into the Arrhenius equations, using an assigned time-averaged mantle residence

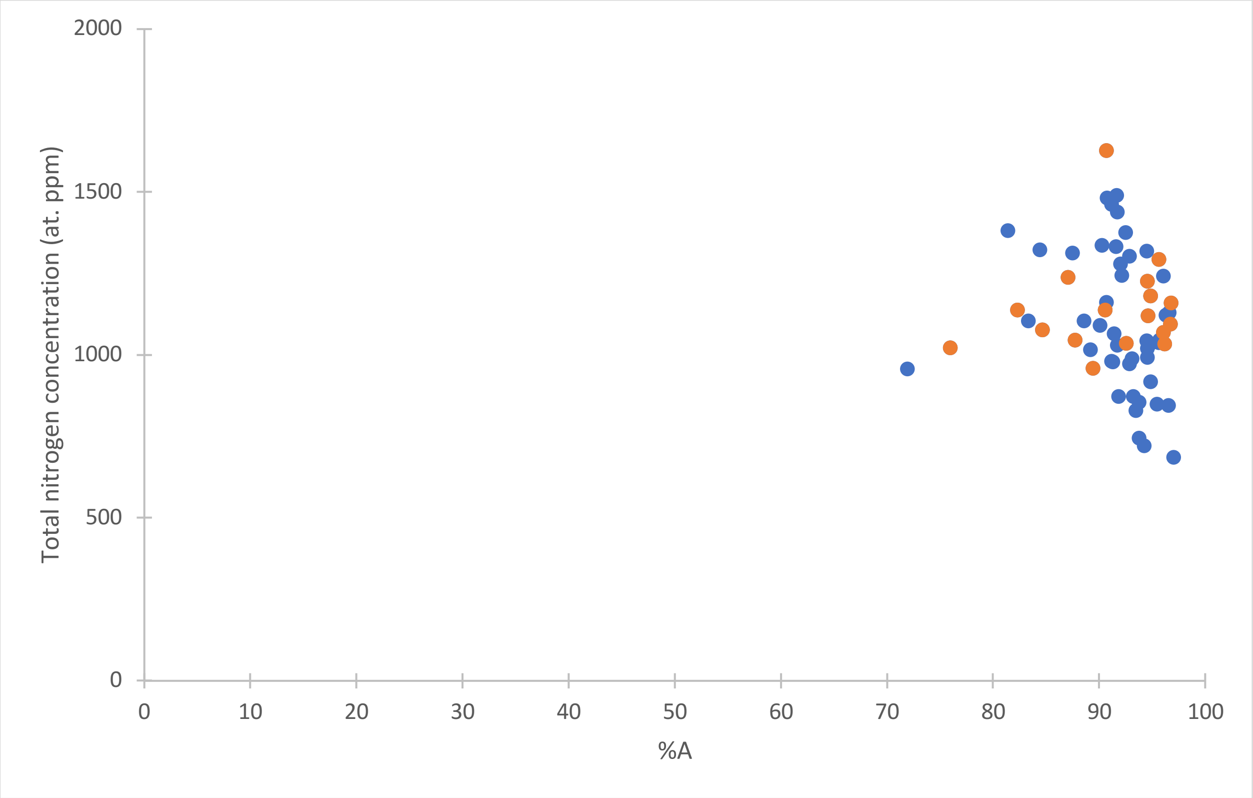

Figure 4.22: Plot of total nitrogen concentration (at. ppm) of Type Ib/IaA diamonds against their aggregation states, represented by %A. Orange dots represent diamonds in the larger size group, while blue dots represent diamonds in the smaller size group.

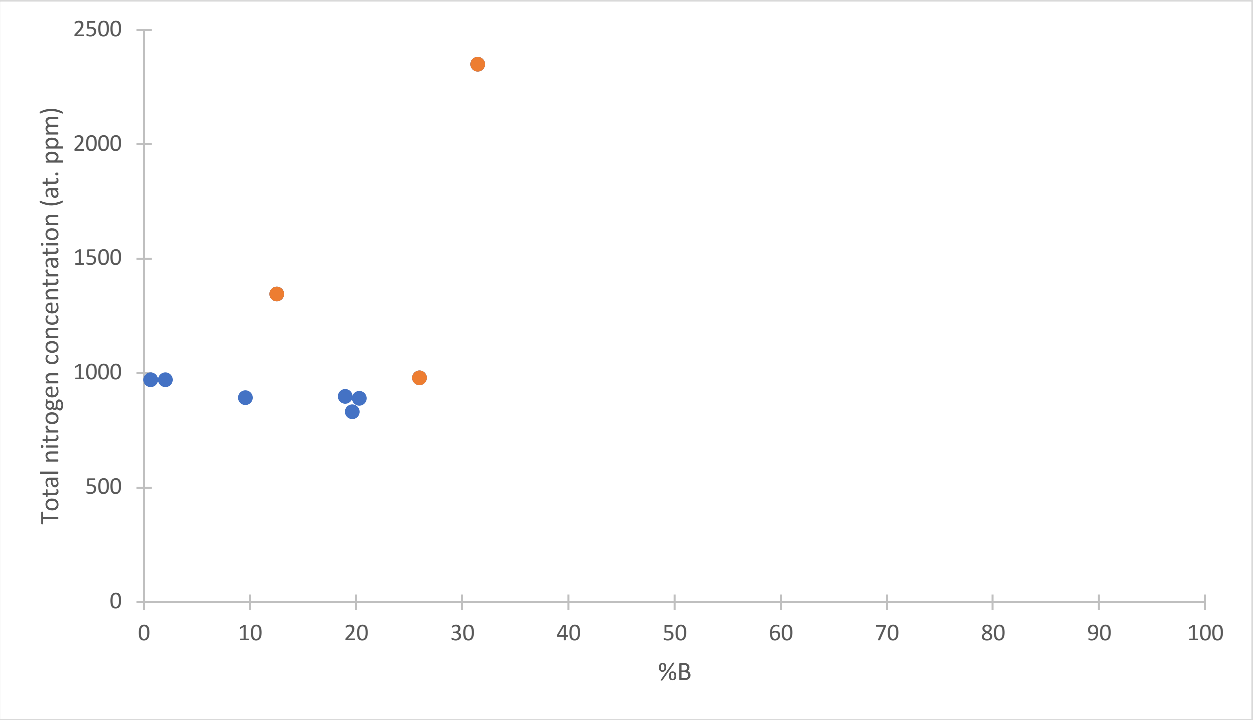

Figure 4.23: Plot of total nitrogen concentration (at. ppm) of Type IaA and Type IaAB diamonds against their aggregation states, represented by %B. Orange dots represent diamonds in the larger size group, while blue dots represent diamonds in the smaller size group.

temperature (Taylor et al., 1990; Taylor et al., 1996; Leahy and Taylor, 1997). A previous study on Misery diamonds indicated a range of time-averaged mantle residence temperatures between 1030 and 1320 °C, with the vast majority falling in the range of 1050 to 1125 °C (Krebs et al., 2016). Based on this result, the time-averaged mantle residence temperature adopted for the estimation of the mantle residence times of diamonds is 1100 °C. Note that this value is just an assumption to investigate the disparity between the residence times of diamonds with different nitrogen aggregation states, especially for the cases of colourless cores enclosed by yellow outer layers.

Experimental data show that the aggregation rate from C- to A-centres is dependent on the morphology of diamonds, with cube sectors requiring a higher activation energy than octahedral sectors (Taylor et al., 1996). Thus, irregular shaped diamonds were not included in the calculation unless they showed clearly recognizable cubic or octahedral faces, documented by surface features such as tetragons or trigons, respectively. It is observed that all C-centre bearing diamonds with identifiable morphology are cuboids and that irregular shaped diamonds with surface features that allow classification all possess tetragons, i.e., were originally cuboids as well.

Based on their types, diamonds are categorized into three groups for calculation of their mantle residence times: (i) Type IaA and Type IaAB; (ii) Type Ib/IaA; and (iii) Type Ib/IaA outer layer with Type IaA or Type IaAB core. Type IaA growth zones with 100 % A-centres were assigned a B-centre proportion of 0.5 % for estimation of mantle residence times. The mantle residence times of diamonds with 3 – 5 mm and < 3 mm sizes are shown separately below. However, due to limited sample size and a limitation to only yellow diamonds, the statistics demonstrated here do not necessarily reflect the general trends of the mantle residence times of all Misery diamonds.

For diamonds of size 3 – 5 mm: the first group ranges from about 0.5 to 1.8 Ga, with a median value of 0.9 Ga; the second group spans a range of approximately 12,000 to 67,000 years, with a median value of 40,000 years; the third group has a range for outer layers from around 7,000 to 51,000 years, with a median value of 16,500 years, whereas for the cores the range is approximately 0.02 to 0.5 Ga, with a median value of 0.03 Ga.

For diamonds of size < 3 mm: the first group has a range of about 0.05 to 1.5 Ga, with a median value of 0.9 Ga; the second group ranges from around 6,000 to 65,000 years, with a median value of 24,000 years; the third group has a range for outer layers from approximately 6,000 to 52,000 years, with a median value of 21,000 years, whereas the cores span a range of around 0.02 to 0.2 Ga, with a median value of 0.03 Ga.

It is observed that the median values are similar for diamonds in the larger and smaller size groups, implying that the two size groups likely originated from the same diamond population and thus can be studied as a whole.

The second group and the Type Ib/IaA overgrowths in the third group share a similar range of mantle residence times, suggesting that they might have formed at about the same period of time from the same diamond forming fluids, and thus have a common origin.

The cores in the third group show a mantle residence time range overlapping with that of the first group at the younger end of the range, which means the younger or shallower diamonds in the first group might have formed together with the cores at around the same period of time, providing they had resided at about the same depth in the mantle with the same time-averaged mantle temperature. The calculation of mantle residence times is, however, sensitive to the time-averaged mantle temperature: a decrease in residence temperature by 50 °C can result in an increase of residence time from 0.1 to 1 Ga. Thus, the relatively broad range of mantle residence time in the first group is likely due to the diamonds crystallizing at different depths in the mantle, where mantle residence temperatures increase with depth along a conductive geotherm.

In addition, the concentric growth zoning with contrasting CL brightness and variations in carbon isotope composition between different growth zones observed in some B′-centre bearing diamonds (refer to Section 4.4.4.3) indicate that they have undergone episodic growth, and thus every growth layer of a single diamond might have resided in the mantle for different lengths of time. Given that the total nitrogen concentration and aggregation state are calculated from the IR spectrum of diamond, which is an integrated signal collected over the optical path of the diamond, one should bear in mind that a false value of mantle residence time may be deduced from an episodic diamond.

4.5.6. Carbon isotope composition

The overall range of $\delta^{13}C$ in Misery diamonds is from −27.1 to −2.9 ‰, with a mode and median at −4.9 ‰ and −4.8 ‰, respectively. In order to compare the carbon isotope compositions of different size groups, diamonds of size 3 – 5 mm and diamonds of size < 3 mm are considered separately.

For diamonds of size 3 – 5 mm, the range is between –27.1 to –3.3 ‰, with a median value of −4.8 ‰. Except for the Type IIa core of one diamond (MS-L19) which shows strong ^{13}C depletion, all data fall in the range of –6.0 to –3.3 ‰.

For diamonds of size < 3 mm, the range is from –6.6 to –2.9 ‰, with a median value of −4.9 ‰. The results show that diamonds of smaller and larger sizes indeed share a similar range of carbon isotope composition and median value.

The distribution of $\delta^{13}C$ displayed by Misery diamonds is similar to that observed from peridotitic diamonds worldwide (Fig. 4.24), where all diamonds except the core of MS-L19 lie in a confined range that agrees with the range of mantle values (−8 to −2 ‰; Cartigny, 2005), suggesting that Misery diamonds predominantly formed from a peridotitic source.

The results are consistent with a previous study on Misery diamonds and their mineral inclusions, where the diamonds also mainly derived from peridotitic sources (approximately 81% of studied diamonds have peridotitic inclusions; Chinn et al., 1998). However, about 16% diamonds with eclogitic inclusions were recovered from Misery and among these a minor proportion has $\delta^{13}C$ values in the range of mantle carbon (Chinn et al., 1998). Thus, it cannot be ruled out that some of the analyzed diamonds might actually have an eclogitic instead of a peridotitic origin.

The unusual diamond (MS-L19) found in this study, which has a colourless Type IIa core and a yellow outer layer with $\delta^{13}C$ values of –27.1 ‰ and –5.0 ‰, respectively, is believed to have formed in two distinct diamond fluids at different periods of time. There are two possibilities: (i) the core formed in an eclogitic source, then after residing in the mantle for a period of time, a mantle-derived fluid reached the diamond and formed an overgrowth on it; or (ii) the core and outer layer both precipitated from diamond fluids of eclogitic origin but with highly distinct $\delta^{13}C$ values and nitrogen contents.

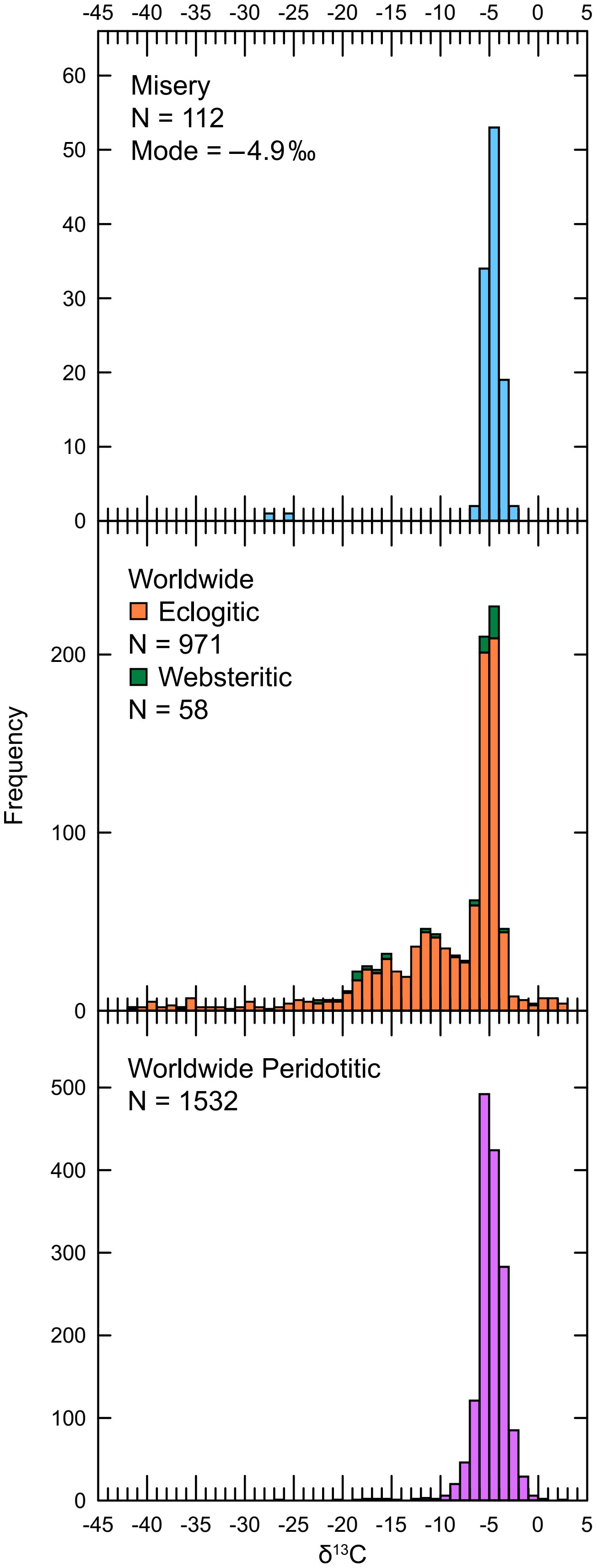

Figure 4.24: Distribution of δ^{13}C values in Misery yellow diamonds, compared to eclogitic, websteritic and peridotitic diamonds worldwide (from the database of Stachel et al., 2017). The mode of δ^{13}C values in Misery yellow diamonds is calculated using Isoplot (Ludwig, 1999).

4.6. Conclusions

Misery yellow diamonds generally have high nitrogen concentrations, showing a median value of 1066 at. ppm. They are also rich in hydrogen, judging from the IR absorption at 3107 cm^{-1}, where the median integrated peak area is 35 cm^{-2}. Considering the similarities in all the data collected from two size groups of Misery yellow diamonds, they likely originated from the same diamond population and hence their data can be summarized as a whole.

Misery yellow diamonds are dominated by mixed Type Ib/IaA – 62 diamonds (87 %) are Type Ib/IaA with an A-centre proportion between 72 and 97 %; nine diamonds (13 %) are Type IaA or Type IaAB, with a B-centre proportion between 1 and 31 %. All Type Ib/IaA diamonds for which a primary shape was fully, partially preserved are cuboids and all irregular-shaped diamonds for which surface characteristics allowed assignment of a primary morphology were also cuboids.

Among the Type Ib/IaA diamonds, four diamonds are found to have colourless cores which contained B′-centres, five diamonds possess colourless cores of pure Type IaA, and one diamond has a colourless Type IIa core. The combination of colourless cores and yellow outer layers is strong evidence of diamond formation in at least two growth events, where the most extreme mantle residence time difference is 0.5 Ga (core) and 7,000 years (outer layer), assuming a time-averaged mantle residence temperature of 1100 °C.

C-centre containing diamonds usually show dark homogeneous CL, growth bands of alternating brightness levels can be observed occasionally. Combinations of bright core and dark rim observed in CL images of numerous diamonds support the interpretation of episodic diamond growth. Yellow diamonds formed in two temporally distinct growth events have previously been observed at Chidliak (Chapter 3) and Qilalugaq (Banas et al., 2017), suggesting that this characteristic is possibly common among yellow diamonds recovered from Canada's Arctic, or even worldwide.

Apart from the core of one diamond, which shows an exceptionally low $\delta^{13}C$ value of −27.1 ‰, Misery diamonds generally display a confined $\delta^{13}C$ range between –6.6 and –2.9 ‰, suggesting that they are predominantly derived from peridotitic sources. The highly ^{13}C depleted core (−27.1 ‰) indicates the likelihood that some eclogitic diamonds exist in the sample sets. This diamond might have crystallized in an eclogitic source from subducted carbon, and then formed an overgrowth layer ($\delta^{13}C$ of –5.0 ‰) during later infiltration of a mantle fluid. In any case, this unusual diamond serves as additional strong evidence of episodic diamond growth at Misery.

4.7. Future work

Mineral inclusion data should be collected from Misery yellow diamonds to better understand the mechanism of their formation and to confirm their source paragenesis. Moreover, collection of photoluminescence (PL) and CL spectra would provide additional information on the distribution of impurities on diamonds to better understand their growth structures.

5. Conclusions

5.1. Comparison of the two localities

Yellow diamonds from the Chidliak CH-7 and the Ekati Misery kimberlites are mostly nitrogen-rich, as both diamond sets have a median nitrogen content over 1000 at. ppm. CH-7 yellow diamonds display a wider range of nitrogen concentration (14 – 3782 at. ppm) compared to Misery yellow diamonds (685 – 2351 at. ppm).

Considering the spectral features, diamonds with discernible C-centre peaks or C-centre-related characteristics dominate in both yellow diamond sets (64 % for CH-7; 87 % for Misery). As C-centres absorb light effectively and even a very small portion in the lattice is enough to cause a vibrant yellow colour, they are considered the main cause of colouration for these diamonds.

It has been reported that natural diamonds containing C-centre are rare, comprising < 0.1 % of natural diamonds worldwide (Fritsch, 1998). However, the proportions in the CH-7 and Misery diamond suites (counting from the total number of diamonds received) are 4.3 % (94 out of 2164 diamonds) and 4.7 % (62 out of 1324 diamonds), respectively, which are significantly higher than the global proportion.

A-centre concentrations are generally high, with 67 % of CH-7 and 94 % of Misery yellow diamonds exhibiting an A-centre proportion ≥ 80 %. The high A-centre absorption may mask the C-centre peaks in IR spectra, making C-centres undetectable when a lower spectral resolution is used. Thus, a higher spectral resolution of 1 cm^{-1} is necessary for such measurements.

Although some diamonds tend to have a more intense yellow colour with higher concentrations of C-centres, this is not a universal rule as saturated yellow diamonds with comparatively low C-centre contents are also frequently observed. The fluorescence properties of these diamonds, such as the strong yellow to orange fluorescence detected in CH-7 yellow diamonds, associated with the 480 nm band or NV-centres, and the medium to weak, yellow to green fluorescence detected in both CH-7 and Misery yellow diamonds, possibly correlated to nickel-related defects or H3 centre, indicate that the existence of additional defects complement the colouration of these diamonds. Thus, C-centres are not the single decisive factor causing the body colour of some yellow diamonds and that a mixture of colour-causing optical centres should always be considered.

Type IaA or Type IaAB with B′-centres are not prevalent in yellow diamonds (18 % for CH-7; 13 % for Misery). Most of the Type Ia diamonds do not follow the linear proportionality between the integrated absorption of the B′ peak and concentration of nitrogen in B-centres. Thus, they are classified as "irregular" diamonds, which are thought to be a consequence of platelet degradation due to short-lived heating and/or shear stresses. As "irregular" diamonds do not demonstrate the linear proportionality between the strength of N3 centre and the integrated absorption of the B′ peak either, it is not possible to estimate the strength of N3 centre from that of the B′ peak in most of the yellow diamonds.

Episodically grown diamonds, composed of B′-centre containing colourless cores and C-centre containing yellow outer layers, are detected among CH-7 and Misery yellow diamonds. Nitrogen thermometry shows that the cores resided for a long time in the mantle before the outer layers formed, assuming a common time-averaged mantle residence temperature of 1100 °C. The cores exhibit mantle residence time ranges of 0.2 – 1.1 Ga and 0.02 – 0.5 Ga, while the yellow outer layers span a range of 5 – 34 years and 6,000 – 52,000 years for CH-7 and Misery diamonds, respectively. Based on the assumption of a common residence temperature of 1100 °C, the time difference between the episodic growth events is larger in CH-7 yellow diamonds compared to Misery yellow diamonds; the colourless cores at CH-7 resided in the mantle for a significantly longer period of time whereas their outer layers only formed shortly before kimberlite eruption.

CL images reveal the internal growth structure of diamonds, in which episodically grown diamonds with co-existing B′- (located at the core) and C-centres (located at the outer layer) show cores and rims with contrasting brightness levels. The bright cores emit blue luminescence in colour CL, which is believed to be associated with the N3 centre. Blue luminescence is also observed in the colourless Type IIa core of an unusual Misery yellow diamond, but it is more likely to be associated with the A-band, which is related to lattice dislocation as a result of plastic deformation. Luminescence originating from the A-band is particularly intense in regions of low nitrogen content and can be misinterpreted as blue luminescence generated by N3 centres, which has similar emission wavelengths.

Carbon isotopic compositions and nitrogen contents in distinct growth zones of numerous diamonds were found to be different, and the contrast in values is especially obvious in CH-7 yellow diamonds. This observation further consolidates the interpretation that many of the studied diamonds crystallized in at least two growth events, from different diamond forming fluids at distinct points of time. CH-7 yellow diamonds display a wider $\delta^{13}C$ range, between −18.7 and −3.6 ‰, with a mode at −6.3 ‰, than Misery yellow diamonds, which excluding an outlier show a $\delta^{13}C$ range between −6.6 and −2.9 ‰, with a mode at –4.9 ‰. One Misery diamond with a colourless Type IIa core is an exceptional case, where the core (−27.1 ‰) shows a strongly ^{13}C depleted signature, whereas the rim (−5.0 ‰) has $\delta^{13}C$ falling in the range of mantle values. The results suggest that CH-7 yellow diamonds may derive predominantly from eclogitic (or websteritic) substrates while Misery diamonds are mainly peridotitic. However, it should be noted that the $\delta^{13}C$ ranges for peridotitic, ecologitic and websteritic diamonds strongly overlapped. Thus, it is possible that some CH-7 yellow diamonds relate to peridotitic source rocks and that some Misery yellow diamonds originated from eclogitic sources.

5.2. Future Work

The existence of episodically grown diamonds in the larger size group (3 – 5 mm) of Misery diamonds indicated that this feature is not limited to small yellow diamonds. Moreover, the prevalence of episodically grown diamonds in CH-7 and Misery, and similar observations at Qilaluguq, suggest that many yellow diamonds formed in at least two temporally distinct growth events. In future studies, yellow diamonds from other localities outside Canada can also be examined to further investigate if this observation is restricted to Canada's Arctic or can be extended globally.

Bibliography

Aulbach, S., Stachel, T., Viljoen, S. K., Brey, G. P. and Harris, J. W. (2002). Eclogitic and websteritic diamond sources beneath the Limpopo Belt – is slab-melting the link? *Contributions to Mineralogy and Petrology* **143**, 56–70.

Banas, A., Stachel, T., Smit, K. V and Armstrong, K. (2017). Yellow and white diamonds from Qilalugaq kimberlites: two generations of diamond growth. *11th International Kimberlite Conference* 11IKC–4536.

Bleeker, W. (2003). The late Archean record: a puzzle in ca. 35 pieces. *Lithos* **71**, 99–134.

Blitz, J. P. and Klarup, D. G. (2002). Signal-to-noise ratio, signal processing, and spectral information in the instrumental analysis laboratory. *Journal of Chemical Education* **79**, 1358.

Boyd, S., Pillinger, C., Milledge, H. and Seal, M. (1992). C and N isotopic composition and the infrared absorption spectra of coated diamonds: evidence for the regional uniformity of CO_2-H_2O rich fluids in lithospheric mantle. *Earth and Planetary Science Letters* **108**, 139–150.

Breeding, C. M. and Shigley, J. E. (2009). The 'Type' classification system of diamonds and its importance in gemology. *Gems & Gemology* **45**, 96–111.

Bursill, L. A. and Glaisher, R. W. (1985). Aggregation and dissolution of small and extended defect structures in Type Ia diamond. *American Mineralogist* **70**, 608–618.

Carlson, J. A., Ravenscroft, P. J., Lavoie, C. and Cunning, J. (2016). Ekati Diamond Mine Northwest Territories, Canada NI 43-101 technical report. 428p.

Cartigny, P. (2005). Stable isotopes and the origin of diamond. *Elements* **1**, 79–84.

Cartigny, P., Palot, M., Thomassot, E. and Harris, J. W. (2014). Diamond formation: a stable isotope perspective. *Annual Review of Earth and Planetary Sciences* **42**, 699–732.

Chapman, J., Brown, G. and Sechos, B. (1996). The typical gemmological characteristics of Argyle diamonds. *Australian Gemmologist* **19**, 339–346.

Chinn, I. L., Gurney, J. J. and Kyser, K. T. (1998). Diamonds and mineral inclusions from the NWT, Canada. *7th International Kimberlite Conference*.

Clifford, T. N. (1966). Tectono-metallogenic units and metallogenic provinces of Africa. *Earth and Planetary Science Letters* **1**, 421–434.

Collins, A. T. (2001). The colour of diamond and how it may be changed. *The Journal of Gemmology* **27**, 341–359.

Collins, A. T. and Mohammed, K. (1982). Optical studies of vibronic bands in yellow luminescing natural diamonds. *Journal of Physics C: Solid State Physics* **15**, 147–158.

Collins, A. T., Kanda, H. and Kitawaki, H. (2000). Colour changes produced in natural brown diamonds by high-pressure, high-temperature treatment. *Diamond and Related Materials* **9**, 113–122.

Creaser, R. A., Grütter, H., Carlson, J. and Crawford, B. (2004). Macrocrystal phlogopite Rb–Sr dates for the Ekati property kimberlites, Slave Province, Canada: evidence for multiple intrusive episodes in the Paleocene and Eocene. *Lithos* **76**, 399–414.

Davies, G. (1976). The A nitrogen aggregate in diamond-its symmetry and possible structure. *Journal of Physics C: Solid State Physics* **9**, L537–L542.

Davies, G. and Hamer, M. F. (1976). Optical studies of the 1.945 eV vibronic band in diamond. *Proceedings of the Royal Society A: Mathematical, Physical and Engineering Sciences* **348**, 285–298.

Davies, R. M., Griffin, W. L., O'Reilly, S. Y. and Andrew, A. S. (2003). Unusual mineral inclusions and carbon isotopes of alluvial diamonds from Bingara, eastern Australia. *Lithos* **69**, 51–66.

De Stefano, A., Kopylova, M. G., Cartigny, P. and Afanasiev, V. (2009). Diamonds and eclogites of the Jericho kimberlite (Northern Canada). *Contributions to Mineralogy and Petrology* **158**, 295–315.

Dobrinets, I. A., Vins, V. G. and Zaitsev, A. M. (2013). HPHT-Treated Diamonds. Berlin, Heidelberg, Germany: Springer. 295p.

Dominion Diamond Mines (2017). Dominion diamond announces positive results of misery deep pre-feasibility study and provides update on fox deep project at Ekati Mine. Dominion Diamond Mines. URL: https://www.ddmines.com/dominion-diamond-announces-positive-results-of-misery-deep-pre-feasibility-study-and-provides-update-on-fox-deep-project-at-ekati-mine/.

Driscoll, W. G. and Vaughan, W. (1978). Handbook of optics. New York: McGraw-Hill. 1600p.

Evans, T. and Sauter, D. H. (1961). Etching of diamond surfaces with gases. *Philosophical Magazine* **6**, 429–440.

Field, J. E. (1979). The properties of diamond. 1st ed. New York: Academic Press. 674p.

Fisher, D. (2009). Brown diamonds and high pressure high temperature treatment. *Lithos* **112**, 619–624.

Fitzgerald, C., Grütter, H., Pell, J. and Pilotto, D. (2018). 2018 Technical Report: Mineral resource update for the Chidliak project, Baffin Island, Nunavut, Canada. Vancouver, BC 210p.

Fritsch, E. (1998). The nature of color in diamonds. In *The Nature of Diamonds* (ed. Harlow, G. E.), pp. 23–27. Cambridge: Cambridge University Press.

Fritsch, E., Hainschwang, T., Massi, L. and Rondeau, B. (2007). Hydrogen-related optical centers in natural diamond: an update. *New Diamond and Frontier Carbon Technology* **17**, 63–89.

From, R. E., St-Onge, M. R. and Camacho, A. L. (2014). Preliminary characterization of the Archean orthogneiss complex of Hall Peninsula, Baffin Island, Nunavut. *Canada-Nunavut Geoscience Office: Summary of Activities 2013* 53–62.

Gaillou, E., Post, J. E., Rose, T. and Butler, J. E. (2012). Cathodoluminescence of natural, plastically deformed pink diamonds. *Microscopy and Microanalysis* **18**, 1292–1302.

Gali, A., Lowther, J. E. and Deák, P. (2001). Defect states of substitutional oxygen in diamond. *Journal of Physics: Condensed Matter* **13**, 11607–11613.

Gem Diamonds (2012). Gem Diamonds half year 2012 results. 31p.

Goldschmidt, V. M. (1937). The principles of distribution of chemical elements in minerals and rocks. The seventh Hugo Müller Lecture, delivered before the Chemical Society on March 17th, 1937. *Journal of the Chemical Society (Resumed)* 655–673.

Goss, J. P., Briddon, P. R., Papagiannidis, S. and Jones, R. (2004). Interstitial nitrogen and its complexes in diamond. *Physical Review B* **70**, 235208.

Goss, J. P., Briddon, P. R., Hill, V., Jones, R. and Rayson, M. J. (2014). Identification of the structure of the 3107 cm^{-1} H-related defect in diamond. *Journal of Physics: Condensed Matter* **26**, 145801.

Government of Western Australia (2015). Department of Mines and Petroleum: Ellendale information sheet 1. URL: http://www.dmp.wa.gov.au/Documents/Environment/Ellendale_Information_Sheet.pdf.

Grütter, H. S. (2009). Pyroxene xenocryst geotherms: techniques and application. *Lithos* **112**, 1167–1178.

Hainschwang, T., Notari, F., Fritsch, E. and Massi, L. (2006). Natural, untreated diamonds showing the A, B and C infrared absorptions ("ABC diamonds"), and the H2 absorption. *Diamond and Related Materials* **15**, 1555–1564.

Hainschwang, T., Notari, F., Fritsch, E., Massi, L., Rondeau, B., Breeding, C. M. and Vollstaedt, H. (2008). HPHT treatment of CO_2 containing and CO_2-related brown diamonds. *Diamond and Related Materials* **17**, 340–351.

Hainschwang, T., Fritsch, E., Notari, F. and Rondeau, B. (2012a). A new defect center in type Ib diamond inducing one phonon infrared absorption: the Y center. *Diamond and Related Materials* **21**, 120–126.

Hainschwang, T., Fritsch, E., Massi, L., Rondeau, B. and Notari, F. (2012b). The C center isolated nitrogen-related infrared absorption at 2688 cm^{-1}: perfect harmony in diamond. *Journal of Applied Spectroscopy* **79**, 737–743.

Hainschwang, T., Fritsch, E., Notari, F., Rondeau, B. and Katrusha, A. (2013). The origin of color in natural C center bearing diamonds. *Diamond and Related Materials* **39**, 27–40.

Harris, J. W., Hawthorne, J. B., Oosterveld, M. M. and Wehmeyer, E. (1975). A classification scheme for diamond and a comparative study of South African diamond characteristics. *Physics and Chemistry of the Earth* **9**, 765–783.

Harte, B. (2010). Diamond formation in the deep mantle: the record of mineral inclusions and their distribution in relation to mantle dehydration zones. *Mineralogical Magazine* **74**, 189–215.

Harte, B., Gurney, J. J. and Harris, J. W. (1980). The formation of peridotitic suite inclusions in diamonds. *Contributions to Mineralogy and Petrology* **72**, 181–190.

Heaman, L. M., Kjarsgaard, B. A. and Creaser, R. A. (2003). The timing of kimberlite magmatism in North America: implications for global kimberlite genesis and diamond exploration. *Lithos* **71**, 153–184.

Heaman, L. M., Pell, J., Grütter, H. S. and Creaser, R. A. (2015). U–Pb geochronology and Sr/Nd isotope compositions of groundmass perovskite from the newly discovered Jurassic Chidliak kimberlite field, Baffin Island, Canada. *Earth and Planetary Science Letters* **415**, 183–199.

Hoffman, P. F. (1988). United plates of America, the birth of a craton: early proterozoic assembly and growth of Laurentia. *Annual Review of Earth and Planetary Sciences* **16**, 543–603.

Hogberg, K., Stachel, T. and Stern, R. A. (2016). Carbon and nitrogen isotope systematics in diamond: Different sensitivities to isotopic fractionation or a decoupled origin? *Lithos* **265**, 16–30.

Hollis, J. A., Frei, D., Van Gool, J. A. M., Garde, A. A. and Persson, M. (2006). Using zircon geochronology to resolve the Archaean geology of southern West Greenland. *Geological Survey of Denmark and Greenland Bulletin* **10**, 49–52.

Howell, D. (2012). Strain-induced birefringence in natural diamond: a review. *European Journal of Mineralogy* **24**, 575–585.

Jackson, G. D., Hunt, P. A., Loveridge, W. D. and Parrish, R. R. (1990). Reconnaissance geochronology of Baffin Island, N.W.T. *Radiogenic Age and Isotopic Studies* **3**, 123–148.

Jenke, G. and Cowan, D. R. (1994). Geophysical signature of the Ellendale Lamproite Pipes, Western Australia. *Exploration Geophysics* **25**, 171–171.

Jones, R., Briddon, P. R. and Öberg, S. (1992). First-principles theory of nitrogen aggregates in diamond. *Philosophical Magazine Letters* **66**, 67–74.

King, J. and Wang, W. (2017). Diamond with unusual fluorescence distribution. *Gems & Gemology* **53**, 228–229.

King, J. M., Shigley, J. E., Gelb, T. H., Guhin, S. S., Hall, M. and Wang, W. (2005). Characterization and grading of natural-color yellow diamonds. *Gems & Gemology* **41**, 88–115.

Kirkley, M. B., Gurney, J. J., Otter, M. L., Hill, S. J. and Daniels, L. R. (1991). The application of C isotope measurements to the identification of the sources of C in diamonds: a review. *Applied Geochemistry* **6**, 477–494.

Kitawaki, H. (2007). Gem diamonds: causes of colors. *New Diamond and Frontier Carbon Technology* **17**, 119–126.

Koivula, J. I., Kammerling, R. C., Fritsch, E., Fryer, C. W., Hargett, D. and Kane, R. E. (1989). The characteristics and identification of filled diamonds. *Gems & Gemology* **25**, 68–83.

Krebs, M. Y., Pearson, D. G., Stachel, T., Stern, R. A., Nowicki, T. and Cairns, S. (2016). Using microdiamonds in kimberlite diamond grade prediction: a case study of the variability in diamond population characteristics across the size range 0.2 to 3.4 mm in Misery kimberlite, Ekati Mine, NWT, Canada. *Economic Geology* **111**, 503–525.

Lang, A. R. (1967). Causes of birefringence in diamond. *Nature* **213**, 248–251.

Leahy, K. and Taylor, W. R. (1997). The influence of the Glennie Domain deep structure on the diamonds in Saskatchewan kimberlites. *Geologiya i Geofizika* **38**, 451–460.

Liggins, S. (2010). Identification of point defects in treated single crystal diamond. University of Warwick. 203p.

Lockhart, G., Grütter, H. and Carlson, J. (2004). Temporal, geomagnetic and related attributes of kimberlite magmatism at Ekati, Northwest Territories, Canada. *Lithos* **77**, 665–682.

Ludwig, K. R. (1999). Using Isoplot/Ex, version 2.01: A geochronological toolkit for Microsoft Excel. *Berkeley Geochronology Center (Special Publication)* **1**, 1–49.

McCallum, M. E., Huntley, P. M., Falk, R. W. and Otter, M. L. (1994). Morphological, resorption and etch feature trends of diamonds from kimberlite populations within the Colorado-Wyoming State Line district, USA. In *Proceedings of the 5th International Kimberlite Conference*, pp. 32–50.

Mita, Y. (1996). Change of absorption spectra in Type-Ib diamond with heavy neutron irradiation. *Physical Review B* **53**, 11360–11364.

Moore, M. and Lang, A. R. (1974). On the origin of the rounded dodecahedral habit of natural diamond. *Journal of Crystal Growth* **26**, 133–139.

Nailer, S. G., Moore, M., Chapman, J. and Kowalski, G. (2007). On the role of nitrogen in stiffening the diamond structure. *Journal of Applied Crystallography* **40**, 1146–1152.

Nimis, P. and Taylor, W. R. (2000). Single clinopyroxene thermobarometry for garnet peridotites. Part I. Calibration and testing of a Cr-in-Cpx barometer and an enstatite-in-Cpx thermometer. *Contributions to Mineralogy and Petrology* **139**, 541–554.

Nowicki, T., Crawford, B., Dyck, D., Carlson, J., McElroy, R., Oshust, P. and Helmstaedt, H. (2004). The geology of kimberlite pipes of the Ekati property, Northwest Territories, Canada. *Lithos* **76**, 1–27.

Nowicki, T. E., Coopersmith, H. and Pilotto, D. (2016). Mineral resource estimate for the Chidliak project, Baffin Island, Nunavut. URL: https://www.pdiam.com/assets/docs/technical-reports/msc16_006r-mineral-resource-estimate-for-the-chidliak-project_2016-06-16.pdf.

Omar, M., Pandya, N. S. and Tolansky, S. (1954). The etching of diamond. I. Octahedron faces. *Proceedings of the Royal Society A: Mathematical, Physical and Engineering Sciences* **225**, 33–40.

Orlov, Y. L. (1977). The mineralogy of the diamond. New York: John Wiley & Sons. 235p.

Pandeya, D. C. and Tolansky, S. (1961). Micro-disk patterns on diamond dodecahedra. *Proceedings of the Physical Society* **78**, 12–16.

Pell, J., Grütter, H., Neilson, S., Lockhart, G., Dempsey, S. and Grenon, H. (2013a). Exploration and discovery of the Chidliak Kimberlite Province, Baffin Island, Nunavut: Canada's newest diamond district. In *Proceedings of 10th International Kimberlite Conference*, pp. 209–227. New Delhi: Springer India.

Pell, J., Clements, B., Grütter, H., Neilson, S. and Grenon, H. (2013b). Following kimberlite indicator minerals to source in the Chidliak Kimberlite Province, Nunavut. *Geological Survey of Canada, Open file 7374* 47–52.

Pollack, H. N. and Chapman, D. S. (1977). On the regional variation of heat flow, geotherms, and lithospheric thickness. *Tectonophysics* **38**, 279–296.

Popov, Y. A., Pevzner, S. L., Pimenov, V. P. and Romushkevich, R. A. (1999). New geothermal data from the Kola superdeep well SG-3. *Tectonophysics* **306**, 345–366.

Salustro, S., Pascale, F., Mackrodt, W. C., Ravoux, C., Erba, A. and Dovesi, R. (2018). Interstitial nitrogen atoms in diamond. A quantum mechanical investigation of its electronic and vibrational properties. *Physical Chemistry Chemical Physics* **20**, 16615–16624.

Sarkar, C., Heaman, L. M. and Pearson, D. G. (2015). Duration and periodicity of kimberlite volcanic activity in the Lac de Gras kimberlite field, Canada and some recommendations for kimberlite geochronology. *Lithos* **218–219**, 155–166.

Scott, D. J. (1999). U-Pb geochronology of the eastern Hall Peninsula, southern Baffin Island, Canada: a northern link between the Archean of West Greenland and the Paleoproterozoic Torngat Orogen of northern Labrador. *Precambrian Research* **93**, 5–26.

Scott, D. J. and Campbell, L. M. (1993). Evolution of the Paleoproterozoic Torngat Orogen, Labrador Canada: recent advances using U-Pb geochronology and Nd isotopic systematics. *Abstracts with Programs - Geological Society of America* **25**, 237.

Scott, D. J., Stern, R. A., St-Onge, M. R. and McMullen, S. M. (2002). U–Pb geochronology of detrital zircons in metasedimentary rocks from southern Baffin Island: implications for the Paleoproterozoic tectonic evolution of Northeastern Laurentia. *Canadian Journal of Earth Sciences* **39**, 611–623.

Shigley, J. and Breeding, C. M. (2013). Optical defects in diamond: a quick reference chart. *Gems & Gemology* **49**, 107–111.

Shigley, J. E. and Breeding, C. M. (2015). Visible absorption spectra of colored diamonds. *Gems & Gemology* **51**, 41–43.

Shirey, S. B. and Shigley, J. E. (2013). Recent advances in understanding the geology of diamonds. *Gems & Gemology* **49**, 188–222.

Snyder, D. B. (2010). Mantle lithosphere structure beneath southeast Baffin Island, Nunavut from teleseismic studies. 1-7p.

Sobolev, E. V., Lenskaya, S. V. and Lisoivan, V. I. (1969). Lamellar formations in the structure of natural diamonds. *Journal of Structural Chemistry* **9**, 917–920.

Speich, L., Kohn, S. C., Wirth, R., Bulanova, G. P. and Smith, C. B. (2017). The relationship between platelet size and the B′ infrared peak of natural diamonds revisited. *Lithos* **278–281**, 419–426.

St-Onge, M. R., Jackson, G. D. and Henderson, I. (2006). Geology, Baffin Island (south of 70° N and east of 80° W), Nunavut. *Geological Survey of Canada, Open file 4931*.

St-Onge, M. R., Wodicka, N. and Ijewliw, O. (2007). Polymetamorphic evolution of the Trans-Hudson Orogen, Baffin Island, Canada: integration of petrological, structural and geochronological data. *Journal of Petrology* **48**, 271–302.

St-Onge, M. R., Van Gool, J. A. M., Garde, A. A. and Scott, D. J. (2009). Correlation of Archaean and Palaeoproterozoic units between northeastern Canada and western Greenland: constraining the pre-collisional upper plate accretionary history of the Trans-Hudson orogen. *Geological Society, London, Special Publications* **318**, 193–235.

Stachel, T. (2014). Diamonds. *Mineralogical Association of Canada Short Course* **44**, 1–28.

Stachel, T. and Harris, J. W. (2008). The origin of cratonic diamonds – constraints from mineral inclusions. *Ore Geology Reviews* **34**, 5–32.

Stachel, T. and Harris, J. W. (2009). Formation of diamond in the Earth's mantle. *Journal of Physics: Condensed Matter* **21**, 364206.

Stachel, T. and Luth, R. W. (2015). Diamond formation – Where, when and how? *Lithos* **220–223**, 200–220.

Stachel, T., Brey, G. P. and Harris, J. W. (2005). Inclusions in sublithospheric diamonds: glimpses of deep Earth. *Elements* **1**, 73–78.

Stachel, T., Banas, A., Muehlenbachs, K., Kurszlaukis, S. and Walker, E. C. (2006). Archean diamonds from Wawa (Canada): samples from deep cratonic roots predating cratonization of the Superior Province. *Contributions to Mineralogy and Petrology* **151**, 737–750.

Stachel, T., Harris, J. W. and Muehlenbachs, K. (2009). Sources of carbon in inclusion bearing diamonds. *Lithos* **112**, 625–637.

Stern, R. A., Palot, M., Howell, D., Stachel, T., Pearson, D. G., Cartigny, P. and Oh, A. (2014). Methods and reference materials for SIMS diamond C- and N-isotope analysis. Canadian Centre for Isotopic Microanalysis, Research Report 14-01. University of Alberta, Education and Research Archive. URL: http://hdl.handle.net/10402/era.38738.

Sumida, N. and Lang, A. R. (1981). Cathodoluminescence evidence of dislocation interactions in diamond. *Philosophical Magazine A* **43**, 1277–1287.

Sunagawa, I. (1984). Morphology of natural and synthetic diamond crystals. In *Materials science of the Earth's interior* (ed. Sunagawa, I.), pp. 303–330. Tokyo: Terra Scientific Publishing.

Sunagawa, I. (1990). Growth and morphology of diamond crystals under stable and metastable contitions. *Journal of Crystal Growth* **99**, 1156–1161.

Sweeney, R. J., Prozesky, V. M., Viljoen, K. S. and Connell, S. (1999). The sensitive determination of H in diamond by infrared (FTIR) spectroscopy and micro-elastic-recoil (μ-ERDA) techniques. *Nuclear Instruments and Methods in Physics Research Section B: Beam Interactions with Materials and Atoms* **158**, 582–587.

Tappe, S., Graham Pearson, D., Kjarsgaard, B. A., Nowell, G. and Dowall, D. (2013). Mantle transition zone input to kimberlite magmatism near a subduction zone: origin of anomalous Nd–Hf isotope systematics at Lac de Gras, Canada. *Earth and Planetary Science Letters* **371–372**, 235–251.

Tappert, R. and Tappert, M. C. (2011). Diamonds in nature: a guide to rough diamonds. Berlin, Heidelberg: Springer. 142p.

Taylor, W. R., Jaques, A. L. and Ridd, M. (1990). Nitrogen-defect aggregation characteristics of some Australasian diamonds: time-temperature constraints on the source regions of pipe and alluvial diamonds. *American Mineralogist* **75**, 1290–1310.

Taylor, W. R., Canil, D. and Judith Milledge, H. (1996). Kinetics of Ib to IaA nitrogen aggregation in diamond. *Geochimica et Cosmochimica Acta* **60**, 4725–4733.

Titkov, S. V., Zudin, N. G., Gorshkov, A. I., Sivtsov, A. V. and Magazina, L. O. (2003). An investigation into the cause of color in natural black diamonds from Siberia. *Gems & Gemology* **39**, 200–209.

Titkov, S. V., Shiryaev, A. A., Zudina, N. N., Zudin, N. G. and Solodova, Y. P. (2015). Defects in cubic diamonds from the placers in the northeastern Siberian platform: results of IR microspectrometry. *Russian Geology and Geophysics* **56**, 354–362.

van der Bogert, C. H., Smith, C. P., Hainschwang, T. and McClure, S. F. (2009). Gray-to-blue-to-violet hydrogen-rich diamonds from the Argyle Mine, Australia. *Gems & Gemology* **45**, 20–37.

Whalen, J. B., Wodicka, N., Taylor, B. E. and Jackson, G. D. (2010). Cumberland batholith, Trans-Hudson Orogen, Canada: petrogenesis and implications for paleoproterozoic crustal and orogenic processes. *Lithos* **117**, 99–118.

Wilks, J. and Wilks, E. (1994). Properties and application of diamond. 1st ed. Oxford: Butterworth-Heinemann. 525p.

Woods, G. S. (1986). Platelets and the infrared absorption of Type Ia diamonds. *Proceedings of the Royal Society A: Mathematical, Physical and Engineering Sciences* **407**, 219–238.

Woods, G. S. and Collins, A. T. (1983). Infrared absorption spectra of hydrogen complexes in type I diamonds. *Journal of Physics and Chemistry of Solids* **44**, 471–475.

Yokota, Y., Kotsuka, H., Sogi, T., Ma, J. S., Hiraki, A., Kawarada, H., Matsuda, K. and Hatada, M. (1992). Formation of optical centers in CVD diamond by electron and neutron irradiation. *Diamond and Related Materials* **1**, 470–477.

Zaitsev, A. M. (2001). Optical properties of diamond. Berlin, Heidelberg, Germany: Springer. 502p.

Appendices

Appendix A. Chidliak CH-7

Table A.1: Summary of data collected from the Chidliak CH-7 diamonds. 'X' in the 'B' area' column shows that the B'-centre was not detected; a '?' in the '1405 area' column signifies that the integrated peak area at 1405 cm^{-1} could not be determined due to a low magnitude or overlap with other absorption peaks.

SampleID	Photo	Weight(ct)	Morphology	Color	LWUV	B' position (cm^{-1})	C (at. ppm)	%C	A (at. ppm)	%A	B (at. ppm)	%B	Total N (at. ppm)	3107 area (cm^{-2})	1405 area (cm^{-2})	B' area (cm^{-2})	Type
CH7-L1		0.018	macle	yellow	inert	X	0	0	1860	84	365	16	2225	11	?	X	IaAB
CH7-L2		0.026	octahedron	yellow	inert	X	0	0	2317	88	313	12	2630	6	?	X	IaAB
CH7-L3	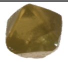	0.021	octahedron	deep yellow	inert	X	346	22	1196	78	0	0	1542	10	?	X	Ib/IaA
CH7-L4		0.012	fragment	pale yellow	inert	X	81	5	1443	95	0	0	1524	20	4	X	Ib/IaA
CH7-L9		0.019	cube	pale yellow	inert	X	48	4	1323	96	0	0	1371	25	4	X	Ib/IaA
CH7-L10	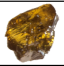	0.019	irregular	brownish yellow	inert	X	521	48	560	52	0	0	1081	28	4	X	Ib/IaA
CH7-L11		0.021	irregular	yellow	inert	X	165	11	1319	89	0	0	1484	24	4	X	Ib/IaA
CH7-L12		0.018	irregular	yellow	inert	X	169	13	1150	87	0	0	1319	21	3	X	Ib/IaA
CH7-L14		0.022	fragment	pale yellow	strong yellow	X	0	0	80	64	45	36	125	21	4	X	IaAB
CH7-L21	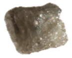	0.018	cube	pale yellow	inert	X	41	4	1065	96	0	0	1106	21	3	X	Ib/IaA
CH7-L22		0.012	irregular	pale yellow	strong yellow	1369	0	0	456	93	33	7	489	15	2	15	IaA
CH7-L24		0.019	fragment	yellow	inert	X	165	10	1565	90	0	0	1730	18	3	X	Ib/IaA
CH7-L25		0.020	aggregate	pale yellow	inert	X	68	3	2102	97	0	0	2170	63	12	X	Ib/IaA
CH7-L26		0.019	octahedron	pale yellow	inert	1376	0	0	858	67	429	33	1287	2	?	60	IaAB
CH7-L27		0.026	octahedron	yellow	inert	1374	0	0	819	97	24	3	843	11	2	16	IaA
CH7-L28		0.021	irregular	orangey yellow	inert	X	227	17	1113	83	0	0	1340	56	9	X	Ib/IaA
CH7-L29		0.019	irregular	orangey yellow	inert	X	132	12	987	88	0	0	1119	25	4	X	Ib/IaA

SampleID	Photo	Weight(ct)	Morphology	Color	LWUV	B' position (cm^{-1})	C (at. ppm)	%C	A (at. ppm)	%A	B (at. ppm)	%B	Total N (at. ppm)	3107 area (cm^{-2})	1405 area (cm^{-2})	B' area (cm^{-2})	Type
CH7-L30		0.023	octahedron	dull yellow	inert	1373	0	0	1019	83	209	17	1228	7	1	21	IaAB
CH7-L31		0.019	fragment	dull yellow	inert	X	214	20	833	80	0	0	1047	8	1	X	Ib/IaA
CH7-L32		0.026	octahedron	yellow	inert	1372	0	0	787	90	83	10	870	1	0	35	IaAB
CH7-L33		0.017	irregular	pale yellow	inert	1373	0	0	1012	72	385	28	1397	3	0	109	IaAB
CH7-L34		0.023	irregular	pale yellow	inert	1368	0	0	610	95	33	5	643	1	0	33	IaA
CH7-L35	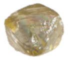	0.020	octahedron	yellow	inert	X	0	0	3782	100	0	0	3782	21	?	X	IaA
CH7-L36		0.019	irregular	pale yellow	inert	1377	0	0	1618	71	673	29	2291	120	22	139	IaAB
CH7-L37		0.028	irregular	pale yellow	strong yellow	X	2	10	11	55	7	35	20	3	1	X	Ib/IaA
CH7-L38		0.020	irregular	pale yellow	strong yellow	X	0	0	16	48	17	52	33	4	1	X	IaAB
CH7-L39		0.018	irregular	pale yellow	strong yellow	X	0	0	17	77	5	23	22	5	1	X	IaAB
CH7-L40		0.021	fragment	yellow	inert	X	330	27	908	73	0	0	1238	24	4	X	Ib/IaA
CH7-L41	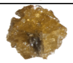	0.012	irregular	yellow	inert	X	221	15	1205	85	0	0	1426	27	5	X	Ib/IaA
CH7-L42		0.030	irregular	yellow	inert	X	115	11	952	89	0	0	1067	9	2	X	Ib/IaA
CH7-L43		0.021	cube	yellow	inert	X	108	8	1228	92	0	0	1336	7	1	X	Ib/IaA
CH7-L44		0.024	irregular	yellow	inert	X	109	9	1147	91	0	0	1256	12	2	X	Ib/IaA
CH7-L45		0.021	cubo-octahedron	yellow	inert	X	123	12	1340	88	0	0	1518	14	2	X	Ib/IaA
CH7-L46		0.016	irregular	deep yellow	inert	X	130	13	880	87	0	0	1010	6	1	X	Ib/IaA

SampleID	Photo	Weight(ct)	Morphology	Color	LWUV	B' position (cm^{-1})	C (at. ppm)	%C	A (at. ppm)	%A	B (at. ppm)	%B	Total N (at. ppm)	3107 area (cm^{-2})	1405 area (cm^{-2})	B' area (cm^{-2})	Type
CH7-L53		0.019	cube	pale yellow	inert	X	90	6	1536	94	0	0	1626	26	4	X	Ib/IaA
CH7-L55		0.027	irregular	pale yellow	inert	1371	0	0	898	85	161	15	1059	20	3	30	IaAB
CH7-L61		0.024	cube	pale yellow	inert	X	56	3	1633	97	0	0	1689	33	6	X	Ib/IaA
CH7-L62		0.019	fragment	pale yellow	inert	X	64	4	1622	96	0	0	1686	28	5	X	Ib/IaA
CH7-L63		0.022	cube	orangey yellow	inert	X	197	20	770	80	0	0	967	34	6	X	Ib/IaA
CH7-L64	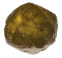	0.021	cubo-octahedron	deep yellow	inert	X	280	20	1115	80	0	0	1395	6	?	X	Ib/IaA
CH7-L65		0.017	fragment	yellow	inert	X	58	22	200	78	0	0	258	1	0	X	Ib/IaA
CH7-L66		0.020	fragment	yellow	inert	X	134	11	1087	89	0	0	1221	1	0	X	Ib/IaA
CH7-L67		0.017	cube	deep yellow	inert	X	234	21	866	79	0	0	1100	12	2	X	Ib/IaA
CH7-L68		0.019	macle	deep yellow	inert	X	173	14	1089	86	0	0	1262	14	3	X	Ib/IaA
CH7-L69		0.027	fragment	yellow	inert	X	110	10	967	90	0	0	1077	16	3	X	Ib/IaA
CH7-L70		0.023	macle	yellow	weak yellow	X	84	9	809	91	0	0	893	31	6	X	Ib/IaA
CH7-L71		0.022	cube	yellow	yellow	X	99	5	1775	95	0	0	1874	107	19	X	Ib/IaA
CH7-L72		0.021	octahedron	yellow	inert	X	131	9	1377	91	0	0	1508	12	2	X	Ib/IaA
CH7-L73		0.022	irregular	yellow	inert	X	53	7	748	93	0	0	801	10	2	X	Ib/IaA
CH7-L74		0.016	cube	yellow	inert	X	145	9	1463	91	0	0	1608	22	3	X	Ib/IaA
CH7-L75		0.022	fragment	pale yellow	strong yellow	X	1	4	15	63	8	33	24	8	1	X	Ib/IaA

SampleID	Photo	Weight(ct)	Morphology	Color	LWUV	B' position (cm^{-1})	C (at. ppm)	%C	A (at. ppm)	%A	B (at. ppm)	%B	Total N (at. ppm)	3107 area (cm^{-2})	1405 area (cm^{-2})	B' area (cm^{-2})	Type
CH7-L76		0.015	cube	pale yellow	yellow	X	98	6	1535	94	0	0	1633	91	17	X	Ib/IaA
CH7-L77		0.025	macle	yellow	inert	X	0	0	1717	88	228	12	1945	16	?	X	IaAB
CH7-L78		0.022	irregular	pale yellow	inert	1373	0	0	770	59	534	41	1304	3	0	115	IaAB
CH7-L79		0.025	irregular	pale yellow	yellow	X	82	4	1834	96	0	0	1916	104	21	X	Ib/IaA
CH7-L81		0.022	cube	pale yellow	inert	X	61	4	1648	96	0	0	1709	28	5	X	Ib/IaA
CH7-L82		0.011	fragment	pale yellow	inert	X	77	5	1486	95	0	0	1563	32	5	X	Ib/IaA
CH7-L84		0.019	cube	pale yellow	inert	X	75	5	1516	95	0	0	1591	28	5	X	Ib/IaA
CH7-L85		0.018	cube	pale yellow	inert	X	76	4	1757	96	0	0	1833	39	7	X	Ib/IaA
CH7-L87		0.017	aggregate	pale yellow	inert	X	0	0	1645	91	155	9	1800	5	?	X	IaA
CH7-L88		0.024	octahedron	pale yellow	purple	1377	0	0	1732	71	693	29	2425	8	1	155	IaAB
CH7-L89		0.020	irregular	brownish yellow	inert	X	132	11	1072	89	0	0	1204	14	3	X	Ib/IaA
CH7-L90		0.021	octahedron	pale yellow	inert	X	0	0	2057	95	103	5	2160	4	?	X	IaA
CH7-L91		0.021	octahedron	dull yellow	yellow	1365	0	0	1247	84	229	16	1476	63	11	43	IaAB
CH7-L92		0.025	irregular	dull yellow	strong yellow	X	9	10	59	69	18	21	86	8	1	X	Ib/IaA
CH7-L93		0.016	fragment	pale yellow	strong yellow	X	2	3	46	74	14	23	62	14	2	X	Ib/IaA
CH7-S1		0.005	cuboid	greenish yellow	inert	X	533	54	451	46	0	0	984	16	3	X	Ib/IaA
CH7-S2	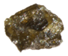	0.006	cuboid	greenish yellow	inert	X	599	64	343	36	0	0	942	20	4	X	Ib/IaA

SampleID	Photo	Weight(ct)	Morphology	Color	LWUV	B' position (cm^{-1})	C (at. ppm)	%C	A (at. ppm)	%A	B (at. ppm)	%B	Total N (at. ppm)	3107 area (cm^{-2})	1405 area (cm^{-2})	B' area (cm^{-2})	Type
CH7-S3		0.012	cuboid	orangey yellow	inert	X	153	10	1360	90	0	0	1513	23	4	X	Ib/IaA
CH7-S4		0.015	octahedron	orangey yellow	inert	X	303	35	554	65	0	0	857	27	5	X	Ib/IaA
CH7-S5		0.014	cuboid	deep yellow	inert	X	249	19	1039	81	0	0	1288	25	5	X	Ib/IaA
CH7-S6		0.014	irregular	deep yellow	inert	X	166	17	796	83	0	0	962	20	4	X	Ib/IaA
CH7-S7		0.019	cuboid	deep yellow	inert	X	207	18	930	82	0	0	1137	11	2	X	Ib/IaA
CH7-S8		0.011	cuboid	deep yellow	inert	X	257	27	698	73	0	0	955	13	2	X	Ib/IaA
CH7-S9		0.009	cuboid	deep yellow	inert	X	115	10	1045	90	0	0	1160	29	5	X	Ib/IaA
CH7-S10	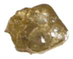	0.013	cuboid	deep yellow	inert	X	94	8	1051	92	0	0	1145	3	1	X	Ib/IaA
CH7-S11		0.009	aggregate	yellow	yellow	1371	0	0	332	68	155	32	487	4	1	9	IaAB
CH7-S12		0.017	cuboid	pale yellow	inert	1366	0	0	144	95	7	5	151	0	0	4	IaA
CH7-S13		0.020	octahedron	yellow	inert	X	187	19	774	81	0	0	961	8	1	X	Ib/IaA
CH7-S14		0.019	fragment	yellow	inert	X	107	15	600	85	0	0	707	0	0	X	Ib/IaA
CH7-S15		0.019	fragment	dull yellow	strong yellow	X	7	13	18	32	31	55	56	4	0	X	Ib/IaA
CH7-S16		0.025	fragment	pale yellow	inert	X	0	0	1488	95	80	5	1568	2	?	X	IaA
CH7-S17		0.011	macle	yellow	inert	X	305	13	2109	87	0	0	2414	11	?	X	Ib/IaA
CH7-S18		0.024	fragment	yellow	inert	X	0	0	1471	90	166	10	1637	2	?	X	IaAB
CH7-S19		0.012	fragment	pale yellow	inert	1373	0	0	856	79	230	21	1086	2	0	88	IaAB

SampleID	Photo	Weight(ct)	Morphology	Color	LWUV	B' position (cm^{-1})	C (at. ppm)	%C	A (at. ppm)	%A	B (at. ppm)	%B	Total N (at. ppm)	3107 area (cm^{-2})	1405 area (cm^{-2})	B' area (cm^{-2})	Type
CH7-S20		0.016	octahedron	pale yellow	inert	1377	0	0	888	74	315	26	1203	20	3	32	IaAB
CH7-S21		0.010	fragment	pale yellow	inert	1373	0	0	787	52	723	48	1510	51	8	126	IaAB
CH7-S22		0.017	fragment	dull yellow	strong yellow	1365	0	0	137	74	48	26	185	2	0	5	IaAB
CH7-S23		0.007	fragment	dull yellow	inert	X	122	7	1733	93	0	0	1855	116	22	X	Ib/IaA
CH7-S24		0.014	fragment	dull yellow	strong yellow	X	4	3	107	93	4	3	115	4	1	X	Ib/IaA
CH7-S25		0.021	fragment	dull yellow	inert	X	0	0	1477	75	496	25	1973	18	4	X	IaAB
CH7-S26		0.010	fragment	dull yellow	strong yellow	1365	0	0	152	57	116	43	268	15	2	13	IaAB
CH7-S27		0.018	irregular	dull yellow	strong yellow	X	5	6	56	70	19	24	80	3	?	X	Ib/IaA
CH7-S28		0.017	cuboid	pale yellow	inert	X	73	4	1598	96	0	0	1671	23	4	X	Ib/IaA
CH7-S35		0.016	cuboid	pale yellow	strong orange	X	0	0	5	31	11	69	16	2	0	X	IaAB
CH7-S44		0.021	fragment	pale yellow	inert	X	30	2	1364	98	0	0	1394	14	2	X	Ib/IaA
CH7-S45		0.014	irregular	brownish yellow	strong yellow	X	0	0	16	28	42	72	58	2	0	X	IaAB
CH7-S52		0.021	fragment	yellow	inert	1374	103	7	1304	85	123	8	1530	7	1	35	Ib/IaAB
CH7-S53		0.017	fragment	pale yellow	inert	1374	0	0	1117	65	597	35	1714	9	1	128	IaAB
CH7-S54		0.020	octahedron	yellow	inert	X	0	0	2024	89	251	11	2275	7	?	X	IaAB
CH7-S55		0.006	irregular	dull yellow	yellow	X	0	0	2592	87	402	13	2994	175	34	X	IaAB
CH7-S56		0.020	cuboid	yellow	inert	X	49	4	1175	96	0	0	1224	20	4	X	Ib/IaA

SampleID	Photo	Weight(ct)	Morphology	Color	LWUV	B' position (cm^{-1})	C (at. ppm)	%C	A (at. ppm)	%A	B (at. ppm)	%B	Total N (at. ppm)	3107 area (cm^{-2})	1405 area (cm^{-2})	B' area (cm^{-2})	Type
CH7-S57		0.012	irregular	pale yellow	inert	X	93	4	2348	96	0	0	2441	153	30	X	Ib/IaA
CH7-S58		0.020	fragment	pale yellow	inert	X	60	3	1784	97	0	0	1844	40	7	X	Ib/IaA
CH7-S59		0.017	cuboid	orangey yellow	inert	X	267	16	1352	84	0	0	1619	62	10	X	Ib/IaA
CH7-S60		0.006	cuboid	orangey yellow	inert	X	336	25	1005	75	0	0	1341	35	6	X	Ib/IaA
CH7-S61		0.014	irregular	yellow	inert	X	163	11	1386	89	0	0	1549	45	9	X	Ib/IaA
CH7-S62		0.019	cubo-octahedron	yellow	inert	X	234	15	1360	85	0	0	1594	22	4	X	Ib/IaA
CH7-S63		0.009	irregular	yellow	inert	X	130	15	748	85	0	0	878	7	1	X	Ib/IaA
CH7-S64		0.014	cuboid	pale yellow	yellow	X	61	7	875	93	0	0	936	55	10	X	Ib/IaA
CH7-S65		0.017	aggregate	pale yellow	yellow	X	44	4	1165	96	0	0	1209	31	6	X	Ib/IaA
CH7-S66		0.018	octahedron	yellow	inert	X	0	0	2049	87	302	13	2351	28	?	X	IaAB
CH7-S67		0.016	cuboid	pale yellow	inert	X	0	0	2086	89	250	11	2336	2	?	X	IaAB
CH7-S68		0.016	fragment	yellow	inert	1372	16	4	351	93	12	3	379	3	0	16	Ib/IaAB
CH7-S70		0.012	irregular	pale yellow	weak yellow	X	54	5	1075	95	0	0	1129	21	4	X	Ib/IaA
CH7-S76		0.022	fragment	pale yellow	weak yellow	X	64	5	1121	95	0	0	1185	22	4	X	Ib/IaA
CH7-S77		0.008	fragment	pale yellow	inert	X	102	5	1754	95	0	0	1856	34	6	X	Ib/IaA
CH7-S79		0.008	fragment	yellow	strong yellow	X	0	0	19	58	14	42	33	4	1	X	IaAB
CH7-S80		0.012	irregular	yellow	weak yellow	X	57	6	969	94	0	0	1026	17	3	X	Ib/IaA

SampleID	Photo	Weight(ct)	Morphology	Color	LWUV	B' position (cm^{-1})	C (at. ppm)	%C	A (at. ppm)	%A	B (at. ppm)	%B	Total N (at. ppm)	3107 area (cm^{-2})	1405 area (cm^{-2})	B' area (cm^{-2})	Type
CH7-S81		0.019	cuboid	orangey yellow	weak yellow	X	235	22	856	78	0	0	1091	45	8	X	Ib/IaA
CH7-S82		0.019	irregular	orangey yellow	green	X	102	9	996	91	0	0	1098	81	16	X	Ib/IaA
CH7-S83		0.014	fragment	yellow	inert	X	173	14	1096	86	0	0	1269	8	1	X	Ib/IaA
CH7-S84		0.016	cuboid	brownish yellow	inert	X	111	9	1083	91	0	0	1194	22	4	X	Ib/IaA
CH7-S85		0.012	irregular	brownish yellow	inert	X	150	19	656	81	0	0	806	11	2	X	Ib/IaA
CH7-S86	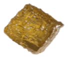	0.019	cuboid	deep yellow	inert	X	195	14	1167	86	0	0	1362	9	2	X	Ib/IaA
CH7-S87		0.013	cuboid	brownish yellow	inert	X	403	23	1344	77	0	0	1747	37	6	X	Ib/IaA
CH7-S88		0.020	irregular	deep brownish yellow	strong yellow	X	0	0	106	80	26	20	132	4	1	X	IaAB
CH7-S89		0.015	irregular	deep brownish yellow	strong yellow	1364	0	0	175	80	44	20	219	5	1	8	IaA
CH7-S90		0.013	fragment	yellow	inert	1371	61	5	1036	79	213	16	1310	2	0	98	Ib/IaAB
CH7-S91		0.016	fragment	yellow	inert	1373	56	4	891	71	302	24	1249	2	0	69	Ib/IaAB
CH7-S92		0.014	fragment	yellow	inert	X	0	0	1784	76	574	24	2358	17	?	X	IaAB
CH7-S93		0.026	fragment	pale yellow	weak green	1369	0	0	455	91	44	9	499	9	1	18	IaA
CH7-S94		0.021	fragment	pale yellow	inert	X	0	0	1586	90	176	10	1762	3	?	X	IaAB
CH7-S95		0.020	fragment	pale yellow	inert	X	81	5	1628	95	0	0	1709	47	8	X	Ib/IaA
CH7-S96		0.018	irregular	pale yellow	inert	X	67	5	1338	95	0	0	1405	36	6	X	Ib/IaA
CH7-S97		0.020	fragment	pale yellow	inert	X	85	4	1929	96	0	0	2014	43	8	X	Ib/IaA

SampleID	Photo	Weight(ct)	Morphology	Color	LWUV	B' position (cm^{-1})	C (at. ppm)	%C	A (at. ppm)	%A	B (at. ppm)	%B	Total N (at. ppm)	3107 area (cm^{-2})	1405 area (cm^{-2})	B' area (cm^{-2})	Type
CH7-S98		0.025	irregular	dull yellow	strong yellow	X	0	0	28	52	26	48	54	4	1	X	IaAB
CH7-S99		0.018	irregular	dull yellow	strong yellow	X	0	0	10	30	23	70	33	3	1	X	IaAB
CH7-S100		0.013	irregular	dull yellow	strong yellow	X	0	0	2	14	12	86	14	1	0	X	IaAB
CH7-S101		0.019	cuboid	dull yellow	yellow	X	43	4	1137	96	0	0	1180	32	6	X	Ib/IaA
CH7-S102		0.019	irregular	dull yellow	strong yellow	X	0	0	16	89	2	11	18	4	1	X	IaAB
CH7-S103		0.014	fragment	dull yellow	strong yellow	X	0	0	21	64	12	36	33	6	1	X	IaAB
CH7-S104		0.019	irregular	dull yellow	strong yellow	X	0	0	24	52	22	48	46	6	1	X	IaAB
CH7-S105		0.016	fragment	dull yellow	strong orange	X	0	0	5	36	9	64	14	1	?	X	IaAB
CH7-S106		0.009	fragment	dull yellow	strong yellow	X	0	0	6	15	35	85	41	2	0	X	IaAB
CH7-S107		0.019	cuboid	dull yellow	inert	X	79	4	1731	96	0	0	1800	14	3	X	Ib/IaA
CH7-S108		0.004	fragment	dull yellow	strong yellow	X	0	0	53	54	46	46	99	7	1	X	IaAB

Appendix B. Ekati Misery Southwest Extension

Table B.1: Summary of data collected on diamonds from the Misery Southwest Extension at the Ekati Mine. 'X' in the 'B' area' column shows that the B'-centre was not detected; a '?' in the '1405 area' column signifies that the integrated peak area at 1405 cm^{-1} could not be determined due to a low magnitude or overlap with other absorption peaks.

Sample ID	Photo	Weight (ct)	Morphology	color	LWUV	B' position (cm^{-1})	C (at. ppm)	%C	A (at. ppm)	%A	B (at. ppm)	%B	Total N (at. ppm)	3107 area (cm^{-2})	1405 area (cm^{-2})	B' area (cm^{-2})	Type
MS-L1		0.390	macle	pale yellow	purple	1376	0	0	1612	69	739	31	2351	2	?	308	IaAB
MS-L2		0.340	irregular	pale yellow	greenish yellow	1373	0	0	727	74	254	26	981	26	4	109	IaAB
MS-L3		0.120	macle	pale yellow	inert	1374	0	0	1178	88	168	12	1346	142	24	41	IaAB
MS-L4		0.420	irregular	orangey yellow	inert	X	166	15	910	85	0	0	1076	24	4	X	Ib/IaA
MS-L5		0.360	irregular	orangey yellow	greenish yellow	X	108	9	1029	91	0	0	1137	24	4	X	Ib/IaA
MS-L6		0.290	cube	orangey yellow	yellow	X	129	12	917	88	0	0	1046	23	4	X	Ib/IaA
MS-L7		0.170	irregular	yellow	yellow	X	78	8	957	92	0	0	1035	28	5	X	Ib/IaA
MS-L8		0.110	irregular	orangey yellow	yellow	X	68	6	1159	94	0	0	1227	48	7	X	Ib/IaA
MS-L9		0.200	cube	orangey yellow	yellow	X	40	4	994	96	0	0	1034	31	5	X	Ib/IaA
MS-L10		0.210	irregular	orangey yellow	yellow	X	246	24	775	76	0	0	1021	18	3	X	Ib/IaA
MS-L11		0.140	cube	yellow	yellow	X	61	5	1060	95	0	0	1121	52	8	X	Ib/IaA
MS-L12		0.130	cube	yellow	yellow	X	153	9	1475	91	0	0	1628	152	26	X	Ib/IaA
MS-L13		0.110	cube	pale yellow	yellow	X	38	3	1121	97	0	0	1159	38	7	X	Ib/IaA
MS-L14		0.150	dodecahedron	yellow	inert	X	102	11	858	89	0	0	960	31	5	X	Ib/IaA
MS-L15		0.100	cube	yellow	yellow	X	37	3	1058	97	0	0	1095	28	5	X	Ib/IaA
MS-L16		0.110	irregular	yellow	yellow	X	62	5	1120	95	0	0	1182	35	7	X	Ib/IaA

Sample ID	Photo	Weight (ct)	Morphology	color	LWUV	B' position (cm^{-1})	C (at. ppm)	%C	A (at. ppm)	%A	B (at. ppm)	%B	Total N (at. ppm)	3107 area (cm^{-2})	1405 area (cm^{-2})	B' area (cm^{-2})	Type
MS-L17		0.120	cube	yellow	yellow	X	57	4	1236	96	0	0	1293	54	10	X	Ib/IaA
MS-L18		0.150	irregular	yellow	yellow	X	43	4	1026	96	0	0	1069	34	5	X	Ib/IaA
MS-L19		0.130	tetrahexahedron	deep yellow	inert	X	202	18	936	82	0	0	1138	17	3	X	Ib/IaA
MS-L20		0.220	cube	orangey yellow	inert	X	161	13	1078	87	0	0	1239	53	8	X	Ib/IaA
MS-S1		0.079	cube	orangey yellow	inert	X	258	19	1124	81	0	0	1382	37	6	X	Ib/IaA
MS-S2		0.081	cube	orangey yellow	inert	X	185	17	920	83	0	0	1105	31	5	X	Ib/IaA
MS-S3		0.035	irregular	orangey yellow	inert	X	207	16	1116	84	0	0	1323	54	9	X	Ib/IaA
MS-S4		0.029	irregular	orangey yellow	yellow	X	94	7	1208	93	0	0	1302	62	10	X	Ib/IaA
MS-S5		0.047	irregular	orangey yellow	inert	X	99	8	1145	92	0	0	1244	30	5	X	Ib/IaA
MS-S6		0.017	irregular	orangey yellow	inert	X	109	10	981	90	0	0	1090	33	6	X	Ib/IaA
MS-S7		0.036	dodecahedron	orangey yellow	yellow	X	130	9	1332	91	0	0	1462	25	4	X	Ib/IaA
MS-S8		0.019	cube	orangey yellow	yellow	X	54	6	801	94	0	0	855	38	7	X	Ib/IaA
MS-S9		0.019	cube	orangey yellow	inert	X	87	9	893	91	0	0	980	40	7	X	Ib/IaA
MS-S10		0.035	irregular	orangey yellow	inert	X	131	10	1205	90	0	0	1336	26	4	X	Ib/IaA
MS-S11		0.022	irregular	orangey yellow	inert	X	120	8	1318	92	0	0	1438	40	7	X	Ib/IaA
MS-S12		0.023	aggregate	orangey yellow	inert	X	111	11	906	89	0	0	1017	32	6	X	Ib/IaA

Sample ID	Photo	Weight (ct)	Morphology	color	LWUV	B' position (cm^{-1})	C (at. ppm)	%C	A (at. ppm)	%A	B (at. ppm)	%B	Total N (at. ppm)	3107 area (cm^{-2})	1405 area (cm^{-2})	B' area (cm^{-2})	Type
MS-S13		0.041	irregular	orangey yellow	yellow	X	92	9	974	91	0	0	1066	46	8	X	Ib/IaA
MS-S14		0.020	irregular	orangey yellow	inert	X	127	12	977	88	0	0	1104	29	5	X	Ib/IaA
MS-S15		0.042	cube	pale yellow	yellow	X	46	4	991	96	0	0	1037	45	9	X	Ib/IaA
MS-S16		0.023	irregular	pale yellow	yellow	X	48	5	869	95	0	0	917	37	7	X	Ib/IaA
MS-S17		0.022	cube	pale yellow	yellow	X	42	4	1080	96	0	0	1122	55	10	X	Ib/IaA
MS-S18		0.041	dodecahedron	pale yellow	yellow	1376	0	0	729	81	170	19	899	62	11	8	IaAB
MS-S19		0.016	cube	pale yellow	yellow	X	86	8	943	92	0	0	1029	43	7	X	Ib/IaA
MS-S20		0.029	dodecahedron	pale yellow	yellow	1375	0	0	967	99	6	1	973	13	2	10	IaA
MS-S21		0.029	irregular	pale yellow	yellow	1378	0	0	712	80	181	20	893	51	9	2	IaAB
MS-S22		0.019	irregular	pale yellow	yellow	1377	0	0	669	80	163	20	832	44	7	4	IaAB
MS-S23		0.029	irregular	pale yellow	yellow	X	46	4	1000	96	0	0	1046	30	5	X	Ib/IaA
MS-S27		0.045	dodecahedron	pale yellow	weak yellow	1376	0	0	954	98	19	2	973	14	3	5	IaA
MS-S40		0.027	cube	yellow	weak yellow	X	39	5	809	95	0	0	848	22	4	X	Ib/IaA
MS-S41		0.060	cube	yellow	inert	X	104	8	1272	92	0	0	1376	39	7	X	Ib/IaA
MS-S42		0.028	irregular	yellow	inert	X	109	9	1052	91	0	0	1161	24	4	X	Ib/IaA
MS-S43		0.031	aggregate	yellow	inert	X	125	8	1365	92	0	0	1490	55	9	X	Ib/IaA

Sample ID	Photo	Weight (ct)	Morphology	color	LWUV	B' position (cm^{-1})	C (at. ppm)	%C	A (at. ppm)	%A	B (at. ppm)	%B	Total N (at. ppm)	3107 area (cm^{-2})	1405 area (cm^{-2})	B' area (cm^{-2})	Type
MS-S44		0.018	irregular	yellow	inert	X	165	13	1148	87	0	0	1313	40	7	X	Ib/IaA
MS-S45		0.043	irregular	yellow	weak yellow	X	113	8	1219	92	0	0	1332	41	8	X	Ib/IaA
MS-S46		0.044	irregular	yellow	inert	X	103	8	1176	92	0	0	1279	55	9	X	Ib/IaA
MS-S47		0.057	irregular	yellow	inert	X	47	6	698	94	0	0	745	24	4	X	Ib/IaA
MS-S48		0.017	cube	dull yellow	inert	X	74	6	1245	94	0	0	1319	51	9	X	Ib/IaA
MS-S49		0.027	irregular	yellow	inert	X	86	9	892	91	0	0	978	32	5	X	Ib/IaA
MS-S50		0.054	fragment	orangey yellow	inert	X	269	28	688	72	0	0	957	35	6	X	Ib/IaA
MS-S51		0.040	irregular	yellow	weak yellow	X	58	6	985	94	0	0	1043	42	7	X	Ib/IaA
MS-S52		0.031	irregular	yellow	yellow	X	70	7	902	93	0	0	972	44	7	X	Ib/IaA
MS-S53		0.023	irregular	orangey yellow	inert	X	55	7	775	93	0	0	830	22	4	X	Ib/IaA
MS-S54		0.019	irregular	yellow	yellow	X	30	4	816	96	0	0	846	28	5	X	Ib/IaA
MS-S55		0.019	cube	yellow	yellow	X	72	8	800	92	0	0	872	43	8	X	Ib/IaA
MS-S56		0.057	cube	yellow	yellow	X	50	4	1193	96	0	0	1243	38	7	X	Ib/IaA
MS-S57		0.016	irregular	yellow	yellow	X	138	9	1343	91	0	0	1481	37	6	X	Ib/IaA
MS-S58		0.062	irregular	yellow	weak yellow	X	69	7	920	93	0	0	989	35	6	X	Ib/IaA
MS-S59		0.024	cube	yellow	yellow	X	42	6	679	94	0	0	721	42	7	X	Ib/IaA

Sample ID	Photo	Weight (ct)	Morphology	color	LWUV	B' position (cm^{-1})	C (at. ppm)	%C	A (at. ppm)	%A	B (at. ppm)	%B	Total N (at. ppm)	3107 area (cm^{-2})	1405 area (cm^{-2})	B' area (cm^{-2})	Type
MS-S60		0.028	irregular	yellow	yellow	X	55	6	938	94	0	0	993	34	6	X	Ib/IaA
MS-S61		0.024	aggregate	yellow	yellow	X	56	5	963	95	0	0	1019	29	5	X	Ib/IaA
MS-S63		0.034	dodecahedron	dull yellow	inert	X	21	3	664	97	0	0	685	4	1	X	Ib/IaA
MS-S64		0.017	irregular	dull yellow	inert	X	60	7	813	93	0	0	873	20	3	X	Ib/IaA
MS-S65		0.030	fragment	dull yellow	inert	X	39	3	1091	97	0	0	1130	51	8	X	Ib/IaA
MS-S66		0.028	irregular	pale yellow	weak yellow	X	55	5	976	95	0	0	1031	33	6	X	Ib/IaA
MS-S67		0.019	octahedron	pale yellow	inert	1373	0	0	810	91	85	9	895	16	3	32	IaA

Appendix C. Surface features of yellow diamonds

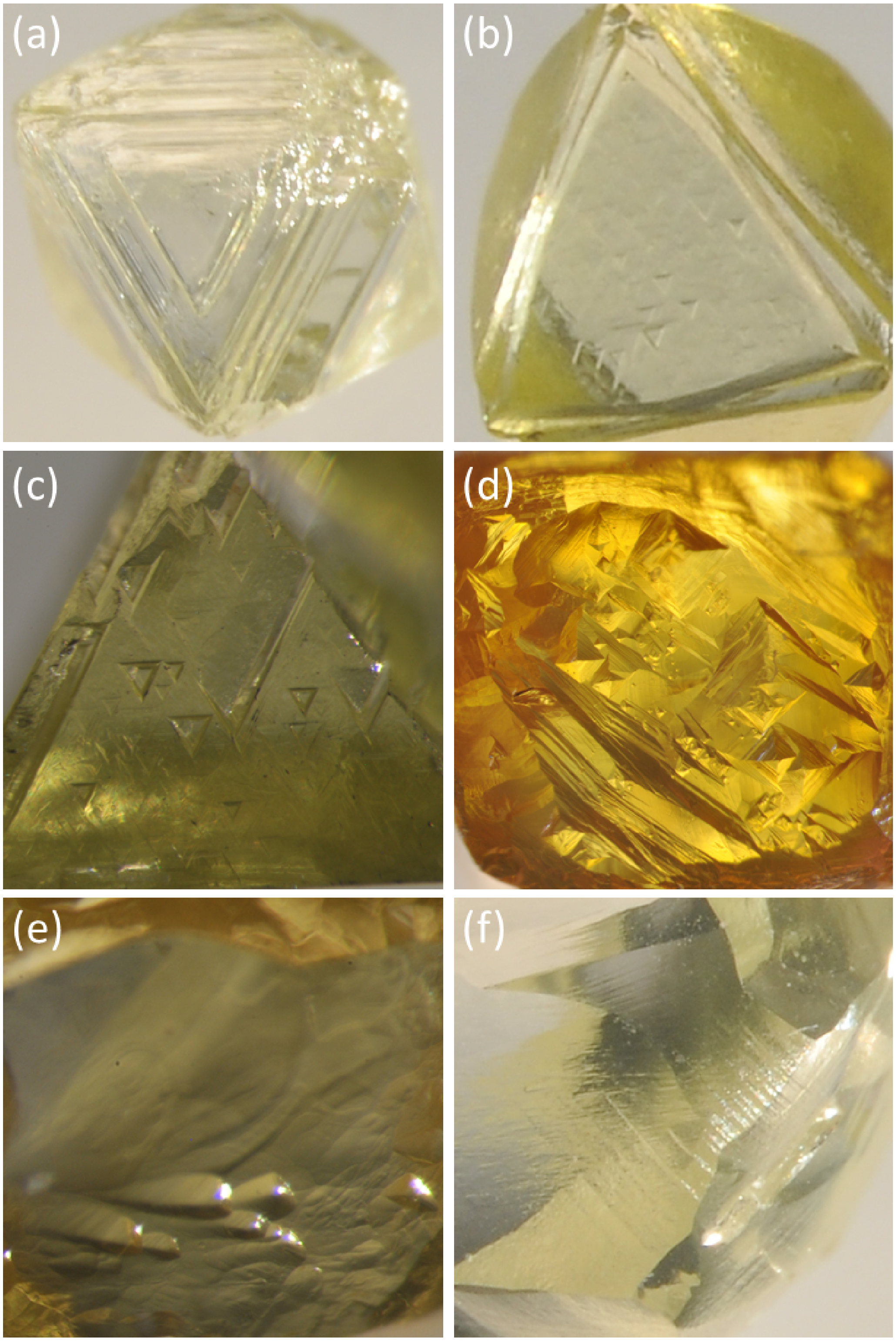

Figure C.1: Surface features observed on yellow diamonds: (a) triangular plates (stacked growth layers), (b) shield-shape laminae, (c) negative trigons, (d) tetragons, (e) hillocks, and (f) plastic deformation lines.